FRACTURE TOUGHNESS OF REINFORCED PLASTIC COMPOSITE MATERIALS

Henry Schmidt

FRACTURE TOUGHNESS OF REINFORCED PLASTIC COMPOSITE MATERIALS

BY

HENRY SCHMIDT, JR.

LIEUTENANT COMMANDER, UNITED STATES NAVY

B.S., UNITED STATES NAVAL ACADEMY

(1961)

SUBMITTED IN PARTIAL FULFILLMENT

OF THE REQUIREMENTS FOR THE DEGREE OF

NAVAL ENGINEER

AND THE DEGREE OF

MASTER OF SCIENCE IN NAVAL ARCHITECTURE

AND MARINE ENGINEERING

AT THE

MASSACHUSETTS INSTITUTE OF TECHNOLOGY

MAY, 1970

FRACTURE TOUGHNESS OF REINFORCED PLASTIC COMPOSITE MATERIALS

BY

HENRY SCHMIDT, JR.

Submitted to the Department of Naval Architecture and Marine Engineering on May 22, 1970, in partial fulfillment of the requirements for the Master of Science degree in Naval Architecture and Marine Engineering and the Professional Degree, Naval Engineer.

ABSTRACT

Double cantilever beam specimens containing various fibers as reinforcement in epoxy and polyester resin matrix materials were tested for fracture toughness. Specimen geometry and test procedures were similar to those used for similar tests on un-reinforced thermoplastic and thermosetting resins. Fibers were oriented perpendicular to direction of crack growth in a single layer at mid thickness of the test specimen. Fracture toughness was found to be sensitive to fiber debonding, fiber density, test specimen web thickness, and distance of crack tip in the matrix material ahead of the point where the last fiber had fractured. Fiber bundle debonding was found to be a function of fiber extensibility, fiber to matrix bond strength, and shear strength of the resin. Debonding in the radial direction around the fiber bundles may have a greater effect on fracture energy than does debonding along the length of the fibers.

THESIS SUPERVISOR: F. J. McGARRY

TITLE: PROFESSOR, DEPARTMENT OF CIVIL ENGINEERING

ACKNOWLEDGMENT

I would like to express my appreciation to Professor Frederick J. McGarry for his guidance and attention to the progress of this work, and for his many suggestions. In addition, I would like to thank Mr. J. F. Mandell for his many suggestions and for his contribution of some of the data to this work. The contribution of comments and criticism from other graduate students, teaching assistants, and research assistants is hereby acknowledged.

The assistance of Mr. James King and Mr. Arthur Rudolf was invaluable for the technical advice and suggestions in preparation of the test specimens from the castings.

TABLE OF CONTENTS

LIST OF FIGURES

LIST OF FIGURES (Continued)

LIST OF FIGURES (Continued)

LIST OF TABLES

LIST OF SYMBOLS

f = force applied - pounds or pounds/inch

$a = f(EI)$

δ = deflection - inches

l = crack length - inches

N = beam parameter

U = elastic strain energy - inch pounds

S = Griffith Surface Work - inch pounds

W = crack width at fracture surface - inches

γ = fracture energy - ergs/cm^2

A = area - inches^2

s = scale factor

$s = \frac{\text{INSTRON Crosshead Rate}}{\text{INSTRON Chart Rate}}$

t = width of crack at fracture surface

t = web thickness of beam specimen - inches

h = beam height - inches

A_f = cross section area of fibers - inches^2

n' = number of fiber bundles in specimen

n = fiber bundle density - bundles/inch

V_f = volume fraction of fibers

I. INTRODUCTION

The increasing use of fiber reinforced plastic matrix composite materials has demonstrated the existing structural potential of these materials for many industrial uses, some of which are aircraft and aero space, construction, corrosion resistant materials, industrial equipment, watercraft and other marine uses, and transportation. During the period from 1957 to 1970, use of these materials in the various industries has shown an average of a seven-fold increase with an even greater growth predicted in the coming decade.* (1) With the increased usage of this type composite material, technology has managed to solve many production and product problems. However, the level of theoretical investigation of these materials has not kept pace nor produced reliable data and criteria enabling the engineer or designer to accurately determine the material necessary to meet his needs in a particular application. The majority of the design practices in use today are based upon past experience or require testing of a prototype to determine if the design and the material are adequate to meet the service requirements.**

Some of the characteristics of fiber reinforced resin matrix composite materials make them particularly desirable in many applications. Such characteristics as being able to be tailored to a specific need, high strength to weight ratio, resistance to many degrading environments, and

---

* Numbers in parentheses indicate references at the end of the text.

** This may be evidenced by the construction and current testing by the U.S. Navy of a full scale midship section of a proposed Minesweeper ship design using a fiber reinforced resin composite hull material.

ease of maintenance are only a few.

These materials are not without their shortcomings. When thermosetting polymer matrices are used in the fabrication of these materials, their usefulness is seriously limited by their brittleness and susceptibility to crack initiation and propagation.[2] When materials show this susceptibility, their application is limited to stress levels very much lower than might be expected in relation to their ultimate tensile stress.

Fracture toughness of a material is a measure of the ability of a material to resist the initiation and unstable propagation of cracks in the material. These cracks may be initiated at flaws in the material or at points in the structure where stress may be concentrated due to design. The fracture toughness testing of fiber reinforced resin composite materials is still in the developmental stages. A great deal of fracture toughness testing has been accomplished with metals which exhibit a brittle behavior,[3][4][5] but it is doubtful whether the procedures developed for these materials may be used for testing of composite materials.

It has been nearly five decades since Griffith[6] set forth his theory of brittle fracture, and this theory has been successfully applied to a wide range of materials. Other investigators such as Irwin,[7] Orowan,[8] and Irwin and Kies[9] have proposed an alteration in the Griffith theory by the combining of any fracture mechanism operating in a material into Griffith's surface energy term (γ). The central idea of Griffith's theory is that the strain energy introduced into a material during loading is replaced by a surface energy as a crack propagates through the material. When the rate of change of strain energy with crack length is equal to the rate of change of surface energy with crack length, unstable crack propa-

gation will result. Fiberglass reinforced resin matrix materials commonly display an effective surface energy (γ) more than 1000 times greater than that shown by either of the components in their bulk form.[10]

This investigation was undertaken in an attempt to determine why fiber reinforced resin matrix materials are tough, and the fracture mechanisms through which this fracture toughness is evidenced. Several investigators have reported studies which are of interest in this work. Mullin, et al.,[11] have experimentally studied some of the basic fracture mechanisms exhibited by single fibers of a variety of materials in an epoxy matrix. A discussion of a number of types of fracture which may occur, depending upon the properties of the particular fiber or matrix material and upon the degree of adhesion between the components, is presented. Outwater and Carns[10] and Outwater and Murphy[12] have also studied the fracture of single fibers imbedded in a matrix material with particular emphasis placed upon the energy necessary to fracture a fiber which debonds from and pulls out of the matrix material. They conclude that this mechanism is the major contributor to the fracture energy of these materials.

II. PROCEDURE

According to the Griffith theory,[6] the fracture surface energy (γ) is the amount of energy required to produce a unit area of fracture surface. This energy may be regarded as one measure of the resistance of a material to the initiation of and the rapid propagation of a crack through the material. Experimentally, a measure of this fracture surface energy (γ) may be obtained using tensile specimens containing defects of a known size. Another method of measuring this energy is the use of a cleavage technique as proposed by Berry.[13][14] Berry, as well as Broutman and McGarry,[15] made use of this technique to measure the surface energy of isotropic glassy polymeric materials. Hoagland[16] applied the technique to measure the plain strain fracture toughness of metals, which may or may not exhibit isotropic properties depending upon the prior history of the metal and sample selection. Berry conducted an extensive analysis of the cleavage technique as to the possible sources of error in the results produced by the technique and the overlying assumptions. Gillis and Gilman[17] also conducted a mathematical analysis of the technique as to the possible sources of error. Both investigators conclude that if the system behaves in an essentially linear manner, the approximations of elementary beam theory are substantially correct. Berry further found that the uncertainty in the value of the fracture surface energy obtained from the tensile samples is usually not less than $\pm$ 30 percent. Although this discrepancy is small when compared to the actual and theoretical values of this parameter, it is much greater than desirable if values of fracture

surface energy for different polymeric materials are to be compared.

The double cantilever beam cleavage technique was selected for use in this study for the following reasons:

1) The values obtained for the fracture surface energy (γ) are more accurate and consistent than those obtained using the tensile technique.
2) The tensile technique develops inherently unstable, rapid crack propagation whereas the cleavage technique results in an inherently stable, slow crack propagation allowing study of the material as the crack propagates through it.
3) The value of the fracture energy may be obtained from a single specimen.
4) Fracture energy may be calculated directly from the recording chart in a straightforward manner.
5) The calculation of fracture energy using the cleavage technique does not require knowledge of the modulus of the material.

Using the cleavage technique, a crack is caused to propagate along the median plane of the beam sample by forces applied at the free ends of the specimen (Figures 1 and 2). The crack is constrained to the median plane by the slots milled in the test specimen. These slots are as proposed by Berry for isotropic materials and are even more necessary for the fiber reinforced specimens which are anisotropic. Since the fibers impart a large amount of additional toughness to the material, the crack has an even greater tendency to leave the slot, particularly when large numbers of fibers are used. Because of this tendency, low deflection rates are required during the test and in some instances, the specimens had to be

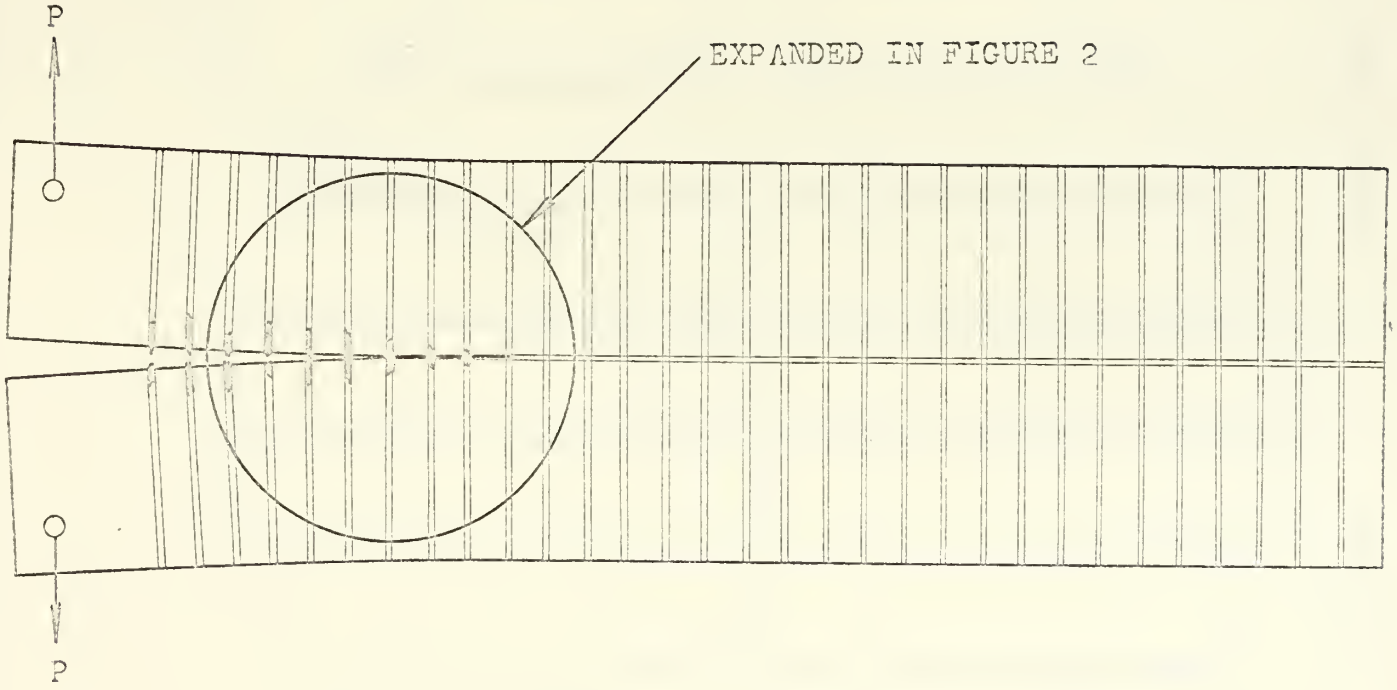

FIGURE 1 SCHEMATIC OF CRACK PROPAGATION

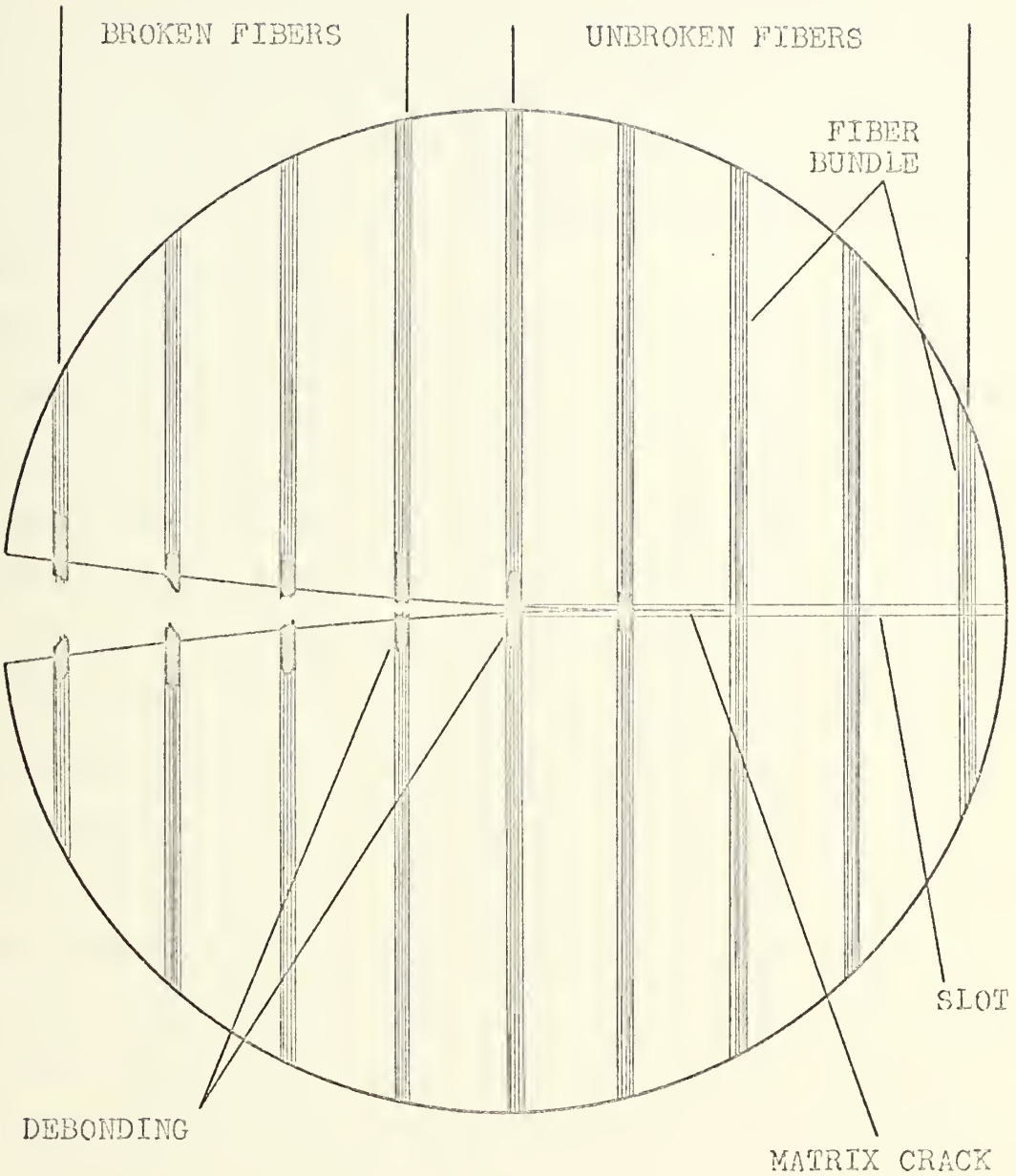

FIGURE 2 SCHEMATIC OF FRACTURE AREA

further modified by the addition of aluminum strips along the length of the beam. The details of specimen preparation and modification are contained in Appendix A. Figure 3 shows the detail of the standard test specimen used. The dimensions as used for the standard test specimen were found to be sufficient to develop the full strength of the fiber as well as be convenient for preparation and machining as discussed in the Discussion of Results section.

The specimens were tested on an INSTRON Universal Testing Machine with a 1000 pound load cell. The specimens are pinned to the loading arms using the holes drilled for such purpose (Figure 1). A suitable chart speed that is compatible with the crosshead rate being used is selected. The specimens are then tested using a constant deflection rate and the fracture energy is calculated directly from the INSTRON recording chart as will be explained in the Results section. As explained previously, low deflection rates (generally .01 inches per minute or less) are required due to the tendency of the crack to leave the slots at higher rates.

Due to the transparency of the matrix materials used, the crack may be readily observed as it propagates through the material. Suitable notation may be made on the recording chart to record the progress of the crack in the matrix and the fracture of the fiber bundles. The behavior of the fibers and the matrix materials also may be observed while subject to the action of the propagating crack.

The matrix materials to be used in this investigation are thermosetting resins. The resins selected were LAMINAC 4173 Polyester Resin (American Cyanimid Company) cured using 2 percent methyl ethyl ketone peroxide, and EPON 828 Epoxy Resin (Shell Chemical Company) cured using 5

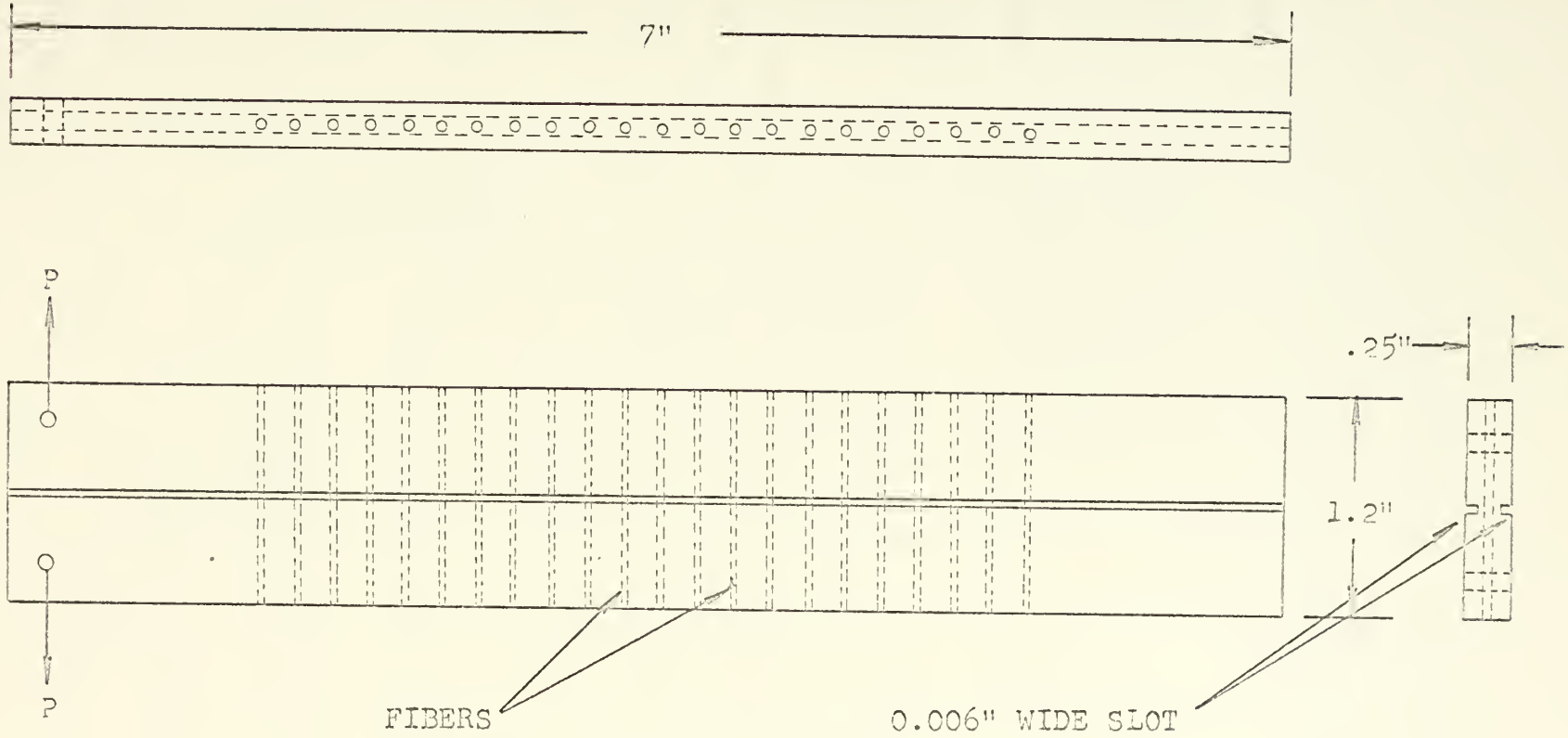

FIGURE 3 CLEAVAGE SPECIMEN

% Curing Agent D. Fibers used in preparing the specimens were as follows:

1) Fiber bundles extracted from Style 181 fiberglass cloth (Stevens Fiberglass), E-glass fibers. (Style 181 cloth)
2) E-glass fiber bundles of essentially rectangular cross section area. (Flat E-glass)
3) Nylon 6 fiber bundles.
4) Beta glass fiber bundles.
5) Thornel Graphite fiber bundles.
6) Bundles of synthetic fiber manufactured by Monsanto Corporation. (Monsanto Type I)
7) Single filament E-glass fibers of .01 and .005 inch diameter.

The properties of the materials used are presented in Appendix B.

The parameters to be investigated in determining the effect on the fracture energy of a fiber reinforced resin matrix material are:

1) Effect of matrix toughness - the two matrix materials were selected to observe the effect on fracture energy of an approximate five fold increase in matrix toughness when used with a given fiber material reinforcement.
2) Effect on fracture energy of different fiber bundle material in the two resin matrices.
3) Effect on fracture energy of changing specimen geometry, notably the specimen height and web thickness.
4) Qualitative effect of fiber debonding on fracture energy.
5) Effect of fiber twist on the fracture energy.
6) Effect of fiber density (number of fiber bundles per inch of test section) on the fracture surface of the specimen.

III. RESULTS

The general procedure for determining the fracture surface energy from a double cantilever beam specimen involves the determination of the beam parameter (N) from the test data. The effective surface energy corresponding to points where the crack length was noted during the test may then be computed. The beam parameter (N) can be determined from the force equation for a generalized beam:[13]

$$f = \frac{a\delta}{l^N}$$

where

f = applied force

a = $f(EI)$

δ = deflection

l = crack length

Values of (N) may then be determined from the graph of log f/δ versus log l, the slope of the curve being equal to (N). With the value of (N) so obtained, the fracture surface energy may then be determined by applying the Griffith relation relating the elastic strain energy of the beams to the surface energy necessary to create the fracture surface.

The elastic strain energy in the beam is given by:

$$U = \frac{1}{2} f \delta$$

$$= \frac{1}{2} \frac{a\delta^2}{l^N}$$

The fracture surface energy of a propagating crack is given by:

$$S = 2\gamma (Wl)$$

where:

S = surface work

W = width of the crack at the fracture surface

Applying the Griffith criteria:

$$\frac{\partial U}{\partial l} = \frac{\partial S}{\partial l}$$

results in:[13]

$$\frac{nf\delta}{2l} = 2\gamma W$$

or:

$$\gamma = \frac{nf\delta}{4Wl}$$

This procedure was found to be unsatisfactory for specimens containing fiber reinforcement (an anistropic material) as the data obtained on the recording chart (Figure 4) is too irregular resulting in inconsistencies in the computed fracture surface energy.

A method which has been found to yield reasonably reproducible results for the fiber reinforced resin matrix composite materials is to divide the change in the area under the force-deflection curve (INSTRON output recording - Figure 4), between points where the crack length was noted on the INSTRON recording chart, by the surface area of the crack between these two points. The length of the crack (l) used in these calculations is generally the length from the first fiber bundle of the test section to the last fiber bundle broken during the test, as determined from the test specimen. The use of cross polarized light to observe the

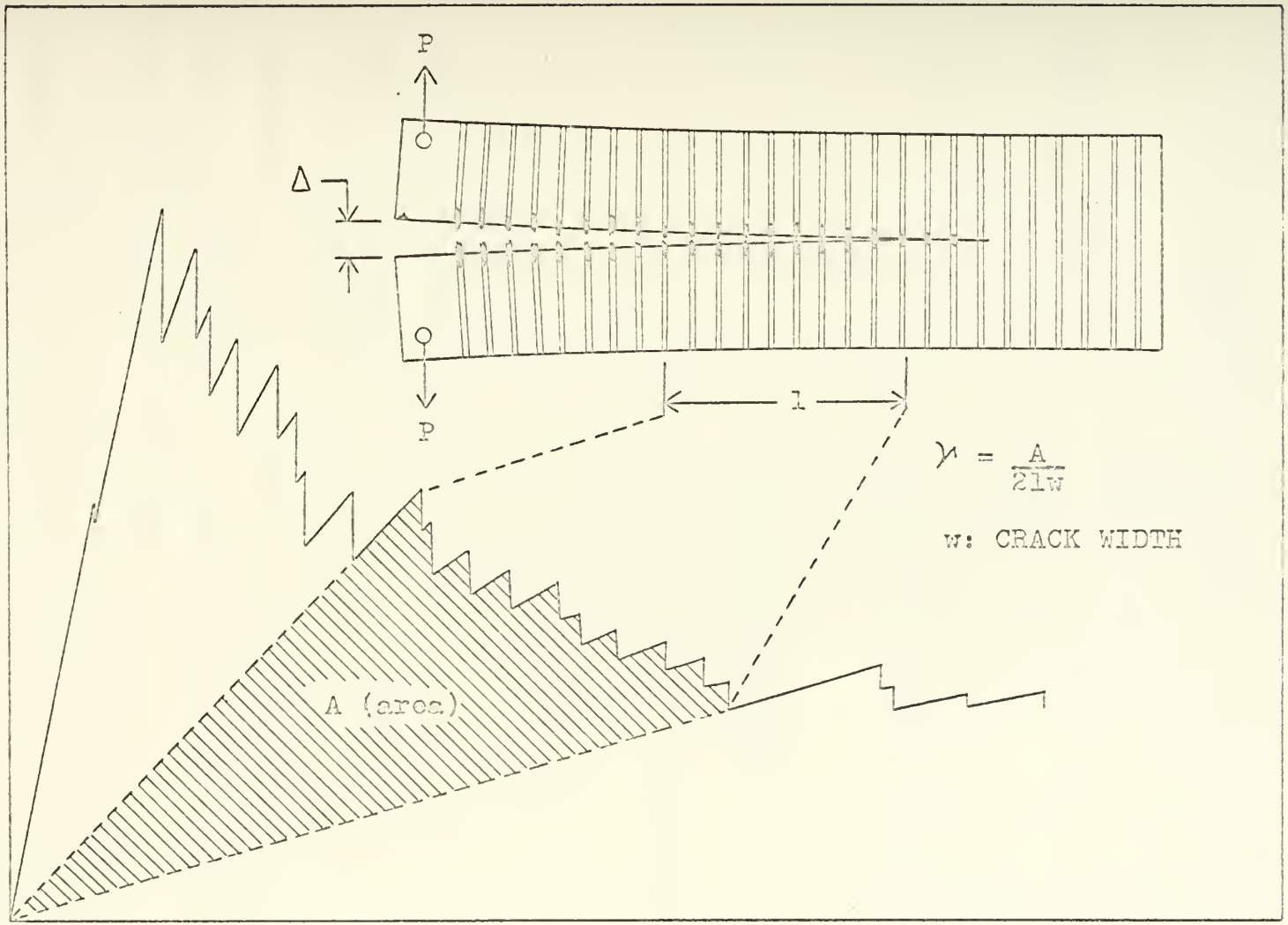

FIGURE 4 TYPICAL INSTRON OUTPUT AND ENERGY CALCULATION.

specimen during the test enables the observer to accurately determine the position of the last broken fiber by observation of the stress patterns in the material.

Using the INSTRON output recording:

$$\gamma = \frac{Afs}{2tl}$$

where:

γ = fracture energy

A = area as measured from force deflection chart

f = applied force scale of the recording chart - pounds/inch

s = scale factor

$$s = \frac{\text{INSTRON crosshead rate}}{\text{INSTRON chart rate}}$$

t = width of the crack at the fracture surface

t = web thickness

l = crack length as measured from the specimen

For specimens without fiber reinforcement, the values obtained for the fracture energy by this method are in good agreement with the values obtained by the more general procedure of determining the beam parameter and utilizing the Griffith criteria.[13][19] For specimens with fiber reinforcement, the values of fracture surface energy obtained by this method are generally within 15 percent or less of the average value for the particular specimen configuration.

The most consistent results are obtained when the crack is allowed to propagate 2 1/2 to 3 inches through the fiber bundle test section. Deviations in the results become more significant when very short or very long

crack lengths are used due to the end effects. This was also found to be true by Berry[13] in tests of isotropic polymeric materials.

The volume fraction of fibers (V_f) contained in a test specimen may be related to the fiber density (n) of the specimen by the following:

$$(1) \qquad V_f = \frac{\text{volume of fibers}}{\text{total volume of specimen}} = \frac{n' A_f h}{thl}$$

where:

n' = number of fiber bundles contained in specimen

A_f = cross section area of fiber bundles

h = length (height) of the fiber bundles

t = web thickness

h = beam height

l = length of specimen

By dividing the numerator and denominator of equation (1) by the length of the specimen, equation (2) results:

$$(2) \qquad V_f = \frac{\frac{n'}{l} A_f}{t}$$

Since n'/l = fiber bundle density (n) and the area of the fiber bundles (A_f) may be considered to be constant for a particular fiber in a particular matrix material:

$$(3) \qquad V_f \propto \frac{n A_f}{t}$$

Using the proportionality of the volume fraction of fibers to the fiber bundle density (n) and the web thickness (t), the trend of percent change in fracture energy with percent change in volume fraction of fibers

may be determined without accurate measurement of the cross section area of the fibers.

The results of the experiments conducted are displayed in the form of tables and graphs at the end of this section. The data from which these tables and graphs are constructed is presented in its entirety as Appendix C.

The results for the web thickness (t) tests for the two matrix materials with no fibers are presented in Table 1 and Figures 5 and 6. For this test series, specimens of standard dimensions as discussed in the Procedures Section were used with the exception that the web thickness (t) was varied from .04 inches to .10 inches in .02 inch increments. For the LAMINAC 4173 polyester resin matrix, the fracture surface energy (γ) increases with increasing web thickness. It is not a linear increase, however, as doubling the web thickness does not result in an increase in fracture surface energy by a similar factor. For the EPON 828 epoxy resin matrix, the fracture surface energy decreased with increasing web thickness. As with the polyester resin, the decrease observed is not linear in that doubling the web thickness does not result in decreasing the fracture energy by a factor of one-half. However, for both of the resins used, the respective increase or decrease of fracture energy is constant with changing web thickness.

The results of a similar series of web thickness tests for fiber reinforced specimens of the two matrix materials is presented in Table 2 and Figures 7 and 8. For this test series, a standard specimen using Style 181 Cloth fiber bundle reinforcement at a density of 10 bundles per inch was prepared. This density was held constant as was the height of the

beams and the specimen length. The web thickness (t) was again varied from .04 inches to .10 inches in .02 inch increments. For specimens with the LAMINAC 4173 polyester resin matrix, the fracture surface energy decreases with increasing web thickness (t). For a web thickness greater than .08 inches the decrease in fracture energy with increasing web thickness appears to be constant. The specimens with a web thickness of .10 inches were modified with aluminum strips which generally results in a higher value of fracture energy than would be obtained for an unmodified specimen. For the specimens using the EPON 828 epoxy resin matrix, fracture surface energy also decreases with increasing web thickness (t).

The dashed line on Figures 7 and 8 represents the fracture energy resulting if web thickness is assumed to be constant at .04 inches. If web thickness had no effect on the fracture energy of these specimens, this curve should be a horizontal, straight line. This would also be indicated in the results by a doubling of the area under the force-deflection curve (Figure 4) if the web thickness is doubled, or the fracture energy computed should be reduced by one-half if the web thickness is doubled, indicating a constant area under the force-deflection curve. These dashed curves on Figures 7 and 8 indicate that the fracture energy for the EPON 828 specimens has very little dependency on the web thickness.

The results of a series of tests to determine the effect of changing the effective height of the specimen arms is presented in Tables 3 and 4 and Figures 9 and 10. For this test series, a standard specimen with a fiber bundle density of 10 bundles per inch of the Style 181 Cloth fiber bundle and a web thickness of .08 inches was used. The height of the beams (h) was varied from .5 inches to 1.0 inches in .1 inch increments. For

both of the matrix materials, LAMINAC 4173 polyester resin and EPON 828 epoxy resin, the results indicate that the fracture energy is constant with increasing beam height. The value of fracture surface energy is slightly higher for the epoxy resin matrix composite than for the polyester resin matrix.

The most extensive series of tests was conducted on composite specimens of Style 181 Cloth fiber bundles in a LAMINAC 4173 polyester resin matrix with specimen web thickness (t) equal to .04 inches. Fiber bundle density was varied from 1 bundle per inch to 60 bundles per inch. The results of this test series are presented in Table 5 and Figures 11 and 11a. Figure 11a is an expanded presentation of the results contained in Figure 11 for low fiber densities. Above a fiber bundle density of 20 bundles per inch, the specimens had to be modified with aluminum strips (see Appendix A) in order to prevent premature failure of the specimen by the crack leaving the slots and running to the upper and lower surfaces of the specimen.

The results for these specimens with a .04 inch web thickness appear to be linearly increasing through a range of bundle density of about 25 bundles per inch at which point the slope begins to increase with further increase in bundle density(n).

The results of a similar series of tests with the Style 181 Cloth fiber bundle reinforcement in the LAMINAC 4173 polyester resin with a web thickness of .08 inches are presented in Table 6 and Figure 12. These specimens indicate an increasing slope of fracture energy with increasing fiber bundle density up to a density of about 25 bundles per inch at which point the curve appears to become linear. This is opposite to the behavior

observed with the lesser web thickness.

The results of a similar series of tests on specimens with Style 181 Cloth fiber bundles in EPON 828 epoxy resin matrix materials are shown in Table 7 and Figure 13. The value of fracture surface energy increases approximately linearly up to a fiber bundle density of about 30 bundles per inch where it begins to level off.

Figure 14 shows the comparison of fracture surface energy for the Style 181 Cloth fiber bundles in the two different matrix materials. Figures 15 and 16 show the results of fracture surface energy divided by the fiber bundle density for the Style 181 Cloth fiber bundles in the two matrix materials. With increasing bundle density, the contribution of the individual fiber bundles to the toughness decreases although the total toughness increases for the epoxy resin system. For the polyester resin composite, the contribution to the fracture energy by the individual bundles appears to reach a minimum value at approximately 25 bundles per inch where the bundle contribution appears to increase with increasing bundle density. This effect was observed for both the .04 inch and .08 inch web thickness specimens.

The next series of tests utilized an E-glass fiber bundle of a flat rectangular cross section with no twist to the fiber bundles. The results for these fibers in the LAMINAC 4173 polyester resin are shown in Table 8 and Figure 17. A great deal of data scatter was associated with these specimens and the results may not be representative of the actual behavior. Table 9 and Figure 18 show the results of the same fiber in the EPON 828 epoxy resin matrix. These results appear to be linearly increasing throughout the range of bundle density investigated. Figure 19 is the

comparison of the flat E-glass fibers in the two matrix materials. Figures 20 and 21 show the results of fracture surface energy divided by fiber bundle density for the flat E-glass fibers in the two matrix materials.

A series of tests was conducted on specimens utilizing a Beta-glass fiber bundle in the LAMINAC 4173 polyester resin and EPON 828 epoxy resin matrices. The results for fracture surface energy of these fibers on the polyester resin matrix are shown in Tables 10 and 11 and Figures 22 and 23. As with the other types of fibers utilized in the tests, specimens with the LAMINAC 4173 polyester resin matrix required modification with aluminum strips at a bundle density of 20 bundles per inch and greater. Specimens of the Beta-glass fiber bundles in the EPON 828 epoxy resin matrix exhibited an almost linear increase in fracture energy with increasing fiber bundle density throughout the range of bundle density investigated. Figure 24 is the comparison of the fracture energy versus the fiber bundle density for the Beta-glass fibers in the two matrix materials. This is an interesting comparison in that it shows the fracture energy for the polyester resin matrix increasing more rapidly than that for the epoxy resin matrix above a bundle density of about 25 bundles per inch. Figures 25 and 26 show the fracture energy divided by the bundle density versus the bundle density for the polyester resin and the epoxy resin matrix specimens respectively. The individual bundle density contribution for the epoxy matrix composite is less than that for the polyester resin matrix composite.

Table 12 and Figure 27 detail the results of a series of specimens containing a Thornel 50 graphite fiber bundle reinforcement in an EPON 828 epoxy resin matrix. These specimens exhibited the greatest fracture energy

of any of the materials investigated. Figure 28 exhibits the decrease in individual fiber bundle contribution to the fracture energy for the Thornel 50 fiber reinforcement, and this decrease is essentially linear within the range of fiber density investigated.

Another series of tests was conducted using a Monsanto Type I experimental fiber as reinforcement in an EPON 828 epoxy resin matrix. Table 13 and Figure 30 display the results of this test series. The results for the fracture energy exhibited by this specimen are high in comparison to the results obtained using glass fiber bundle reinforcement. Figure 29 shows the decrease in the individual fiber bundle contribution to the fracture energy with increasing fiber density for the Monsanto fibers.

Figure 31 shows the relative comparison of the fracture energy obtained with the various fiber bundles as reinforcement with a LAMINAC 4173 polyester resin matrix composite. Figure 32 shows the comparison of the individual fiber bundle contribution to the fracture energy with increasing fiber bundle density for the same composite systems.

Figure 33 shows the comparison of the individual fiber bundle contribution to the fracture energy with increasing bundle density for the EPON 828 epoxy resin matrix system. Figure 34 exhibits the comparison of the fracture energy obtained with the various fiber bundles as reinforcement in an EPON 828 epoxy resin matrix system. This data is perhaps more meaningful in that only a few of the specimens required modification with aluminum strips to prevent premature failure during testing.

When using Figure 31 through Figure 34, care should be exercised to remember the characteristics of the individual fiber bundles used as reinforcement and the comparison of these characteristics between the respec-

tive fibers. Due to the variation in the bundle characteristics, the curves may not be directly compared one against the other.

Using equation (3), the volume fraction of fibers (V_f) was determined for the web thickness tests and the fiber density tests using the Style 181 Cloth fiber bundle reinforcement (Table 14). Using a common base volume fraction (V_f) of 125 K for these two test series, Figure 35 details the percent increase of fracture energy with percent increase in volume fraction of fibers as computed from the base value. The web thickness tests resulted in a much larger percent increase in fracture energy than was observed for the fiber density studies with web thickness equal to .08 inches at comparable percent increases in volume fraction of fibers. It is significant to note that the fiber density tests for the polyester resin composite with web thickness of .04 inches forms a continuation of the web thickness tests for the same resin system of volume fraction increases above 100 percent. Within the volume fraction range from zero to 100 percent, these two curves, obtained from different test specimens, appear to be essentially coincident. The divergence of the web thickness results as compared to the fiber density results indicates that the lateral extent of the matrix material around the fiber bundles may be significant, particularly at low fiber density. This is supported by the results of the polyester resin fiber density results with the two different web thicknesses, the thinner web thickness yielding larger percentage increases in fracture energy with increasing volume fraction of fibers.

Figures 36 and 37 detail the results of percent increase in fracture energy with percent increase in volume fraction of fibers for the various fiber bundle reinforcements in the polyester and epoxy resin matrix mate-

rials respectively. The percent changes for these figures is measured with respect to the specimen with the lowest volume fraction of fibers.

Table 15 details the results of some specific tests conducted as a preliminary investigation of the effect of such parameters as coating on the fiber bundles, twist of the fiber bundles, and toughening of the resin matrix using CTBN rubber particles, and the fracture energy of the model composite.

Additionally, a test specimen series was prepared using a Nylon 6 fiber bundle as reinforcement in the two respective matrix materials. Bundle densities of 10 and 20 bundles per inch were used. The specimens using the polyester resin matrix failed by cracking out the side even when the specimens were modified with aluminum strips. The epoxy matrix specimens at a density of 20 bundles per inch failed by a similar mechanism. Results were obtained with the Nylon 6 fiber bundles at a density of 10 bundles per inch in the epoxy matrix (Table 15). The fracture energy recorded was the highest for any of the specimens tested.

TABLE 1

WEB THICKNESS EFFECT, NON-REINFORCED RESIN

LAMINAC 4173 POLYESTER RESIN

Specimen	Cast	Crosshead Rate Inches/Min	Web Thickness (t) Inches	γ ergs/cm^2 x 10^{-5}
3	7	.05	.04	.497
5	7	.01	.04	.378
9	9	.01	.04	.455
21	13	.01	.04	.320
80	33	.01	.04	.278
108 a	51	.01	.04	.458
109 a	51	.01	.04	.399
158	105	.005	.08	.545
159	105	.005	.08	.595
164	107	.01	.08	.545

EPON 828 EPOXY RESIN

Specimen	Cast	Crosshead Rate Inches/Min	Web Thickness (t) Inches	γ ergs/cm^2 x 10^{-5}
232	139	.01	.04	3.35
233	139	.01	.06	2.65
234	139	.01	.06	2.92
179	114	.005	.08	2.72
200	124	.01	.08	2.33
235	139	.01	.08	2.72
237	139	.01	.10	2.25
238	139	.01	.10	1.85

a - No post cure

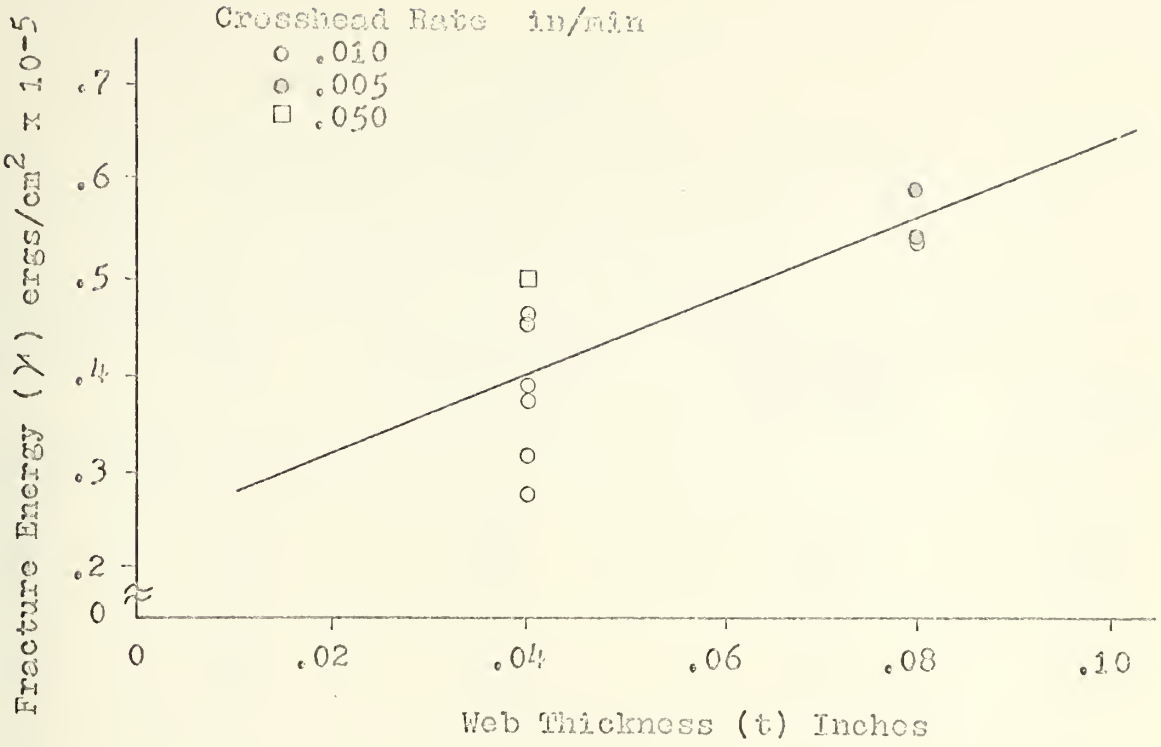

FIGURE 5 FRACTURE ENERGY vs WEB THICKNESS; LAMINAC 4173 POLYESTER RESIN - NON-REINFORCED RESIN.

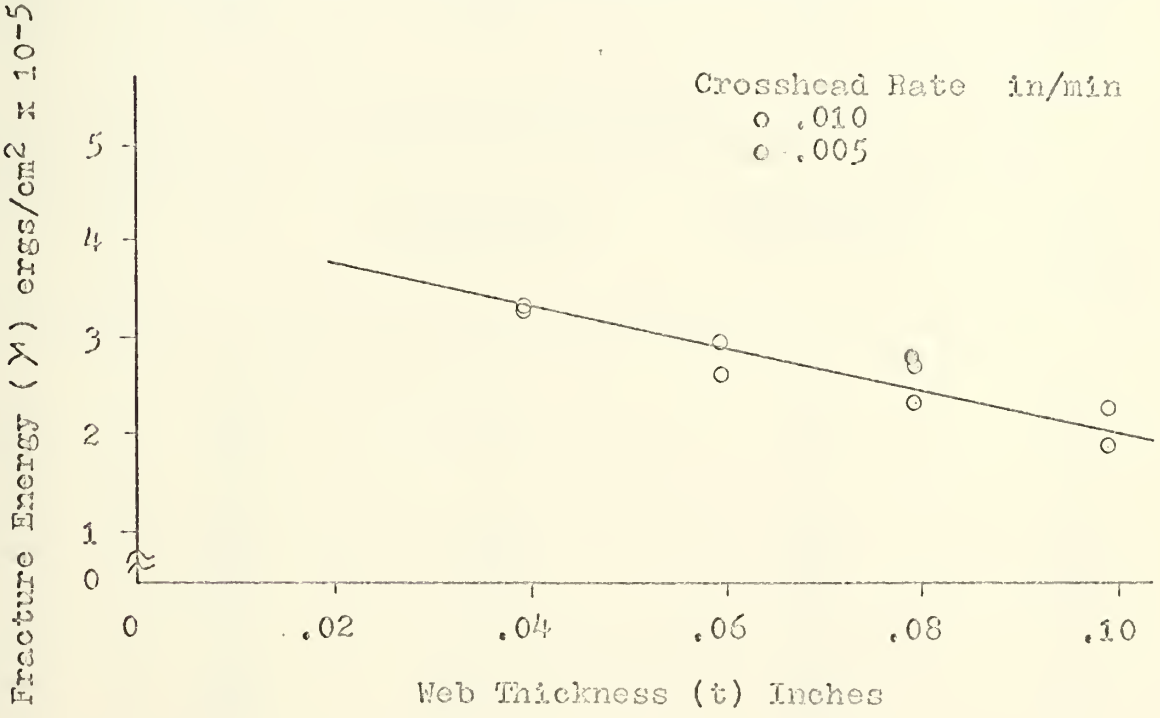

FIGURE 6 FRACTURE ENERGY vs WEB THICKNESS; EPON 828 EPOXY RESIN - NON-REINFORCED RESIN.

TABLE 2

WEB THICKNESS EFFECT, FIBER REINFORCED RESIN

LAMINAC 4173 POLYESTER RESIN

Specimen	Cast	Crosshead Rate Inches/Min	Web Thickness (t) Inches	γ ergs/cm^2 x 10^{-5}
11	9	.01	.04	7.79
12	9	.01	.04	7.11
57	27	.01	.04	6.67
58	27	.01	.06	4.85
246	143	.01	.06	5.36
59	27	.01	.08	3.66
249	145	.01	.08	4.65
231 A	131	.01	.10	3.67
247 A	144	.01	.10	3.67

EPON 828 EPOXY RESIN

Specimen	Cast	Crosshead Rate Inches/Min	Web Thickness (t) Inches	γ ergs/cm^2 x 10^{-5}
175	113	.01	.04	9.83
176	113	.01	.06	6.51
251	146	.01	.06	6.93
177	114	.01	.08	5.25
181	115	.005	.08	5.09
257	149	.01	.08	4.97
178	114	.01	.10	4.48
258	149	.01	.10	3.75
259	149	.01	.10	4.44

A -- Aluminum modified specimens.

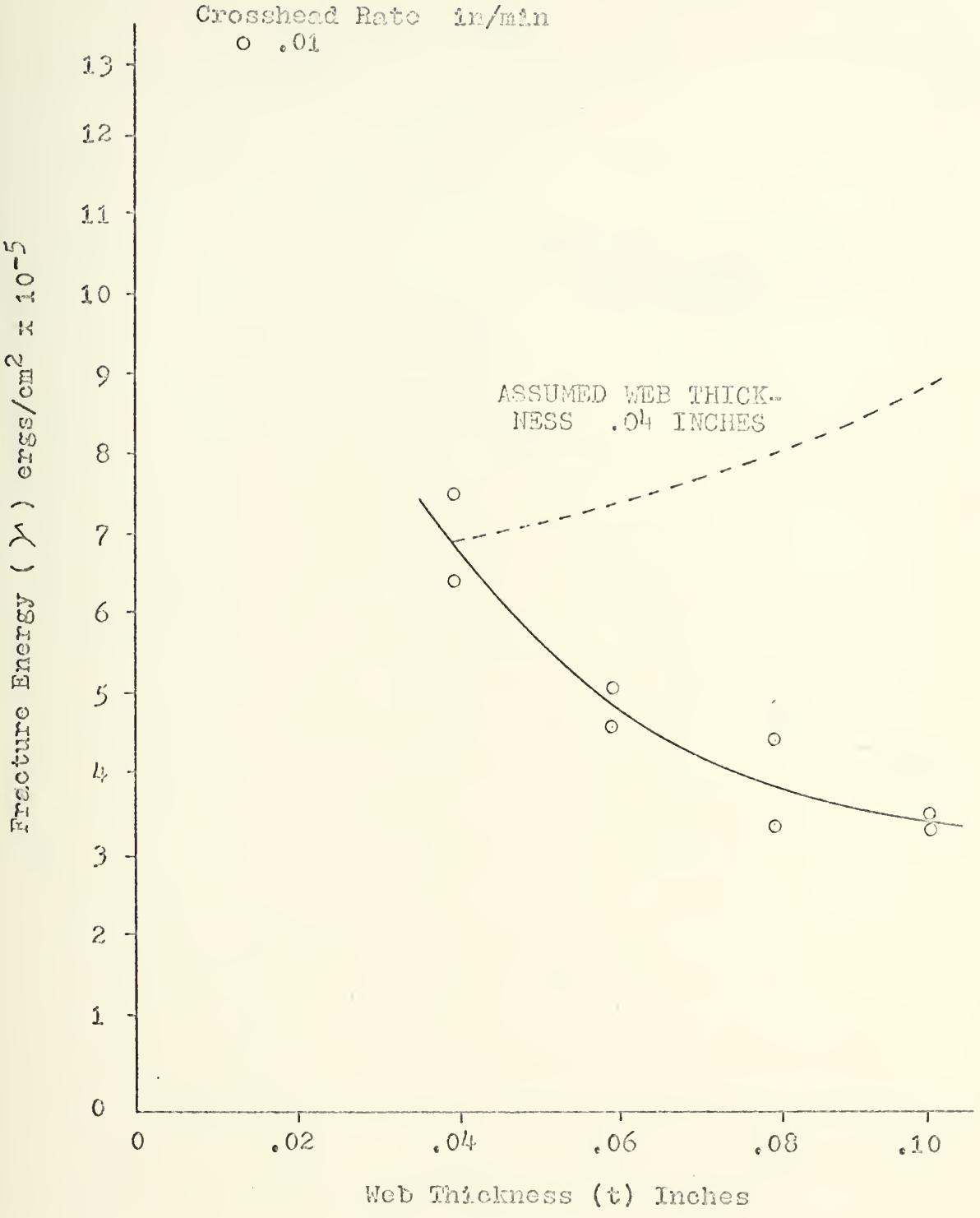

FIGURE 7 FRACTURE ENERGY vs WEB THICKNESS; LAMINAC 4173 POLYESTER RESIN WITH STYLE 181 CLOTH FIBERS AT 10 BUNDLES/INCH.

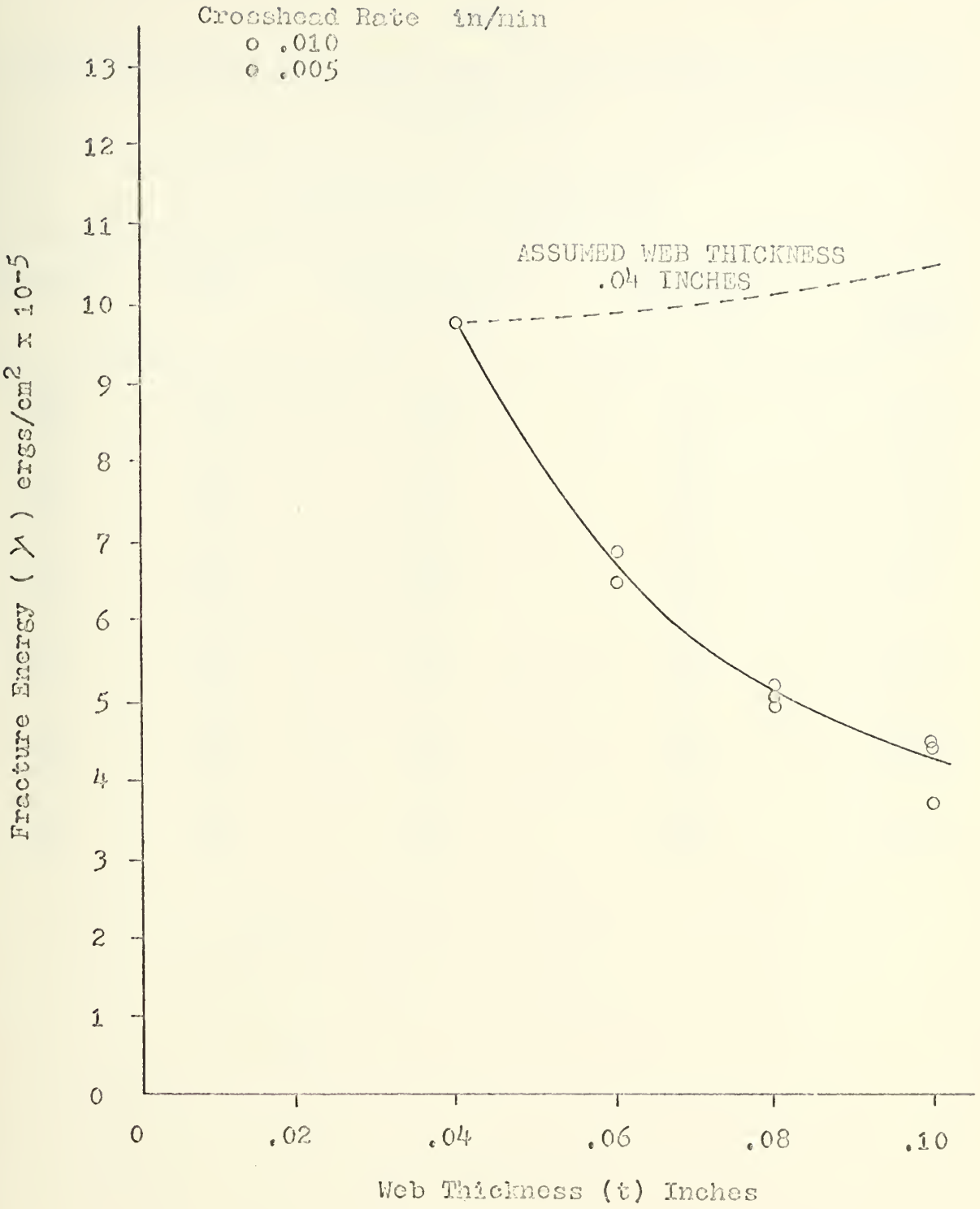

FIGURE 8 FRACTURE ENERGY vs WEB THICKNESS; 828 EPOXY RESIN WITH STYLE 181 CLOTH FIBERS AT 10 BUNDLES/INCH.

TABLE 3

BEAM HEIGHT EFFECT, FIBER REINFORCED RESIN WITH STYLE 181 CLOTH FIBERS

10 BUNDLES/INCH

LAMINAC 4173 POLYESTER RESIN

Specimen	Cast	Crosshead Rate Inches/Min	Beam Height (h) Inches	γ ergs/cm^2 x 10^{-5}
169	110	.005	.50	4.04
171	111	.005	.50	4.37
59	27	.01	.60	3.66
249	145	.01	.60	4.65
170	110	.005	.70	3.78
219	131	.01	.70	4.16
172	111	.005	.80	3.83
220	131	.01	.80	3.71
217	130	.01	.90	3.69
248	144	.01	.90	4.55
218	130	.01	1.00	3.51
250	145	.01	1.00	4.47

TABLE 4

BEAM HEIGHT EFFECT, FIBER REINFORCED RESIN WITH STYLE 181 CLOTH FIBERS

10 BUNDLES/INCH

EPON 828 EPOXY MATRIX

Specimen	Cast	Crosshead Rate Inches/Min	Beam Height (h) Inches	γ ergs/cm^2 x 10^{-5}
173	112	.005	.50	4.92
213	127	.01	.50	3.65
177	114	.01	.60	5.25
181	115	.005	.60	5.09
257	149	.01	.60	4.98
174	112	.005	.70	5.21
253	147	.01	.70	3.60
215	126	.01	.80	5.50
256	148	.01	.80	4.25
216	126	.01	.90	4.20
254	147	.01	.90	4.57
214	127	.01	1.00	3.70
252	146	.01	1.00	3.67

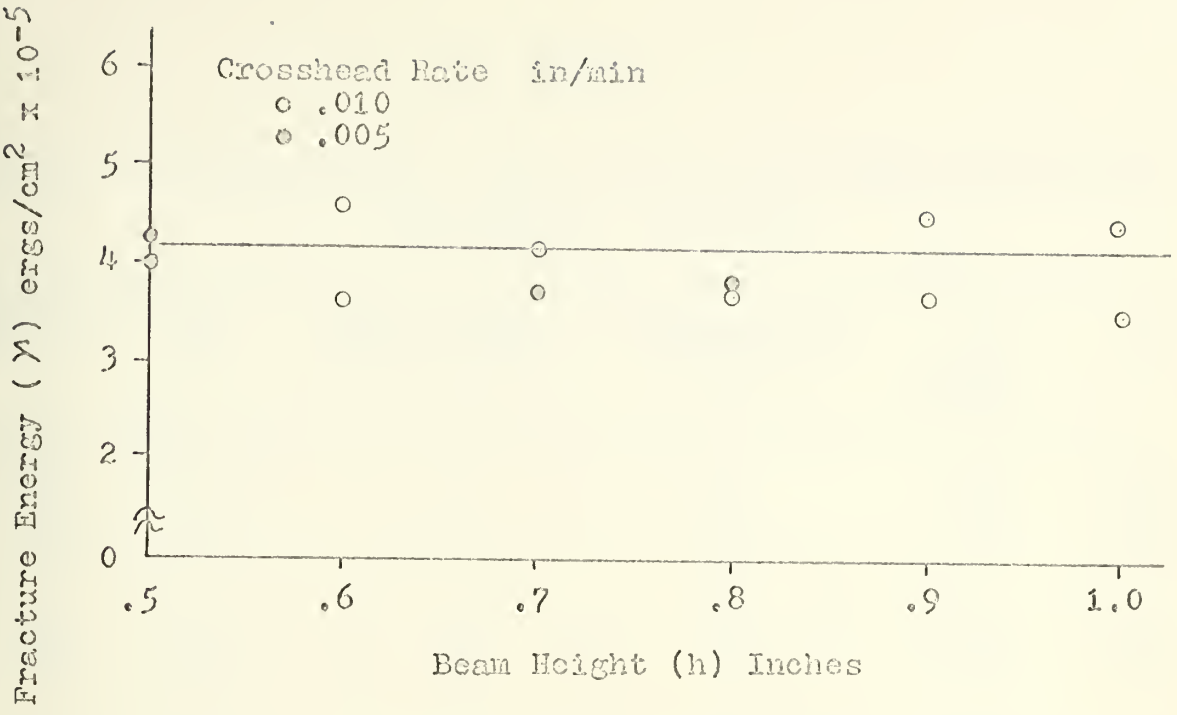

FIGURE 9 FRACTURE ENERGY vs BEAM HEIGHT; LAMINAC 4173 POLYESTER RESIN WITH STYLE 181 CLOTH FIBERS AT 10 BUNDLES/INCH.

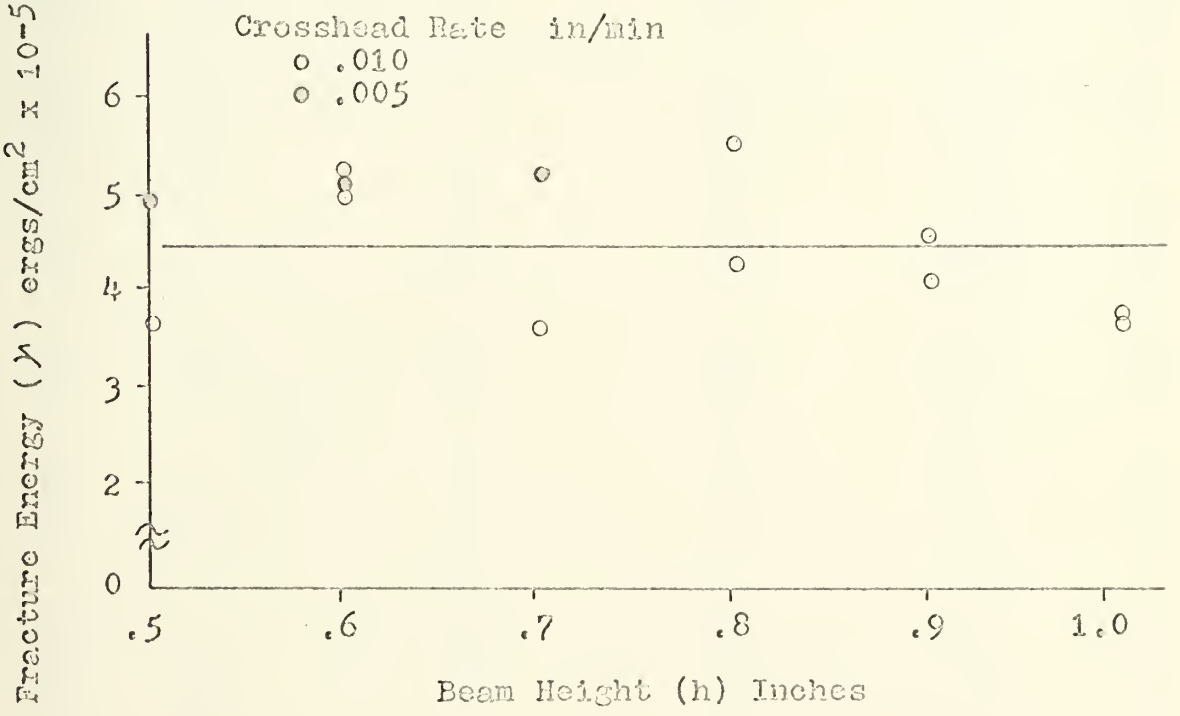

FIGURE 10 FRACTURE ENERGY vs BEAM HEIGHT; EPON 828 EPOXY RESIN WITH STYLE 181 CLOTH FIBERS AT 10 BUNDLES/INCH.

TABLE 5

LAMINAC 4173 POLYESTER RESIN - STYLE 181 CLOTH FIBER BUNDLE REINFORCEMENT

WEB THICKNESS .04 INCHES

Specimen	Cast	Fiber Density (n) Bundles/Inch	Crosshead Rate Inches/Min	γ ergs/cm^2 x 10^{-5}	$\frac{\gamma}{n}$
24	16	1	.01	1.48	1.48
25	16	1	.01	1.81	1.81
26	16	1	.01	1.27	1.27
27	18	2	.01	2.19	1.09
28	18	2	.01	2.33	1.17
29	18	2	.01	2.28	1.14
30	19	3	.01	2.74	.91
31	19	3	.01	2.89	.96
32	19	3	.01	3.10	1.03
124 a	30	3	.05	3.81	1.27
125 a	30	3	.05	3.28	1.09
33	20	4	.01	3.04	.76
34	20	4	.01	3.02	.75
35 A	20	4	.01	3.30	.82
6	8	5	.01	3.99	.80
7	8	5	.01	4.48	.90
8	8	5	.01	4.92	.98
36	21	6	.01	4.45	.74
37	21	6	.01	4.71	.79
38	21	6	.01	4.63	.77
39	22	8	.01	6.15	.77
40	22	8	.005	5.76	.72
41	22	8	.01	5.71	.71
11	9	10	.01	7.79	.78
12	9	10	.01	7.11	.71
57	27	10	.01	6.67	.67
58	27	10	.01	7.26	.73
59	27	10	.01	7.32	.73

TABLE 5 (Continued)

Specimen	Cast	Fiber Density (n) Bundles/Inch	Crosshead Rate Inches/Min	γ ergs/cm^2 x 10^{-5}	$\frac{\gamma}{n}$
42	23	12	.01	8.90	.74
43	23	12	.01	9.59	.80
44	23	12	.005	8.49	.71
45	24	14	.01	8.00	.57
46	24	14	.01	9.20	.66
47	24	14	.002	7.88	.56
49	25	16	.005	10.69	.67
50	25	16	.005	10.43	.65
51	26	18	.005	9.42	.52
52	26	18	.005	10.25	.57
53	26	18	.005	10.74	.60
14	10	20	.01	12.00	.60
14 A	10	20	.005	14.25	.71
15 A	10	20	.05	17.20	.86
54 A	28	30	.005	17.85	.60
55	28	30	.002	14.23	.47
56 A	28	30	.005	16.72	.56
19 A	13	40	.01	27.60	.69
20 A	13	40	.005	19.40	.49
63 A	29	50	.002	30.70	.61
22 A	14	60	.005	55.60	.93

a - No post cure.

A - Specimens modified with aluminum strips.

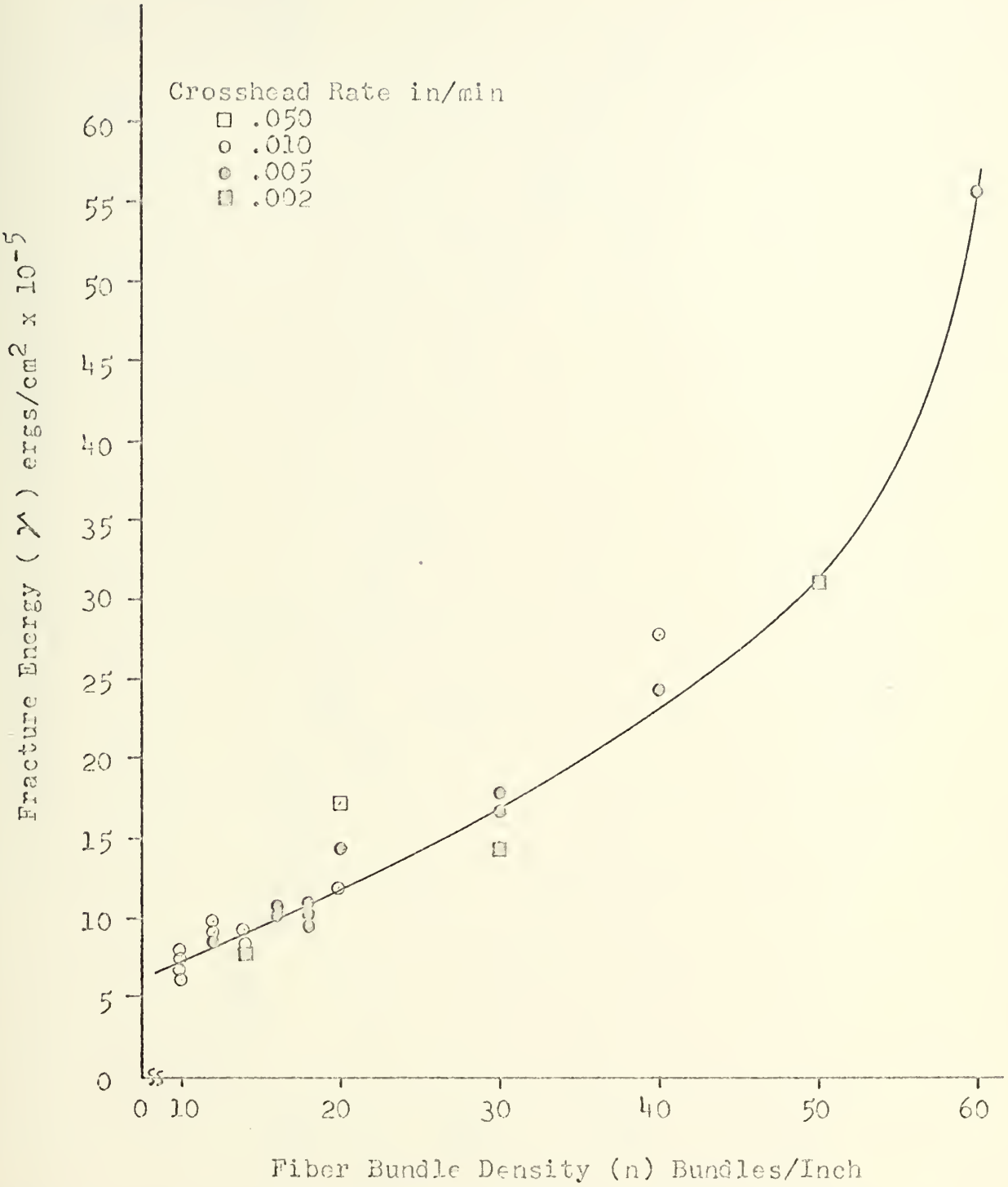

FIGURE 11 FRACTURE ENERGY vs FIBER DENSITY, LAMINAC 4173 POLYESTER RESIN - STYLE 181 CLOTH FIBER BUNDLE REINFORCEMENT, WEB THICKNESS .04 INCHES.

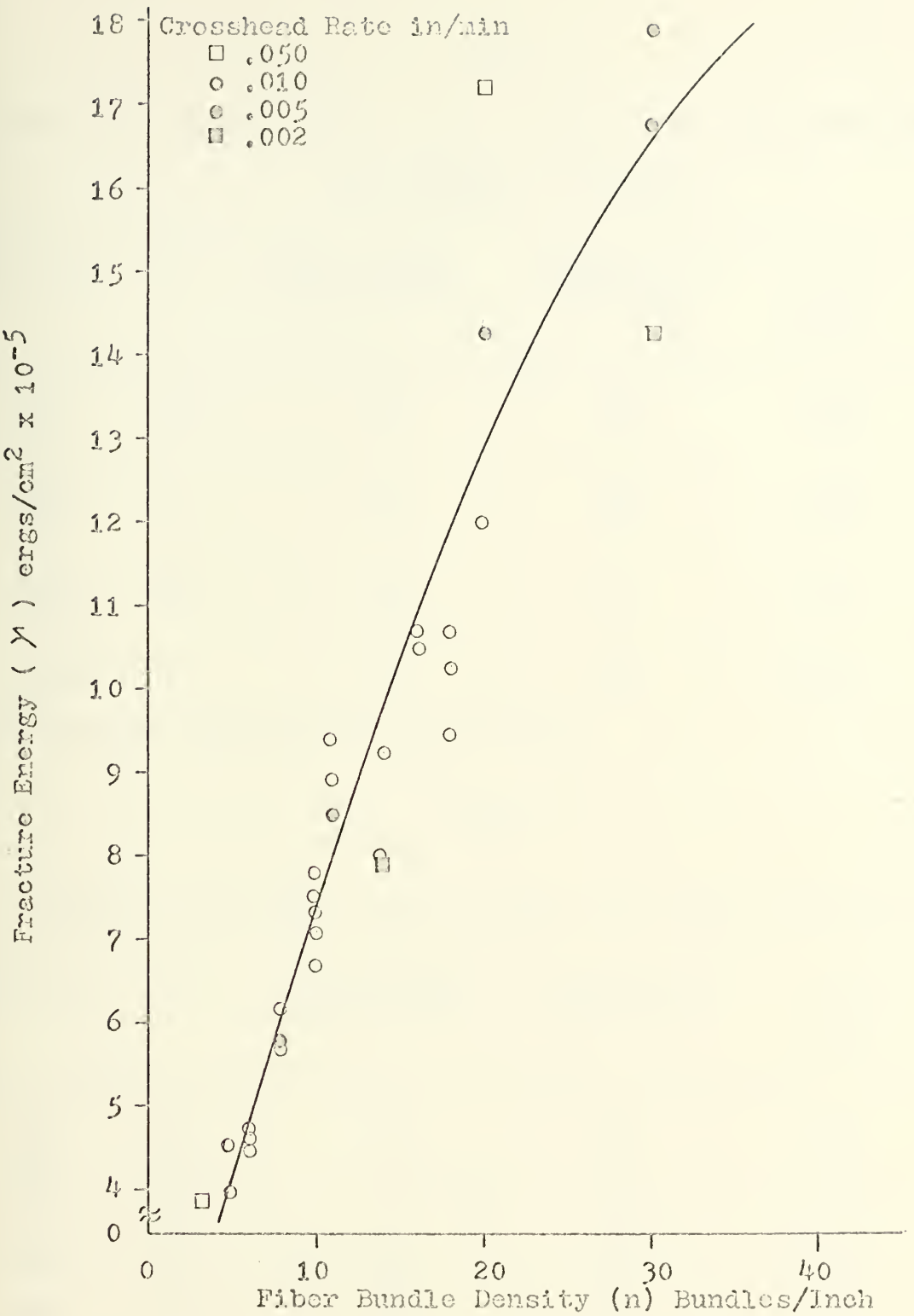

FIGURE 11A FRACTURE ENERGY vs FIBER DENSITY, LAMINAC 4173 POLYESTER RESIN - STYLE 181 CLOTH FIBER REINFORCEMENT, WEB THICKNESS .04 INCHES.

TABLE 6

LAMINAC 4173 POLYESTER RESIN, STYLE 181 CLOTH FIBER BUNDLE REINFORCEMENT

WEB THICKNESS .08 INCHES

Specimen	Cast	Fiber Density (n) Bundles/Inch	Crosshead Rate Inches/Min	γ ergs/cm^2 x 10^{-5}	$\frac{\gamma}{n}$
59	27	10	.01	3.66	.366
249	145	10	.01	4.65	.465
276	----	20	.005	5.03	.251
277 A	----	20	.01	6.20	.311
207	132	30	.01	8.10	.270
209 A	132	30	.01	8.90	.297
278 A	----	40	.005	12.18	.304
279 A	----	40	.01	13.82	.346

A - Specimens modified with aluminum strips.

TABLE 7

EPON 828 EPOXY RESIN, STYLE 181 CLOTH FIBER BUNDLE REINFORCEMENT

Specimen	Cast	Fiber Density (n) Bundles/Inch	Crosshead Rate Inches/Min	γ ergs/cm^2 x 10^{-5}	$\frac{\gamma}{n}$
177	114	10	.01	5.25	.525
181	115	10	.005	5.09	.509
256	149	10	.01	4.98	.498
154	104	20	.005	7.17	.358
155	104	20	.01	7.20	.360
186	118	30	.01	9.47	.316
187	118	30	.005	9.55	.318
190	120	40	.01	10.65	.266
191	120	40	.005	10.72	.268

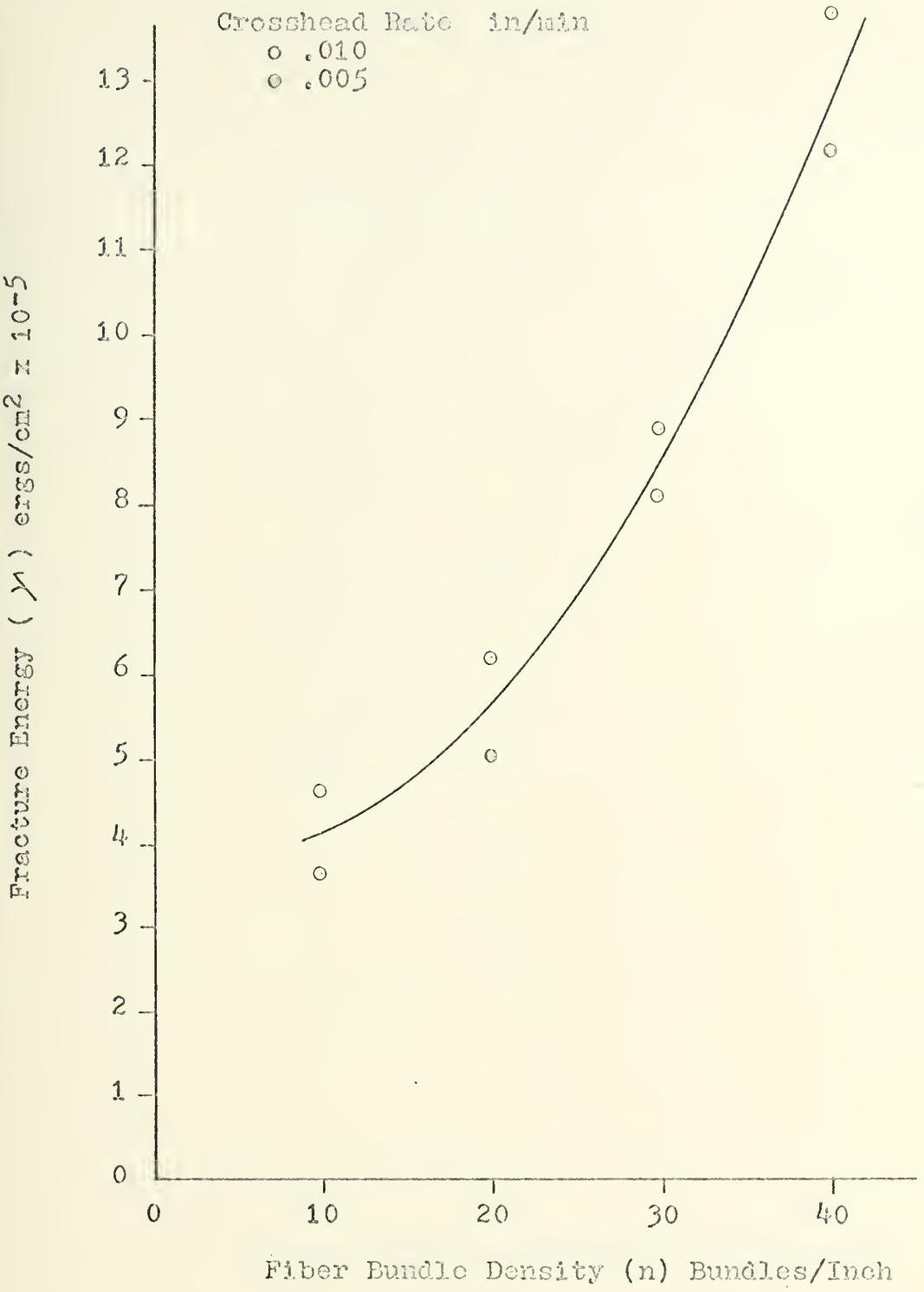

FIGURE 12 FRACTURE ENERGY vs FIBER DENSITY, LAMINAC 4173 POLYESTER RESIN - STYLE 181 CLOTH FIBER REINFORCEMENT, WEB THICKNESS .08 INCHES.

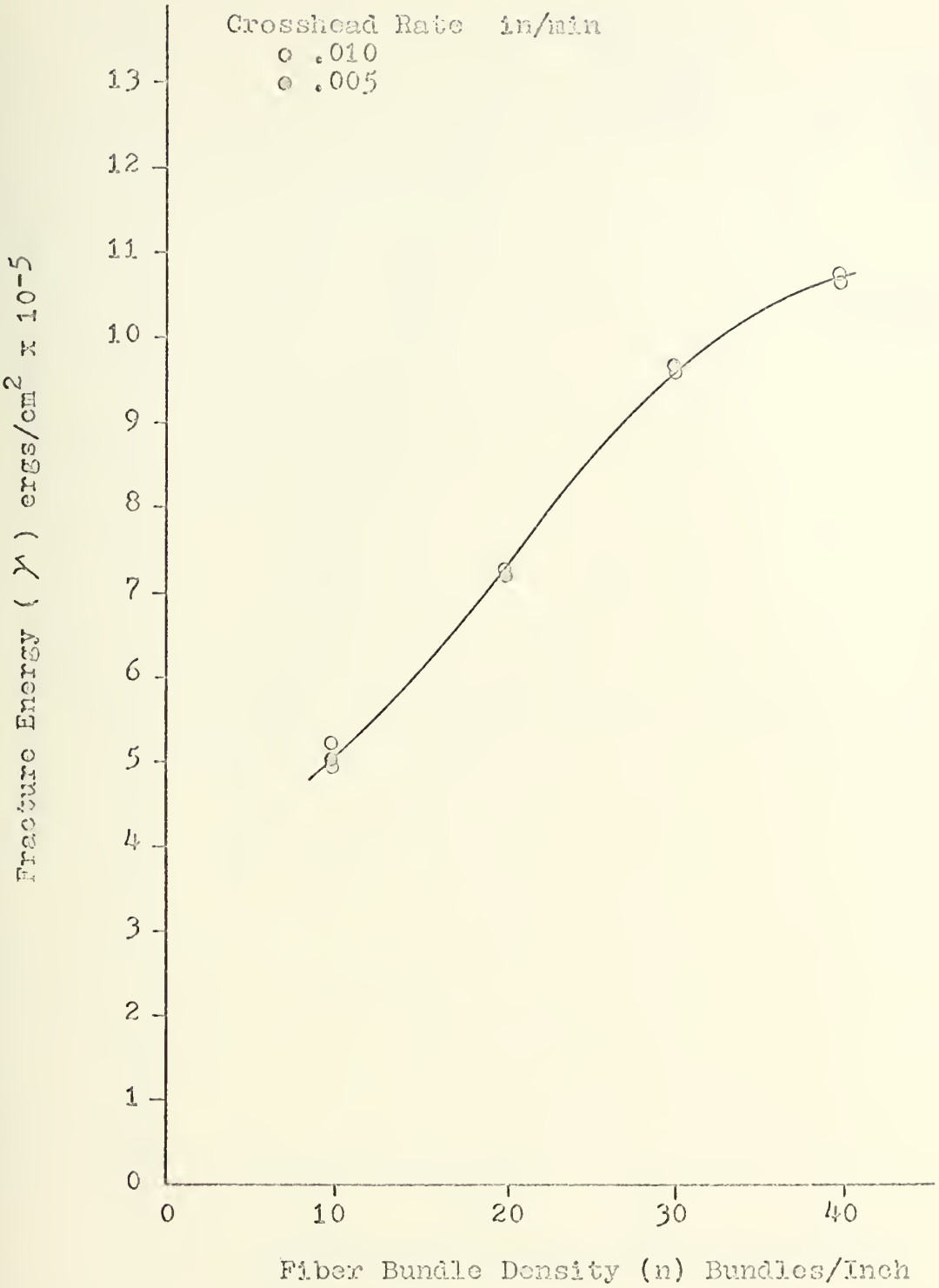

FIGURE 13 FRACTURE ENERGY vs FIBER DENSITY, EPON 828 EPOXY RESIN - STYLE 181 CLOTH FIBER BUNDLE REINFORCEMENT.

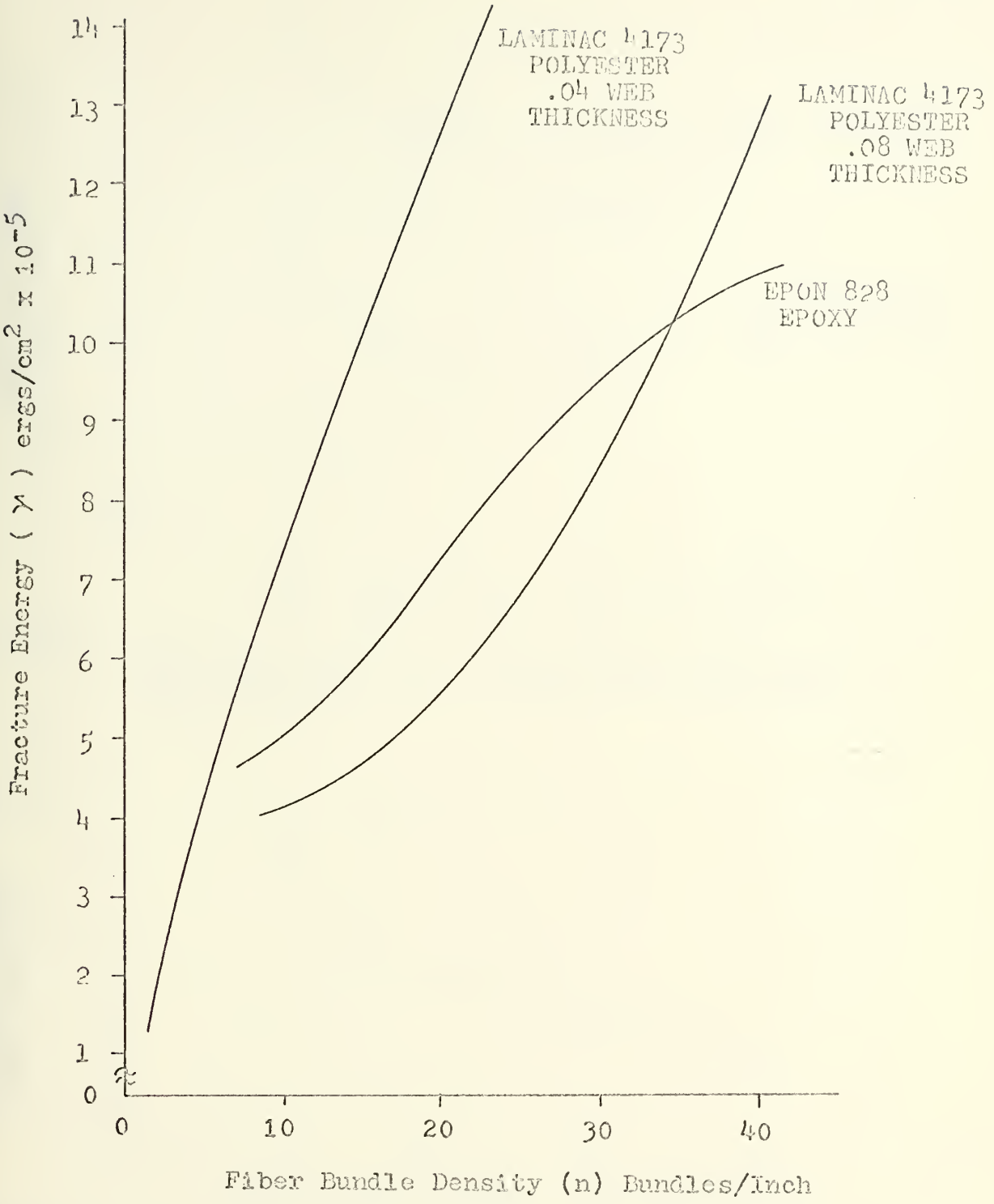

FIGURE 14 COMPARISON OF FRACTURE ENERGY vs FIBER DENSITY FOR STYLE 181 CLOTH FIBERS IN EPON 828 AND LAMINAC 4173 RESIN MATRIX MATERIALS.

FIGURE 15 FIBER CONTRIBUTION TO THE FRACTURE ENERGY; LAMINAC 4173 POLYESTER RESIN - STYLE 181 CLOTH FIBER REINFORCEMENT.

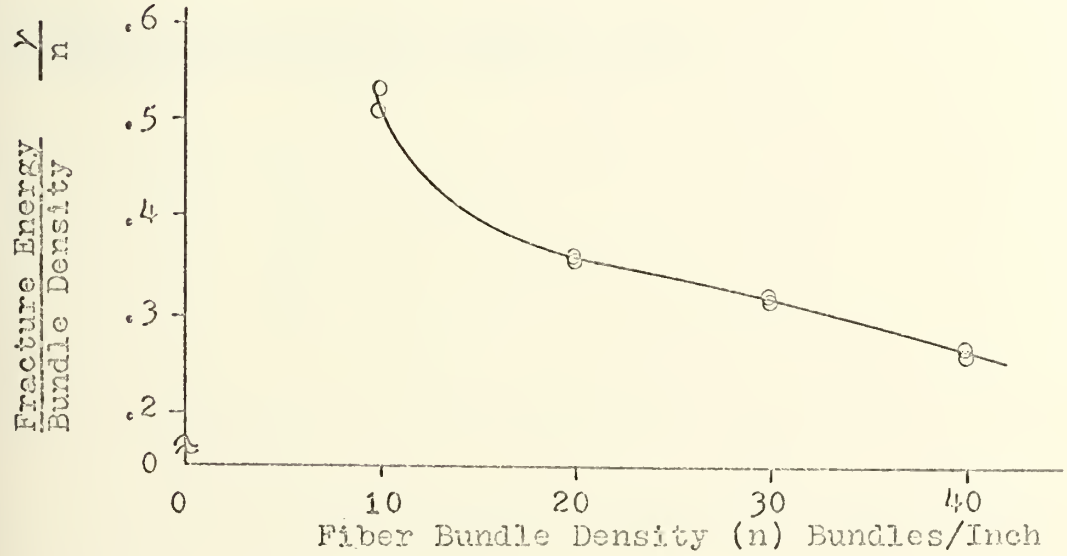

FIGURE 16 FIBER CONTRIBUTION TO THE FRACTURE ENERGY; EPON 828 EPOXY RESIN - STYLE 181 CLOTH FIBER REINFORCEMENT.

TABLE 8

LAMINAC 4173 POLYESTER RESIN, E-GLASS FLAT FIBER BUNDLE REINFORCEMENT

Specimen	Cast	Fiber Density (n) Bundles/Inch	Crosshead Rate Inches/Min	γ ergs/cm^2 x 10^{-5}	$\frac{\gamma}{n}$
162	107	5	.01	2.18	.435
163	107	5	.005	2.29	.458
131	---	10	.01	7.39	.739
132	---	10	.01	6.85	.685
157	105	10	.005	4.21	.421
210	133	10	.01	4.92	.492
211	133	10	.01	4.97	.497
212	133	10	.01	6.00	.600
150 A	102	20	.005	7.50	.375
151 A	102	20	.005	8.70	.435
225 A	136	20	.01	9.10	.455
226 A	136	20	.01	9.70	.485
224 A	135	30	.01	11.25	.375

A - Specimens modified with aluminum strips.

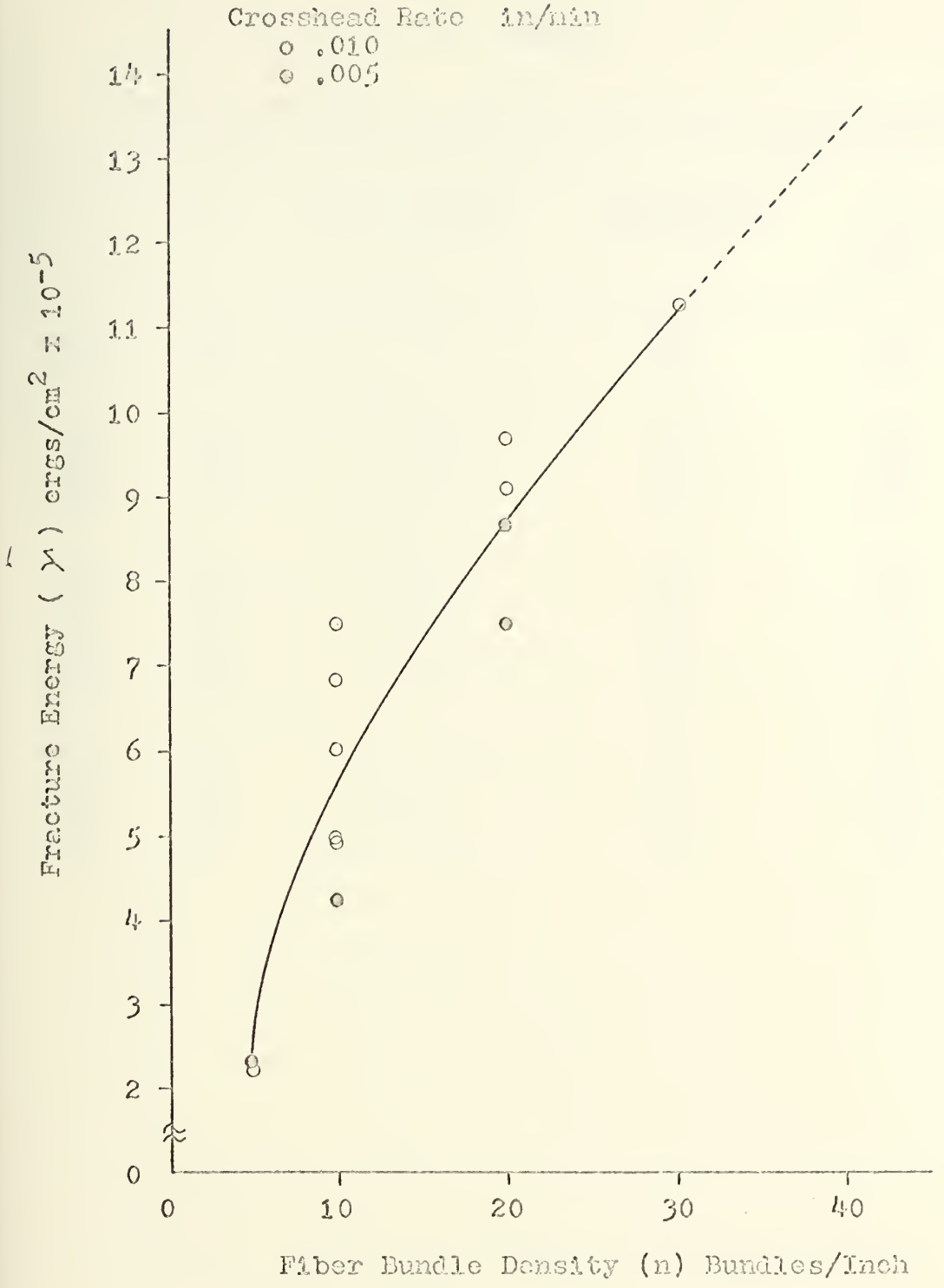

FIGURE 17 FRACTURE ENERGY vs FIBER DENSITY, LAMINAC 4173 POLYESTER RESIN - E-GLASS FLAT FIBER REINFORCEMENT.

TABLE 9

EPON 828 EPOXY RESIN, E-GLASS FLAT FIBER BUNDLE REINFORCEMENT

Specimen	Cast	Fiber Density (n) Bundles/Inch	Crosshead Rate Inches/Min	γ ergs/cm^2 x 10^{-5}	$\frac{\gamma}{n}$
165	108	5	.01	2.60	.520
166	108	5	.005	3.02	.603
160	106	10	.005	3.31	.331
161	106	10	.01	4.05	.405
167	109	10	.005	4.18	.418
168	109	10	.01	3.85	.385
146	100	20	.01	5.00	.250
147	100	20	.01	3.87	.193
148	101	20	.01	6.27	.314
149	101	20	.005	6.12	.306
203	128	20	.01	4.55	.228
204	128	20	.01	5.40	.270
192	121	30	.01	7.42	.248
193	121	30	.005	6.60	.220
205	129	30	.01	7.40	.246
206	129	30	.01	7.55	.252

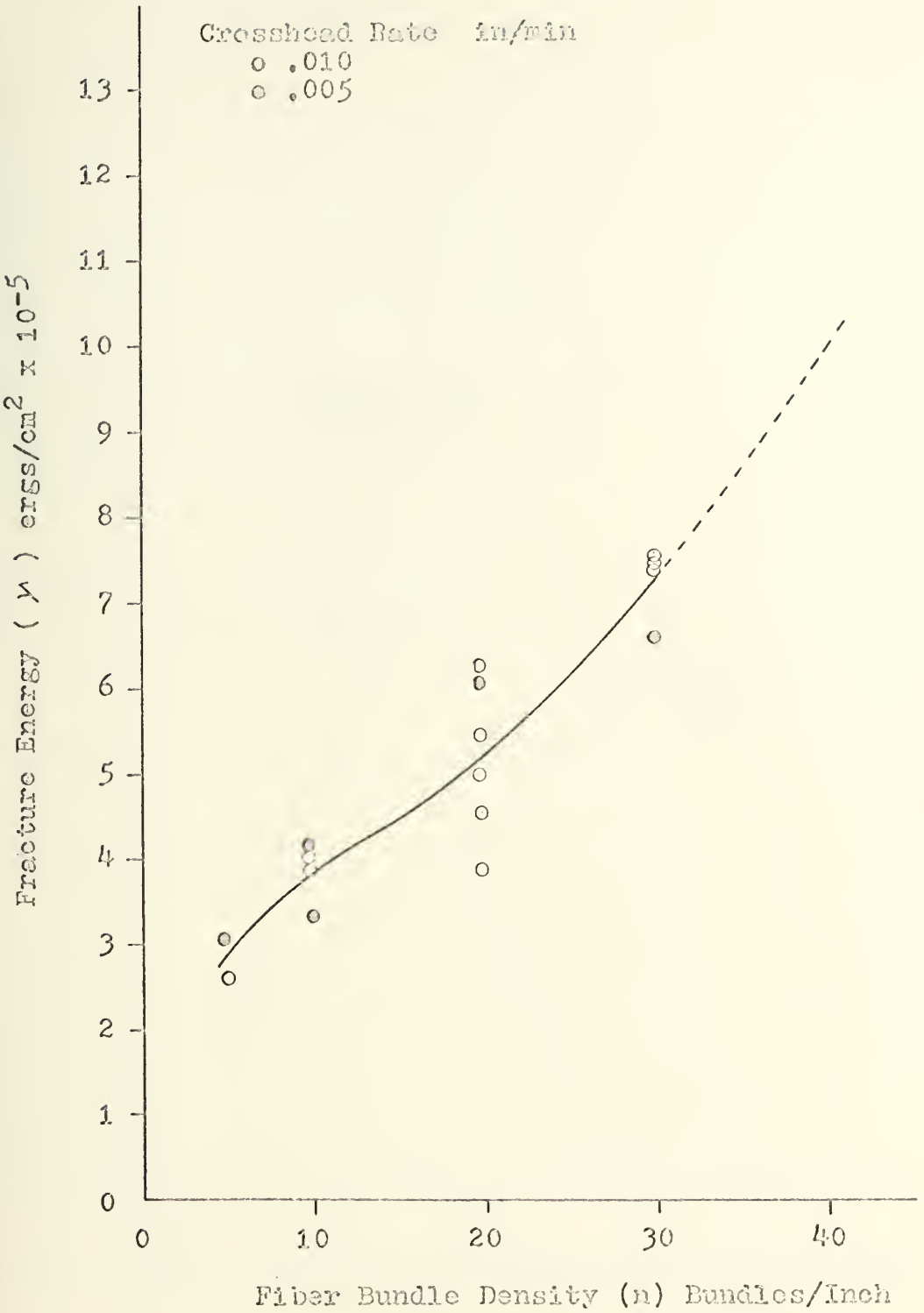

FIGURE 18 FRACTURE ENERGY vs FIBER DENSITY, EPON 828 EPOXY RESIN - E-GLASS FLAT FIBER BUNDLE REINFORCEMENT.

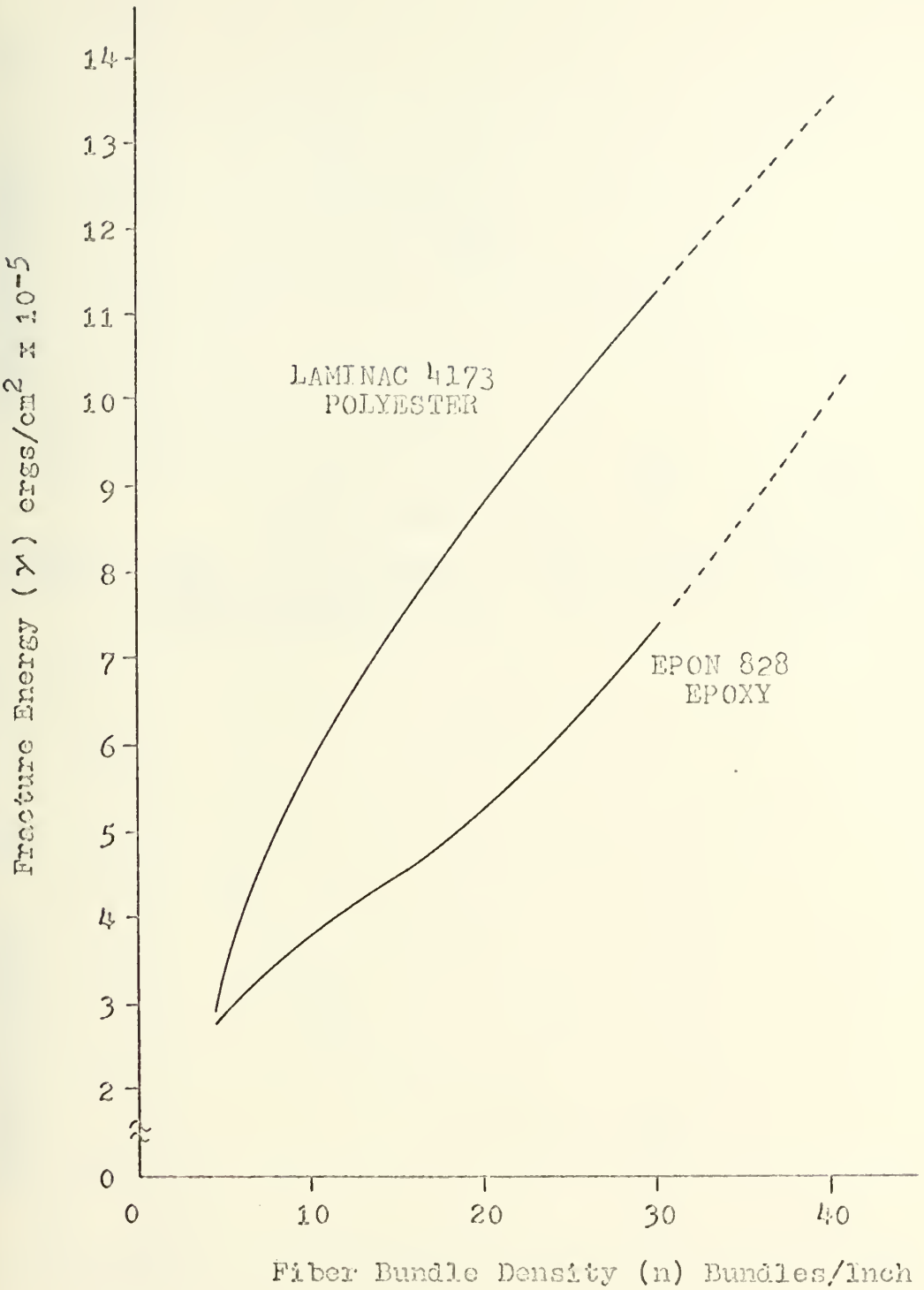

FIGURE 19 COMPARISON OF FRACTURE ENERGY vs FIBER DENSITY FOR FLAT E-GLASS FIBERS IN EPON 828 AND LAMINAC 4173 RESIN MATRIX MATERIALS.

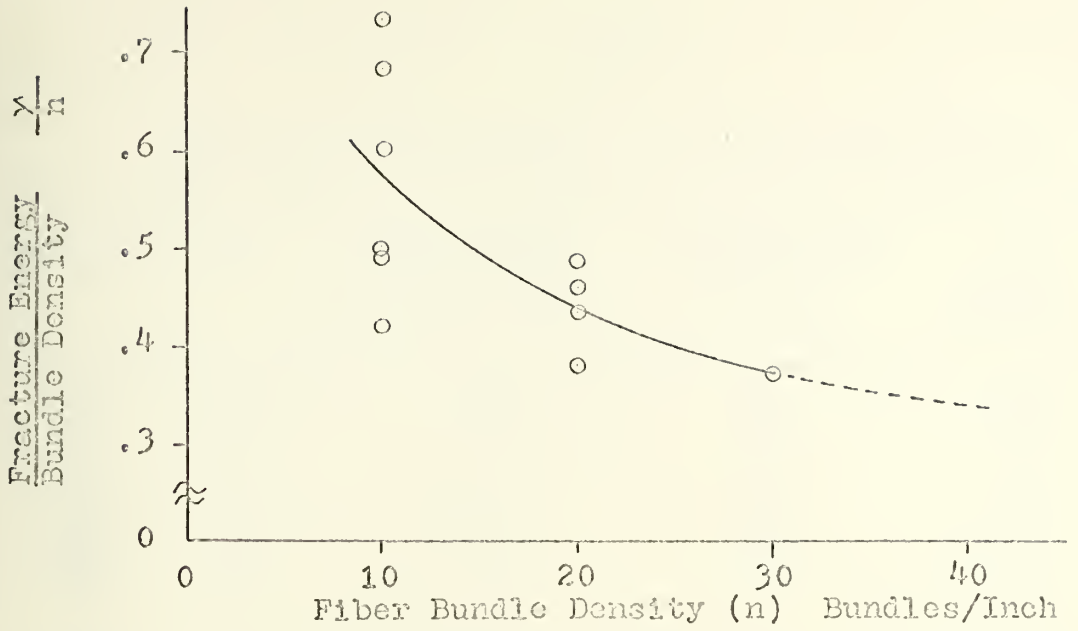

FIGURE 20 FIBER CONTRIBUTION TO THE FRACTURE ENERGY; LAMINAC 4173 POLYESTER RESIN - E-GLASS FLAT FIBER REINFORCEMENT.

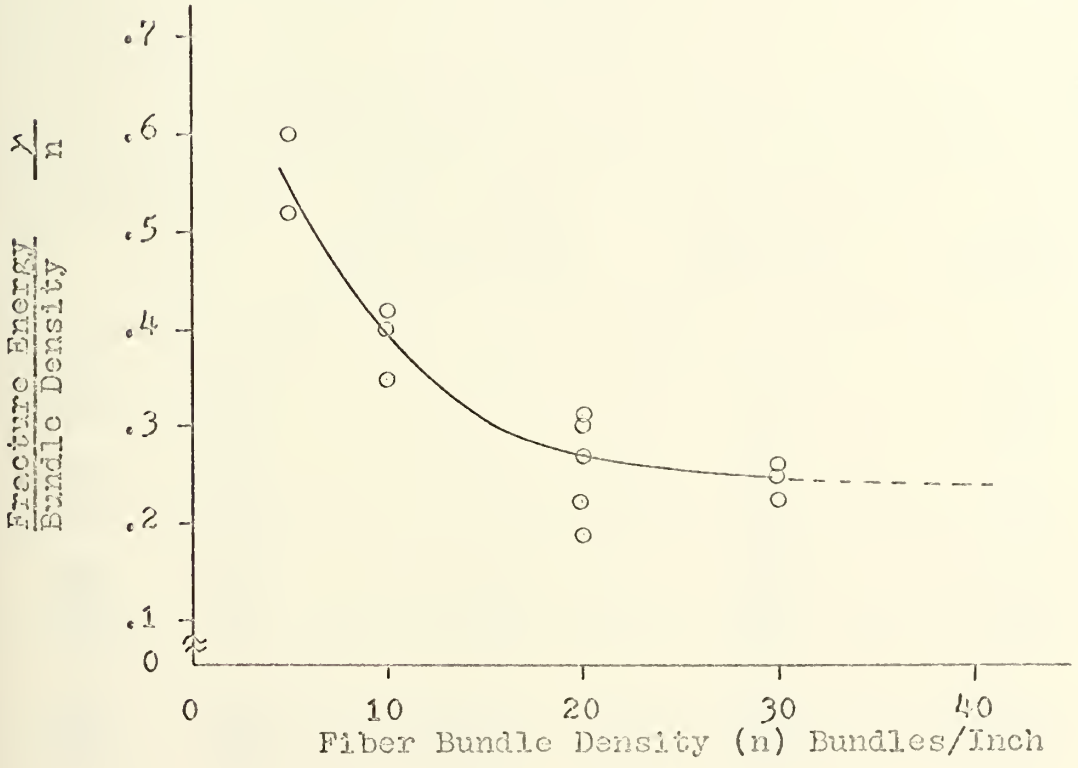

FIGURE 21 FIBER CONTRIBUTION TO THE FRACTURE ENERGY; EPON 828 EPOXY RESIN - E-GLASS FLAT FIBER REINFORCEMENT.

TABLE 10

LAMINAC 4173 POLYESTER RESIN - BETA GLASS FIBER BUNDLES

Specimen	Cast	Fiber Density (n) Bundles/Inch	Crosshead Rate Inches/Min	γ ergs/cm^2 x 10^{-5}	$\frac{\gamma}{n}$
227	137	10	.01	2.90	.290
228	137	10	.01	4.15	.415
229 A	138	20	.01	5.40	.270
230	138	20	.005	5.47	.274
230 A	138	20	.01	5.75	.288
239 A	140	30	.01	10.05	.336
240 A	140	30	.01	9.55	.318

TABLE 11

EPON 828 EPOXY RESIN - BETA GLASS FIBER BUNDLES

Specimen	Cast	Fiber Density (n) Bundles/Inch	Crosshead Rate Inches/Min	γ ergs/cm^2 x 10^{-5}	$\frac{\gamma}{n}$
241	141	10	.01	3.30	.330
242	141	10	.01	3.42	.342
243	142	20	.01	6.25	.312
244	142	20	.01	5.20	.260
268	157	30	.005	8.37	.280
269	157	30	.01	7.50	.250
269 A	157	30	.01	10.40	.347
266	154	40	.01	11.97	.299
267	154	40	.005	11.82	.296
267 A	154	40	.01	9.85	.246

A - Specimens modified with aluminum strips.

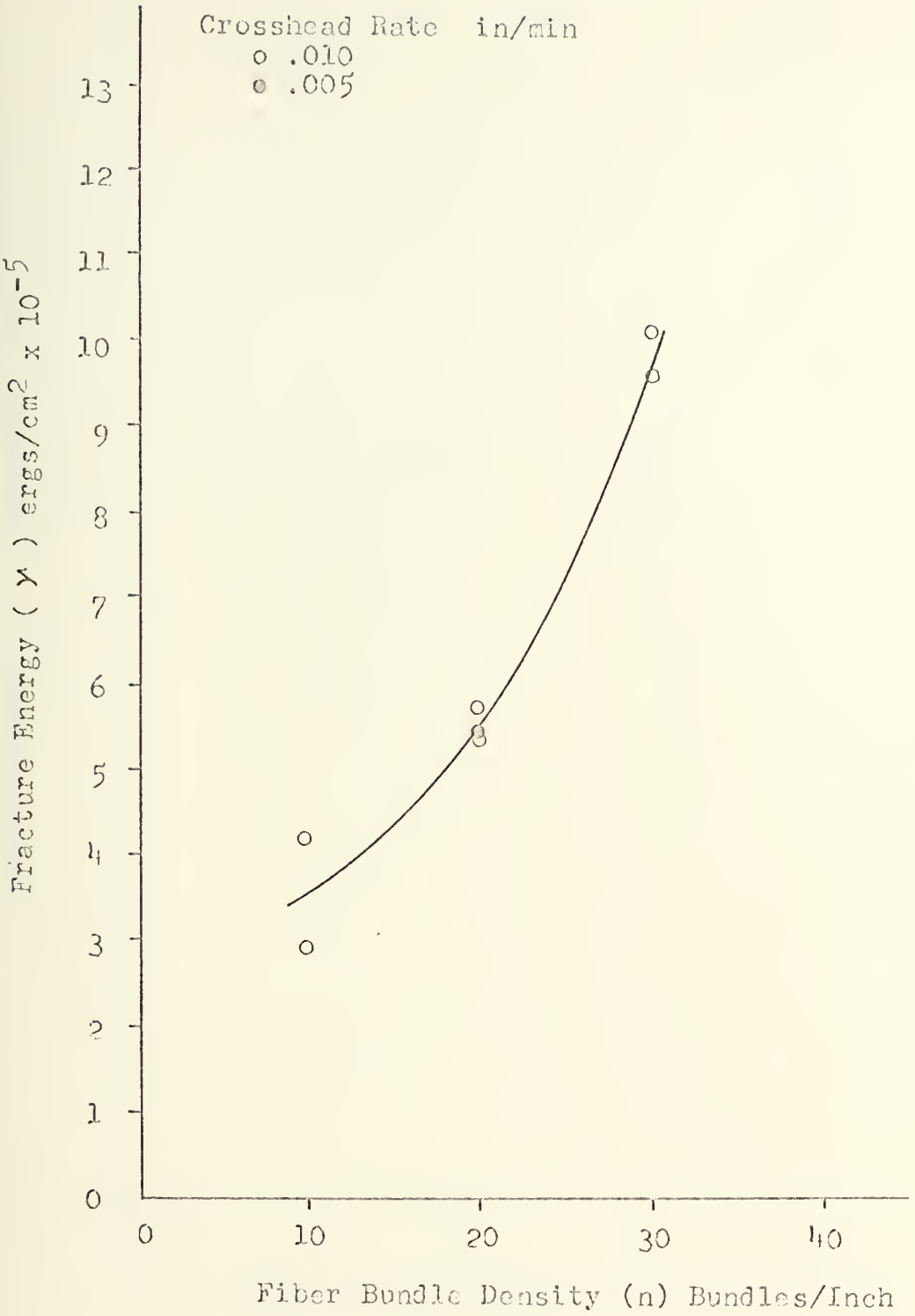

FIGURE 22 FRACTURE ENERGY vs FIBER DENSITY, LAMINAC 4173 POLYESTER RESIN - BETA GLASS FIBER BUNDLES.

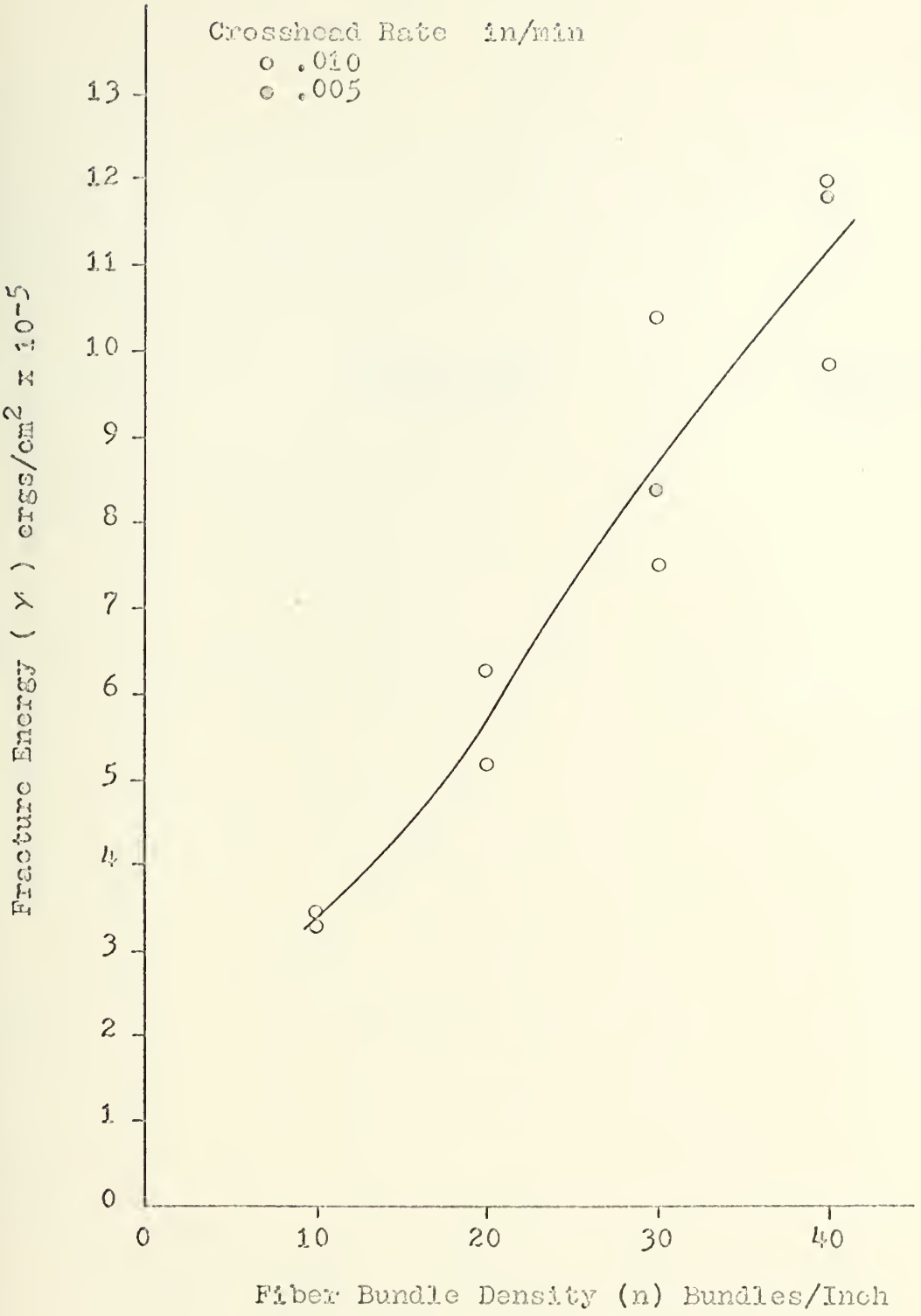

FIGURE 23 FRACTURE ENERGY vs FIBER DENSITY, EPON 828 EPOXY RESIN - BETA GLASS FIBER BUNDLES.

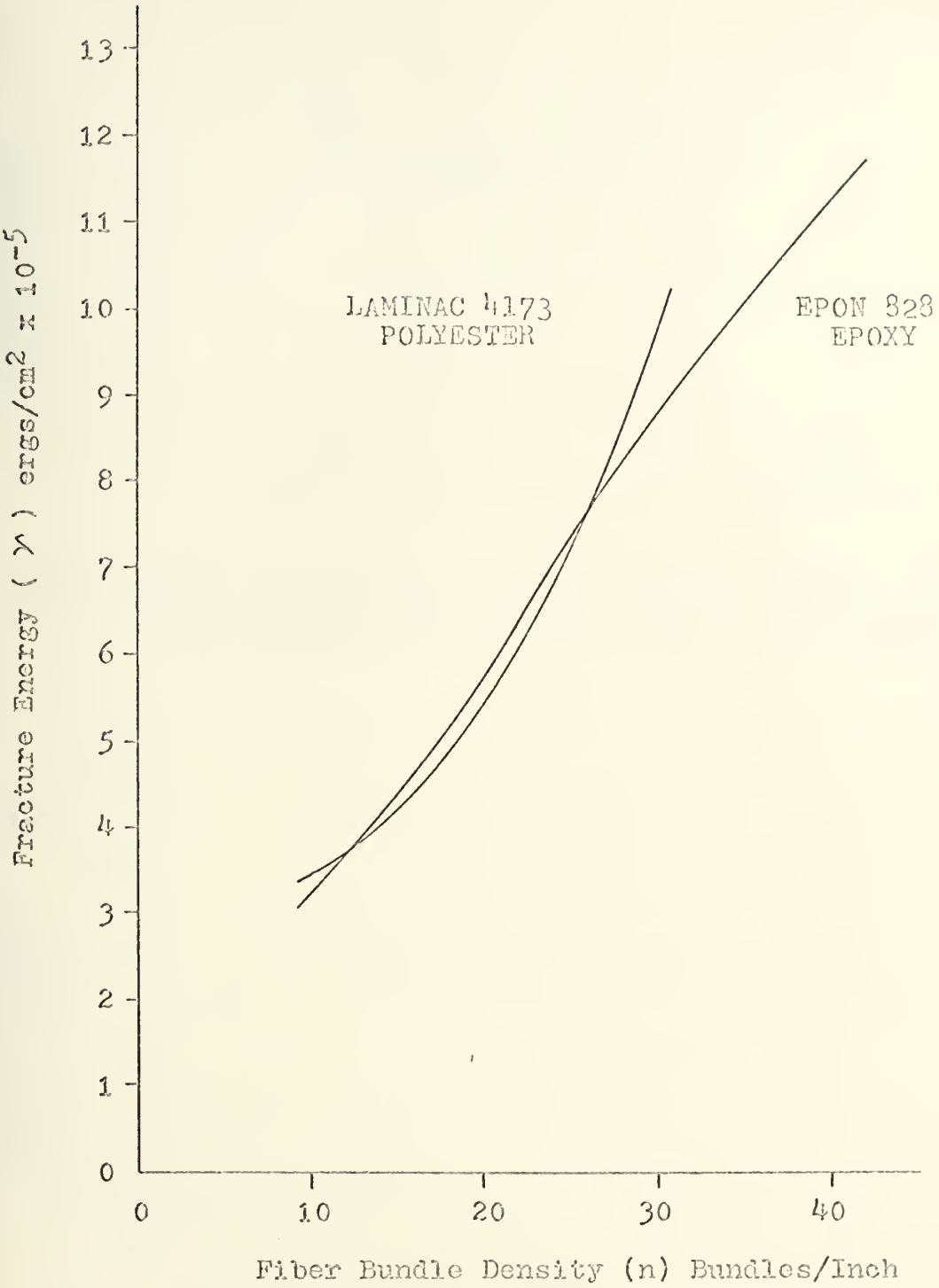

FIGURE 24 COMPARISON OF FRACTURE ENERGY vs FIBER DENSITY FOR BETA GLASS FIBERS IN EPON 828 AND LAMINAC 4173 RESIN MATRIX MATERIALS.

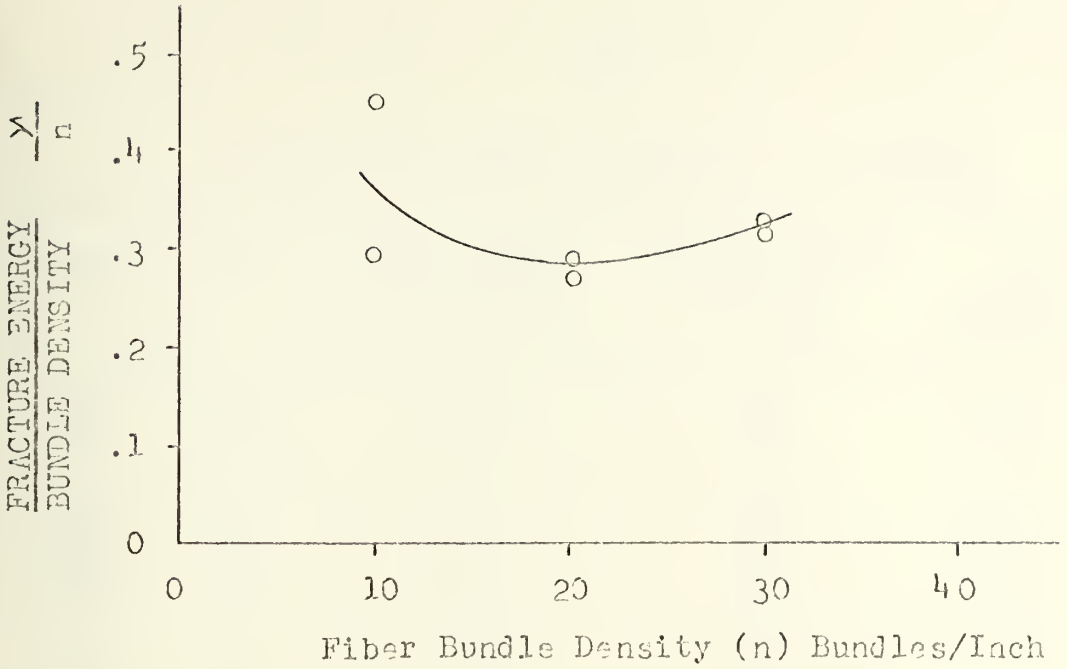

FIGURE 25 FIBER CONTRIBUTION TO THE FRACTURE ENERGY; LAMINAC 4173 POLYESTER RESIN - BETA GLASS FIBER BUNDLES.

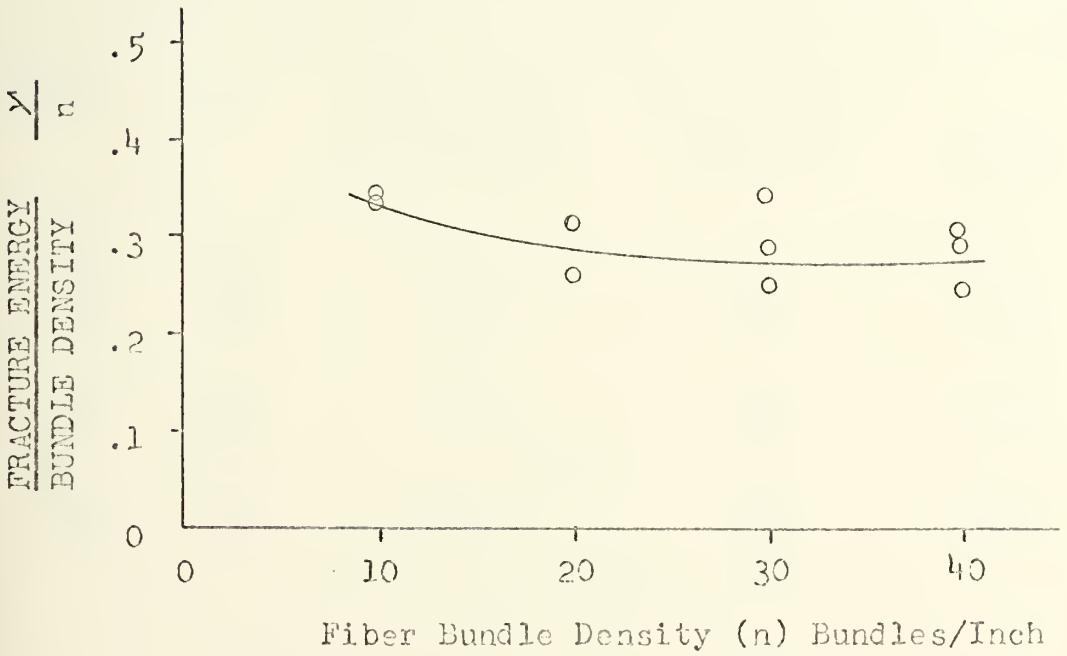

FIGURE 26 FIBER CONTRIBUTION TO THE FRACTURE ENERGY; EPON 828 EPOXY RESIN - BETA GLASS FIBER BUNDLES.

TABLE 12

EPON 828 EPOXY RESIN - THORNEL 50 FIBER BUNDLES

Specimen	Cast	Fiber Density (n) Bundles/Inch	Crosshead Rate Inches/Min	γ ergs/cm^2 x 10^{-5}	$\frac{\gamma}{n}$
196	123	10	.01	8.1	.810
197	123	10	.005	7.7	.770
198	124	20	.01	12.8	.640
199	124	20	.005	----	----
260	150	20	.01	12.8	.640
261 A	150	20	.005	12.5	.625
262	151	30	.005	15.55	.518
263 A	151	30	.005	16.50	.550

TABLE 13

EPON 828 EPOXY RESIN - MONSANTO TYPE I SYNTHETIC FIBER BUNDLES

Specimen	Cast	Fiber Density (n) Bundles/Inch	Crosshead Rate Inches/Min	γ ergs/cm^2 x 10^{-5}	$\frac{\gamma}{n}$
274	160	10	.01	6.05	.605
274	160	10	.01	6.32	.632
275 A	160	10	.01	4.67	.467
272 A	159	20	.01	10.45	.522
273	159	20	.01	13.40	.670
270	158	30	.01	12.92	.431
271 A	158	30	.01	14.20	.474

A - Specimens modified with aluminum strips.

FIGURE 27 FRACTURE ENERGY vs FIBER DENSITY, EPON 828 EPOXY RESIN - THORNEL 50 FIBER BUNDLES.

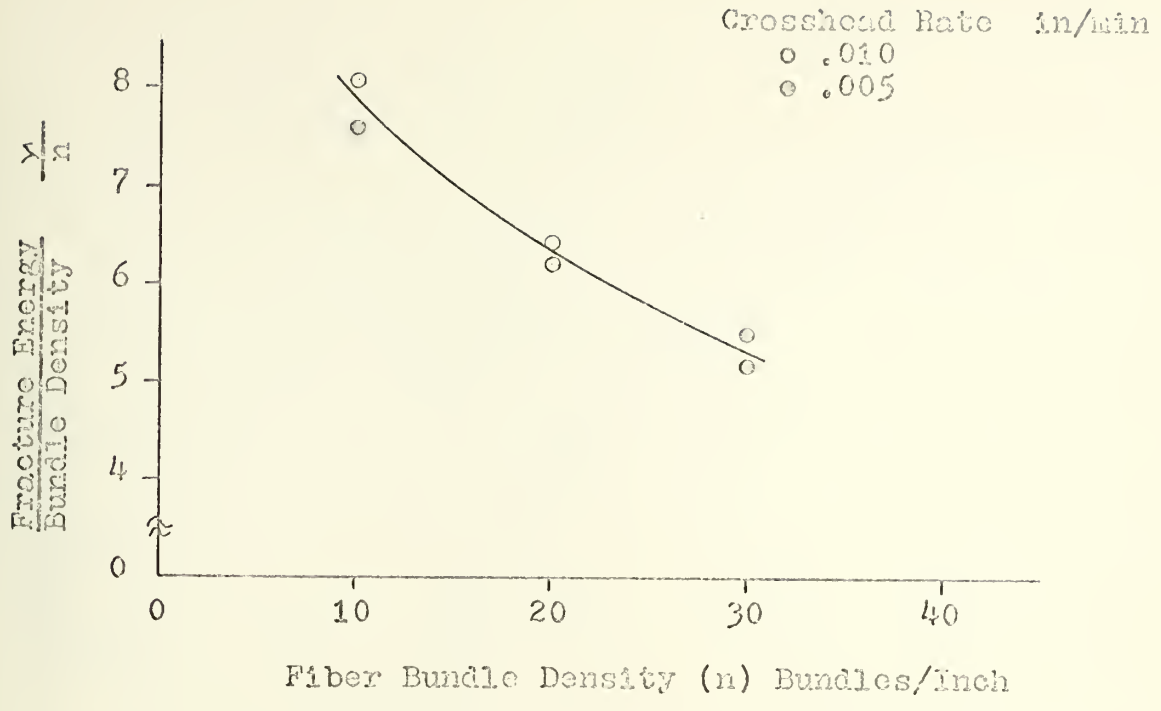

FIGURE 28 FIBER CONTRIBUTION TO THE FRACTURE ENERGY; EPON 828 EPOXY RESIN - THORNEL 50 FIBER BUNDLES.

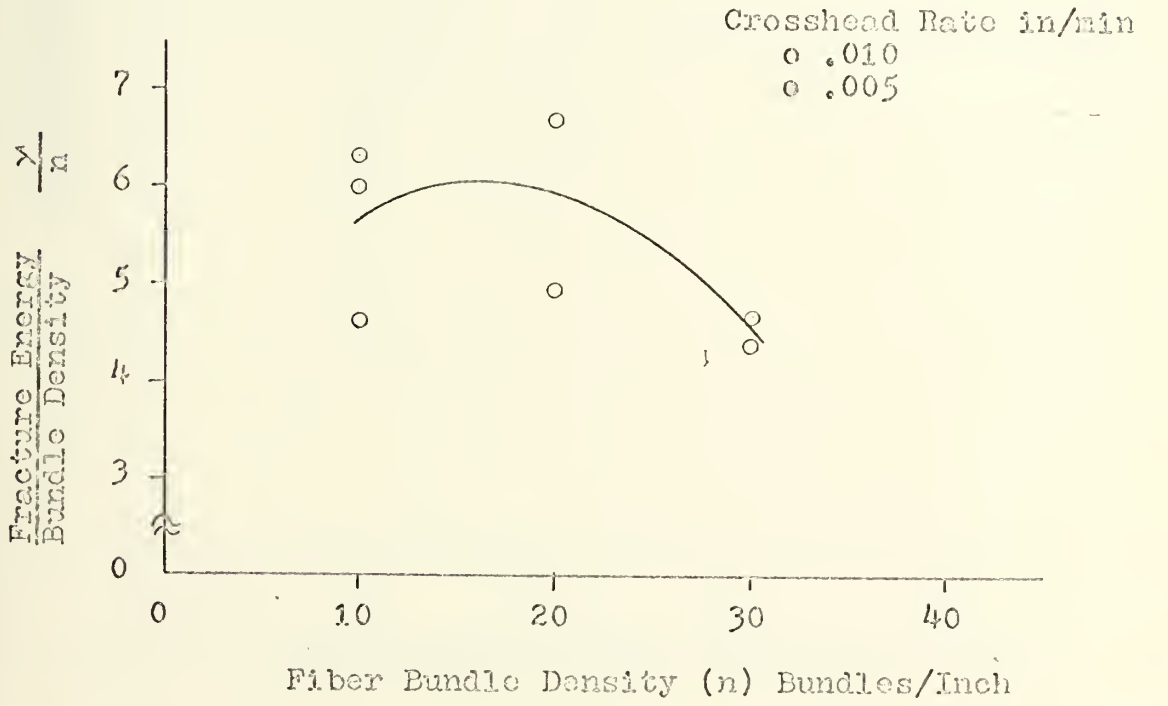

FIGURE 29 FIBER CONTRIBUTION TO THE FRACTURE ENERGY; EPON 828 EPOXY RESIN - MONSANTO TYPE A SYNTHETIC FIBERS.

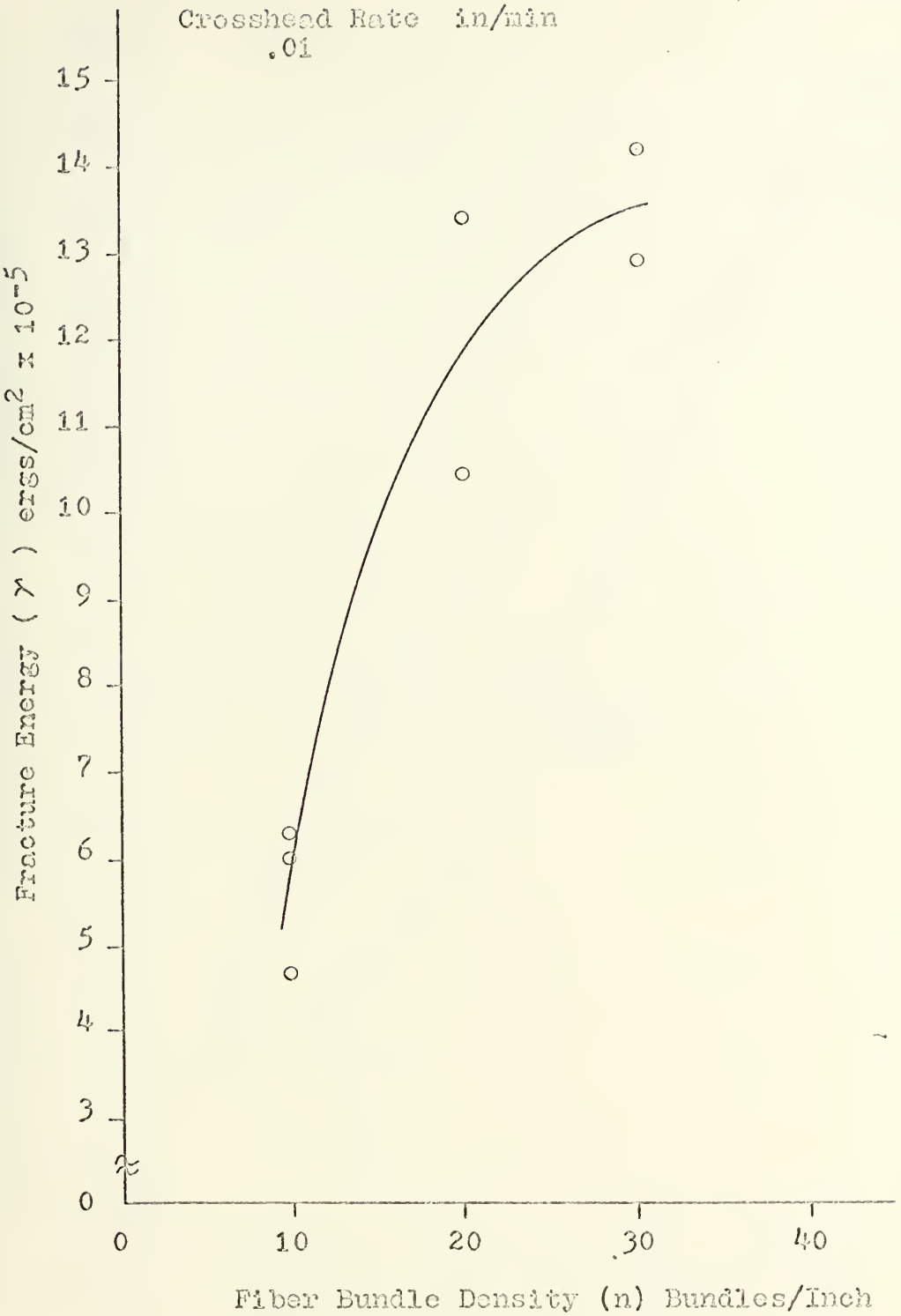

FIGURE 30 FRACTURE ENERGY vs FIBER DENSITY, EPON 828 EPOXY RESIN - MONSANTO TYPE A SYNTHETIC FIBERS.

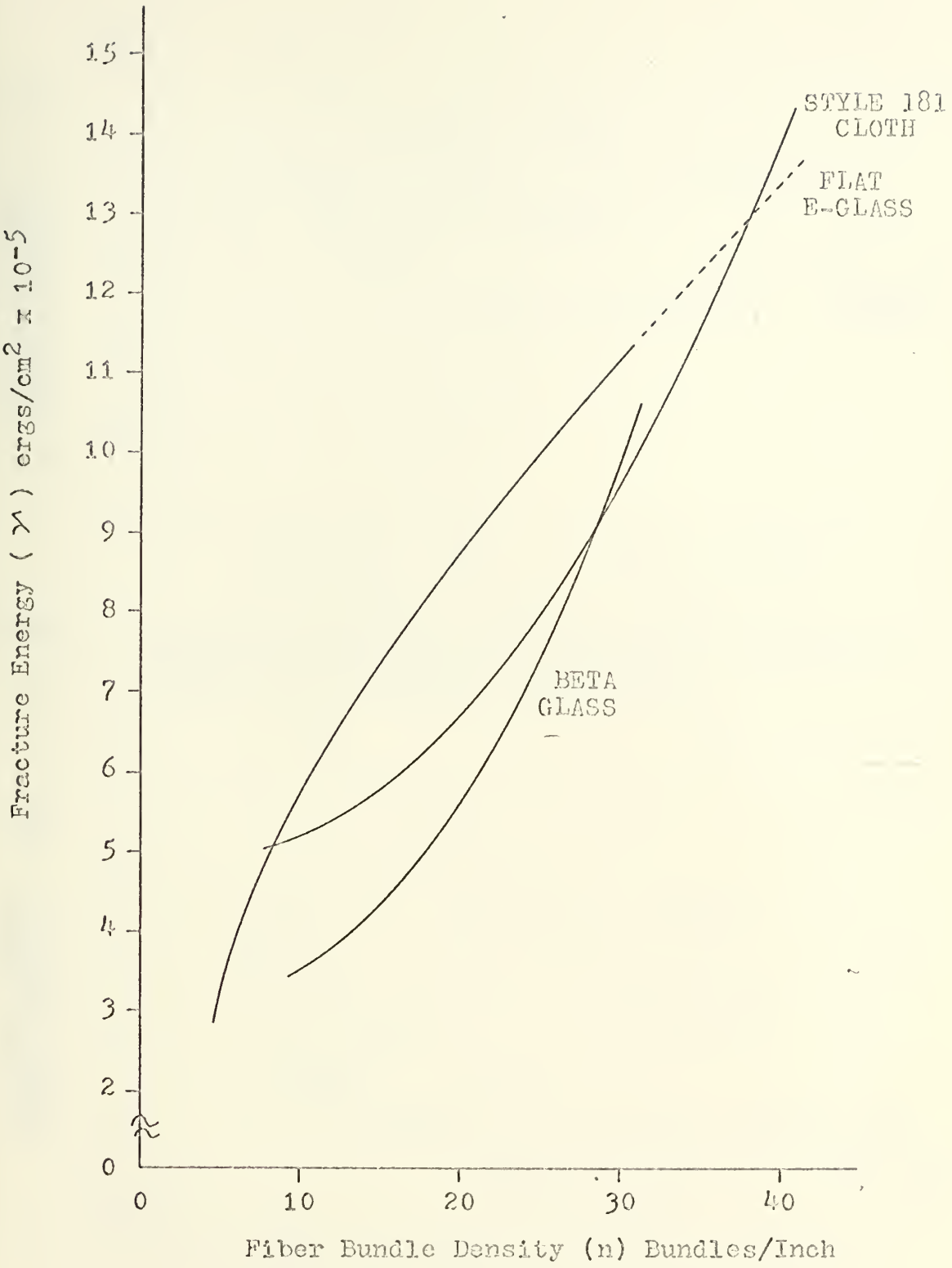

FIGURE 31 COMPARISON OF FRACTURE ENERGY vs FIBER DENSITY FOR VARIOUS FIBER REINFORCING MATERIALS IN LANINAC 4173 POLYESTER RESIN MATRIX.

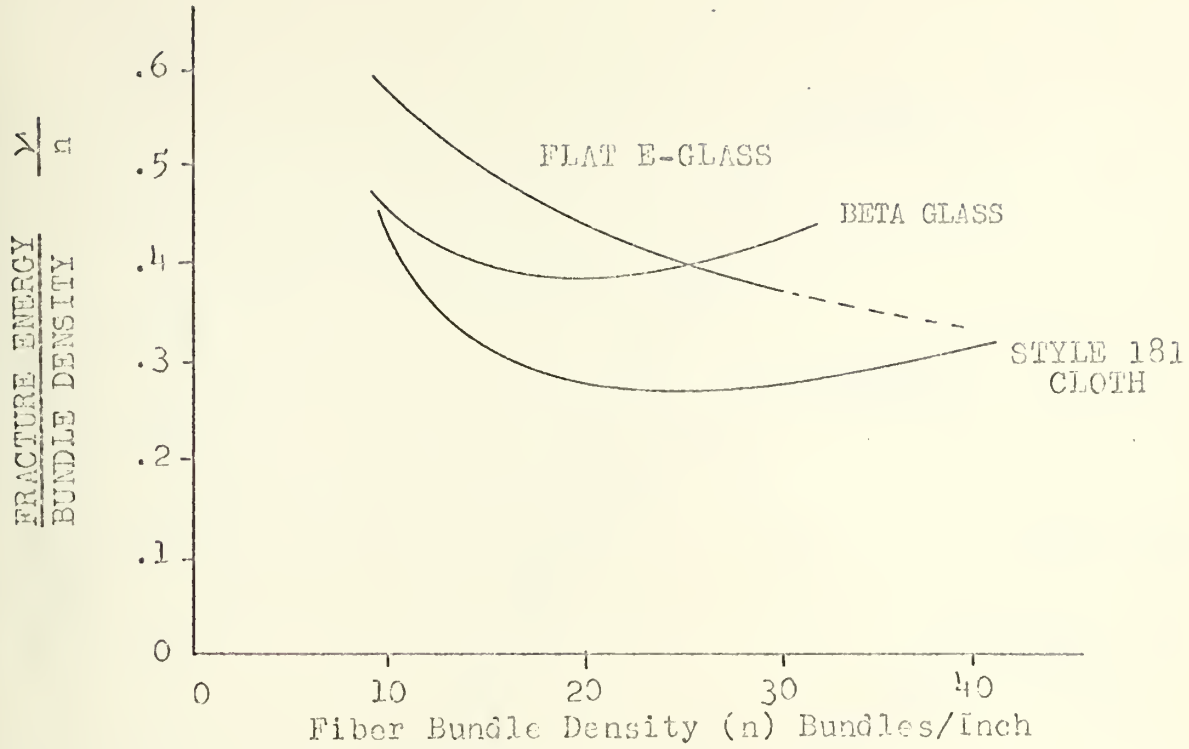

FIGURE 32 COMPARISON OF FIBER CONTRIBUTION TO THE FRACTURE ENERGY FOR VARIOUS FIBER REINFORCING MATERIALS IN LAMINAC 4173 POLYESTER RESIN MATRIX.

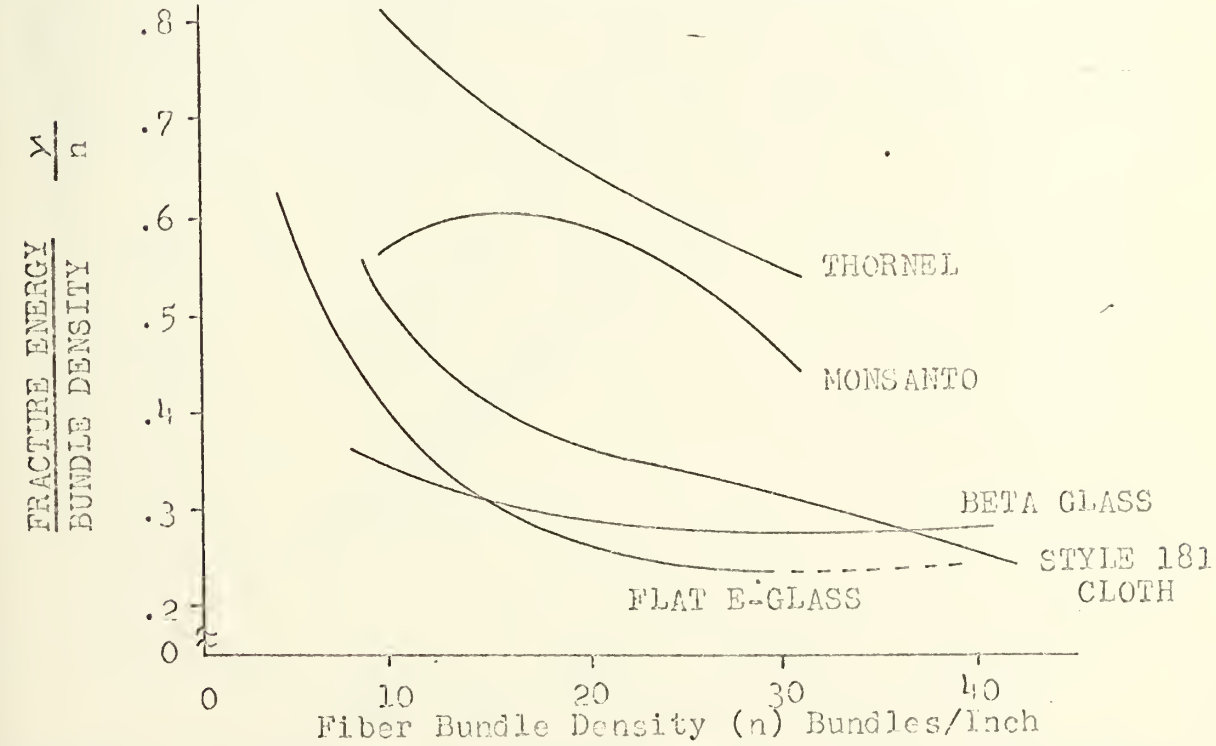

FIGURE 33 COMPARISON OF FIBER CONTRIBUTION TO THE FRACTURE ENERGY FOR VARIOUS FIBER REINFORCING MATERIALS IN EPON 828 EPOXY RESIN MATRIX.

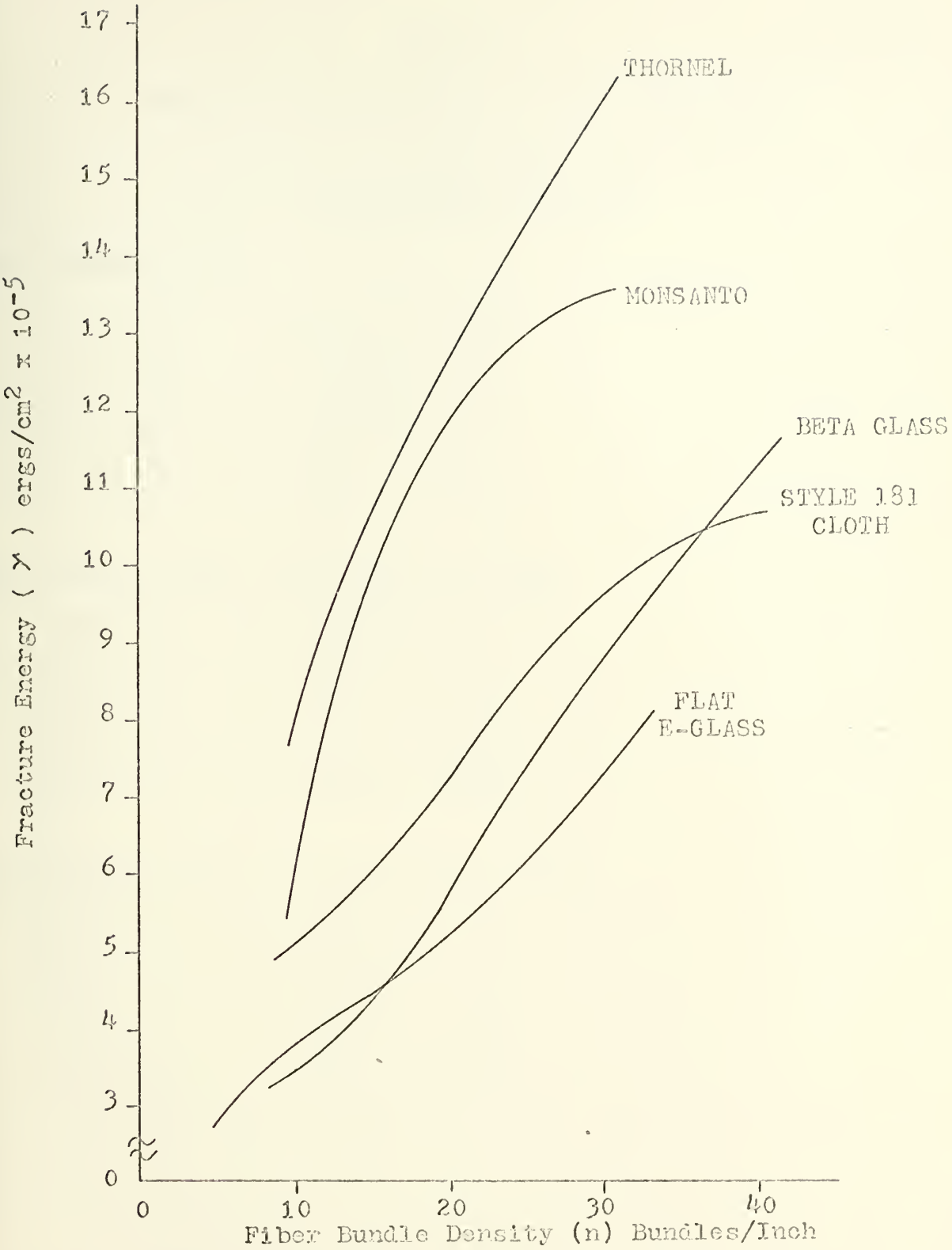

FIGURE 34 COMPARISON OF FRACTURE ENERGY vs FIBER DENSITY FOR VARIOUS FIBER REINFORCING MATERIALS IN EPON 828 EPOXY RESIN MATRIX.

TABLE 14

SUMMARY OF VOLUME FRACTION OF FIBERS' CALCULATIONS

$V_f \propto$ NO FIBERS/UNIT AREA

Web Thickness Tests:

@ t = .10	10/.10 x 1 = 100
@ t = .08	10/.08 x 1 = 125
@ t = .06	10/.06 x 1 = 167
@ t = .04	10/.04 x 1 = 250

Fiber Density Tests - .08 Inch Web Thickness:

@ n = 10	10/.08 x 1 = 125
@ n = 20	20/.08 x 1 = 250
@ n = 30	30/.08 x 1 = 375
@ n = 40	40/.08 x 1 = 500

Fiber Density Tests - .04 Inch Web Thickness:

@ n = 5	5/.04 x 1 = 125
@ n = 10	10/.04 x 1 = 250
@ n = 15	15/.04 x 1 = 375
@ n = 20	20/.04 x 1 = 500

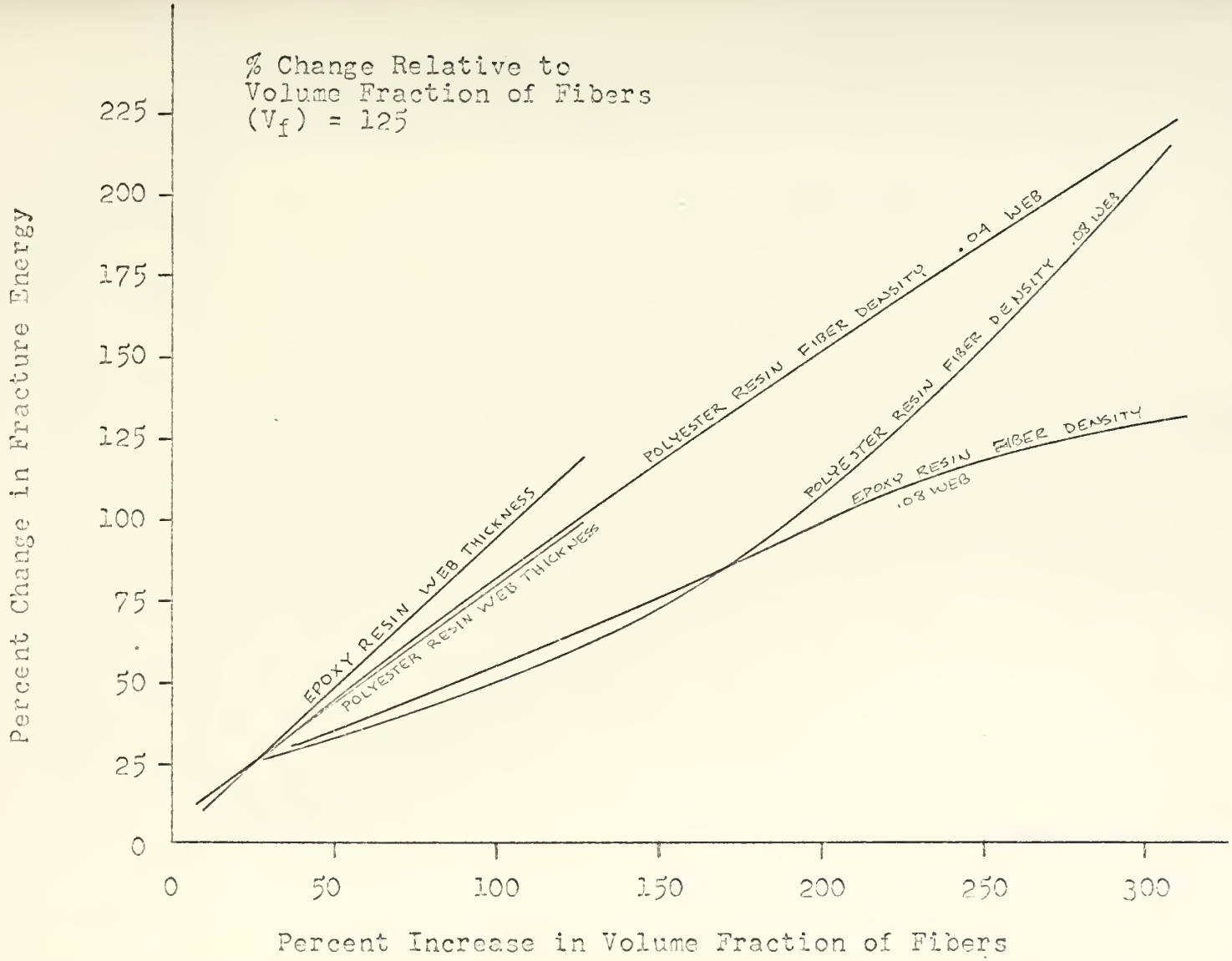

FIGURE 35 VARIATION OF FRACTURE ENERGY CHANGE WITH CHANGE IN VOLUME FRACTION OF FIBERS; STYLE 181 CLOTH FIBERS IN LAMINAC 4173 AND EPON 828 RESIN MATRIX.

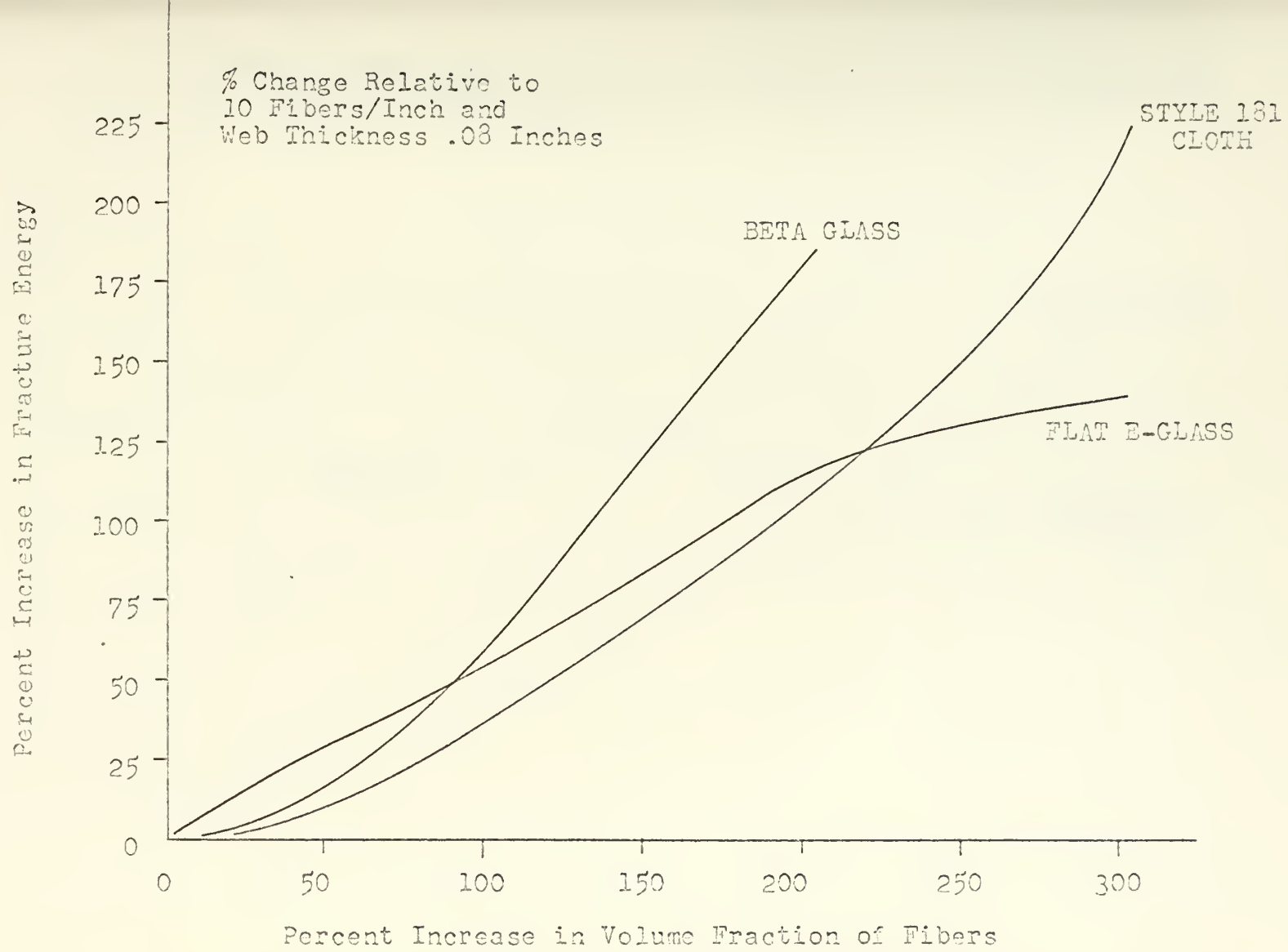

FIGURE 36 VARIATION IN CHANGE IN FRACTURE ENERGY WITH CHANGE IN VOLUME FRACTION OF FIBERS: LAMINAC 4173 POLYESTER RESIN.

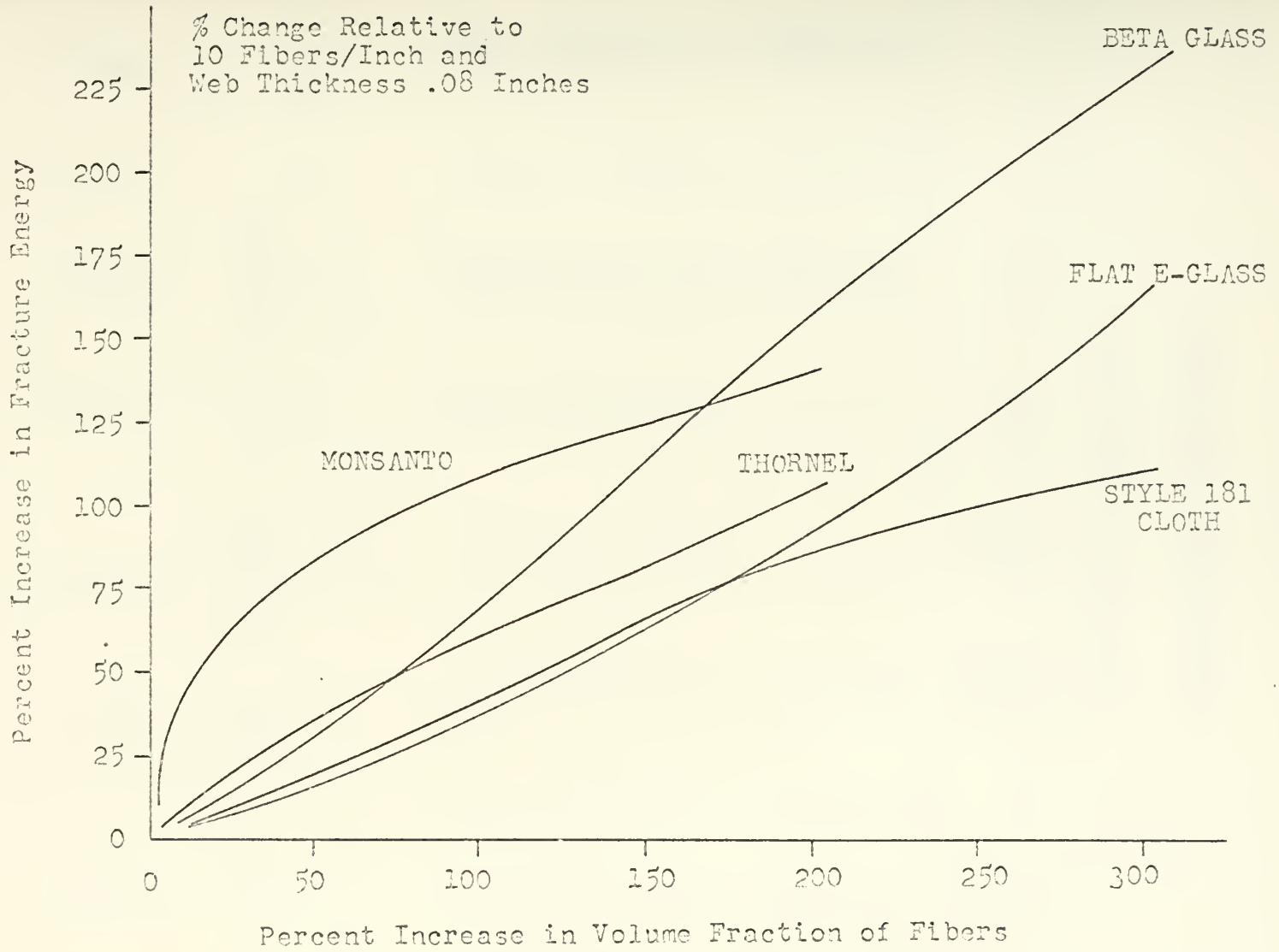

FIGURE 37 VARIATION IN CHANGE IN FRACTURE ENERGY WITH CHANGE IN VOLUME FRACTION OF FIBERS: EPON 828 EPOXY RESIN.

TABLE 15

SPECIAL TEST SPECIMEN RESULTS

CTBN MODIFIED RESIN MATRIX

Specimen	Cast	Matrix Material	Fiber Material	Fiber Density (n)	Crosshead Rate In/Min	CTBN	γ ergs/cm^2 x 10^{-5}	$\frac{\gamma}{n}$
69	34	4173	----	0	.01	4	.542	----
70	34	4173	----	0	.01	4	.564	----
73	35	4173	----	0	.01	8	.65	----
79	35	4173	----	0	.01	8	.66	----
120	62	828	----	0	.01	10	17.60	----
121	62	828	----	0	.01	10	4.18	----
65	45	4173	181	10	.01	8	8.08	.81
66	45	4173	181	10	.01	8	7.62	.76
122	62	828	181	10	.01	10	16.20	1.62
123	62	828	181	10	.01	10	14.10	1.41
133	----	828	.01	10	.01	10	27.65	2.76
134	----	828	.01	10	.01	10	33.00	3.30
18	43	4173	181	40	.01	8	38.80	3.88
99	43	4173	181	40	.01	8	31.90	3.19
128	----	828	181	40	.01	10	55.70	5.57
129	----	828	181	40	.005	10	39.60	3.96

NO POST CURE

Specimen	Cast	Matrix Material	Fiber Material	Fiber Density (n) Bundles/In	Crosshead Rate In/Min	γ ergs/cm^2 x 10^{-5}	$\frac{\gamma}{n}$
108	51	4173	----	0	.01	.458	----
109	51	4173	----	0	.01	.399	----
110	51	4173	181	10	.01	8.650	.86
111	51	4173	181	10	.01	8.100	.81

TABLE 15 (Continued)

TREATED FIBER BUNDLES

Specimen	Cast	Matrix Material	Fiber Material	Fiber Density (n) Bundles/Inch	Crosshead Rate In/Min	γ ergs/cm^2 x 10^{-5}	Bundle Treatment
114	53	4173	181	10	.01	6.73	Heat Cleaned
115	53	4173	181	10	.01	7.15	Heat Cleaned
124	30	4173	181	3	.01	3.81	Paraffin Coated
125	30	4173	181	3	.005	3.28	Paraffin Coated
188	119	4173	181	10	.005	11.28	Plastilease Coated
189	119	4173	181	10	.01	12.30	Plastilease Coated

FLAT E-GLASS BUNDLES TWISTED TO 3 TWISTS PER INCH

Specimen	Cast	Matrix Material	Fiber Density (n)	Crosshead Rate	γ ergs/cm^2 x 10^{-5}
152	103	4173	20	.01	21.62
153	103	4173	20	.005	20.85

NYLON 6 FIBER BUNDLES

Specimen	Cast	Matrix Material	Fiber Density (n)	Crosshead Rate	γ ergs/cm^2 x 10^{-5}
194	122	828	10	.01	19.60
195	122	828	10	.005	16.08

IV. DISCUSSION OF RESULTS

The results of the web thickness with no reinforcement tests for the two matrix materials indicate that there may be a change in the plastic deformation or viscous flow associated with the cleavage fracture of the matrix as the web thickness is increased. The LAMINAC 4173 polyester resin exhibits an increase in fracture energy with increasing web thickness (t). The average value of fracture energy is .48 x 10^5 ergs per square centimeter over the range of web thickness from .04 to .08 inches. If the curve of measured values of fracture energy is extended to a web thickness of .10 inches, the average value for the fracture energy increases to .52 x 10^5 ergs per square centimeter over the range of web thickness from .04 to .10 inches. The maximum variation of the fracture energy from this average value is $\pm$ .12 x 10^5 ergs per square centimeter at .10 and .04 inches web thickness respectively.

The EPON 828 epoxy resin exhibited a decrease in fracture energy with an increase in web thickness. The average value of fracture energy over the range of web thickness investigated is 2.7 x 10^5 ergs per square centimeter. The maximum variation from this average value is $\pm$ .7 ergs per square centimeter at .04 and .10 inches web thickness respectively. The two matrix materials differ radically in behavior with the polyester resin having the greater plastic deformation or viscous flow during fracture as the web thickness is increased.

The results of the web thickness tests of the two matrix materials with Style 181 Cloth glass fiber reinforcement at a fiber density of 10

bundles per inch indicate that the fracture mechanism is very similar for the two different matrix systems. Both the LAMINAC 4173 polyester resin and the EPON 828 epoxy resin systems show a decrease in fracture energy with increasing web thickness. This effect is similar to that observed for the epoxy resin without reinforcement as the web thickness was increased. The decrease in fracture energy associated with increasing web thickness is much more pronounced for the epoxy resin matrix. This is most probably due to the reinforcing of like effects, both the reinforced and nonreinforced specimens exhibiting a decrease in fracture energy with increasing web thickness. The decrease in fracture energy with increasing web thickness for the reinforced polyester resin is not as pronounced due to the offsetting effect of increasing fracture energy with increasing web thickness for the unreinforced polyester resin. The decrease in fracture energy with increasing web thickness can be associated with a decreasing volume fraction of fiber reinforcement as suggested by Outwater and Murphy.[12] This effect is to be expected as the fibers become the principle load bearing elements in the composite material as the volume fraction of fibers is increased. The decreasing slope of the fracture energy curve with increasing web thickness indicates that there may be some minimum value of the fracture energy web thickness relationship which would suggest some minimum volume fraction of fiber reinforcement which must be obtained before a significant effect on the fracture energy may be observed. This effect may be more true for the epoxy than for the polyester resin.

The results of the beam height tests indicate that fracture energy is not a function of this parameter. The force-deflection curve changes with increasing beam height, with greater force required for crack propagation

as the beam height increases. The deflection required for crack propagation in the composite system decreases with increasing beam height. As the .5 inch beam height provides more than sufficient length of fiber necessary to develop the full strength of the fiber, the height of the beam was not expected to influence the fracture energy.

The increasing of the fiber bundle density (increasing the volume fraction of fibers) by decreasing the spacing between the fibers has the same effect as increasing the volume fraction of fibers by decreasing the total amount of matrix surrounding the fibers but holding the fiber spacing constant (web thickness tests). However, decreasing the spacing between the fibers increases the interaction between the bundles and, although the fracture energy increases, the amount is much less than was observed in the web thickness tests for a doubling of the volume fraction of fibers. This is readily apparent in Figure 35 for both the epoxy and polyester resin web thickness tests as compared to the fiber density tests for specimens with a .08 inch web thickness. The linear relationship between percentage increase in fracture energy with percent increase in volume fraction of fiber indicates that the fiber interaction does not change as the volume fraction of fibers is increased by decreasing web thickness for either of the resin materials. For the specimens with a .08 inch web thickness, where the volume fraction of fibers was increased by increasing the fiber density, there is non-linearity to the curves of percent increase in fracture energy vs. percent increase in volume fraction of fibers due to the interaction of the fibers as the density is increased (spacing between fibers is decreased). This is not quite as apparent for the polyester resin composite with the .04 inch web thickness.

The trend in the fracture energy of the various fiber-resin composite

systems with increasing fiber density (volume fraction of fibers) may best be explained by the behavior of the composite system during crack propagation. When the deflection of the beams is increased, the crack in the matrix material propagates through the material, well ahead of where the last fiber bundle has broken (Figure 1). As the crack in the matrix material passes the individual fiber bundles, the area of the specimen in the vicinity of the bundle begins to show a change in refractive index generally manifested as a whitening of the resin matrix (Figure 2). This change in refractive index appears to be a general fracturing of the resin matrix in and around the fiber bundle, and has been termed debonding for lack of a better description. As the deflection of the beams continues, the debonding of the fiber bundles can be observed to progress along the length of the fiber bundle. A change in the stress pattern along the fiber may be observed during the debonding by the use of cross polarized light as was explained earlier. Eventually, the fiber bundle fails and the crack in the matrix material again moves along the specimen. Failure of the fiber bundle and subsequent crack propagation is evidenced by a drop in the load on the INSTRON recording chart (Figure 3). At low fiber density, the bundles tend to fail individually and the crack in the matrix progresses from fiber to fiber in a stick-slip type of behavior. As the fiber density is increased, the bundles tend to fail in groups with the number of fibers failing simultaneously increasing with increasing fiber density. It is significant to note that the tip of the crack in the matrix material is always several fiber bundles ahead of where the bundles are failing, which implies that the stress concentration at the tip of this crack is not sufficient to cause failure of the fibers. Since this stress concentration does not con-

trol the fracture process, the basic Griffith Theory does not apply to this type of material. This may be further substantiated by the fact that the crack in the matrix material tends to propagate around the fiber bundles and not through the matrix material contained within the fiber bundle. A chevron type pattern which is caused by this behavior may be observed on the fracture surface of the matrix material. The actual distance that the matrix crack moves ahead of the last broken fiber appears to be essentially constant for a particular fiber-resin combination and does not change with increasing fiber density. The number of fibers contained within the region between the last broken fiber and the tip of the crack in the matrix material does change with fiber density. This results in a greater number of fibers carrying the load and experiencing the debonding phenomena simultaneously as fiber bundle density increases, further resulting in a larger load recorded on the INSTRON chart with increasing fiber density.

As the crack in the resin matrix material passes the individual fiber bundles, the bundles lose the support of the matrix material surrounding them and become subject to a tensile form of loading. As the fibers are pulled in tension by the deflection of the beams, they tend to elongate which causes the debonding noticed in the vicinity of the fiber bundles. As the debonding occurs, the ability of the matrix to transfer load from the matrix material to the fibers is seriously reduced in the debonded region due to the general fracture of the resin system. As the restraint to fiber elongation is partially released by the fracturing of the matrix, the fiber is free to further elongate causing the debonding to proceed along the length of the fibers (Figure 38).

The debonded region surrounding the fiber bundles will extend some

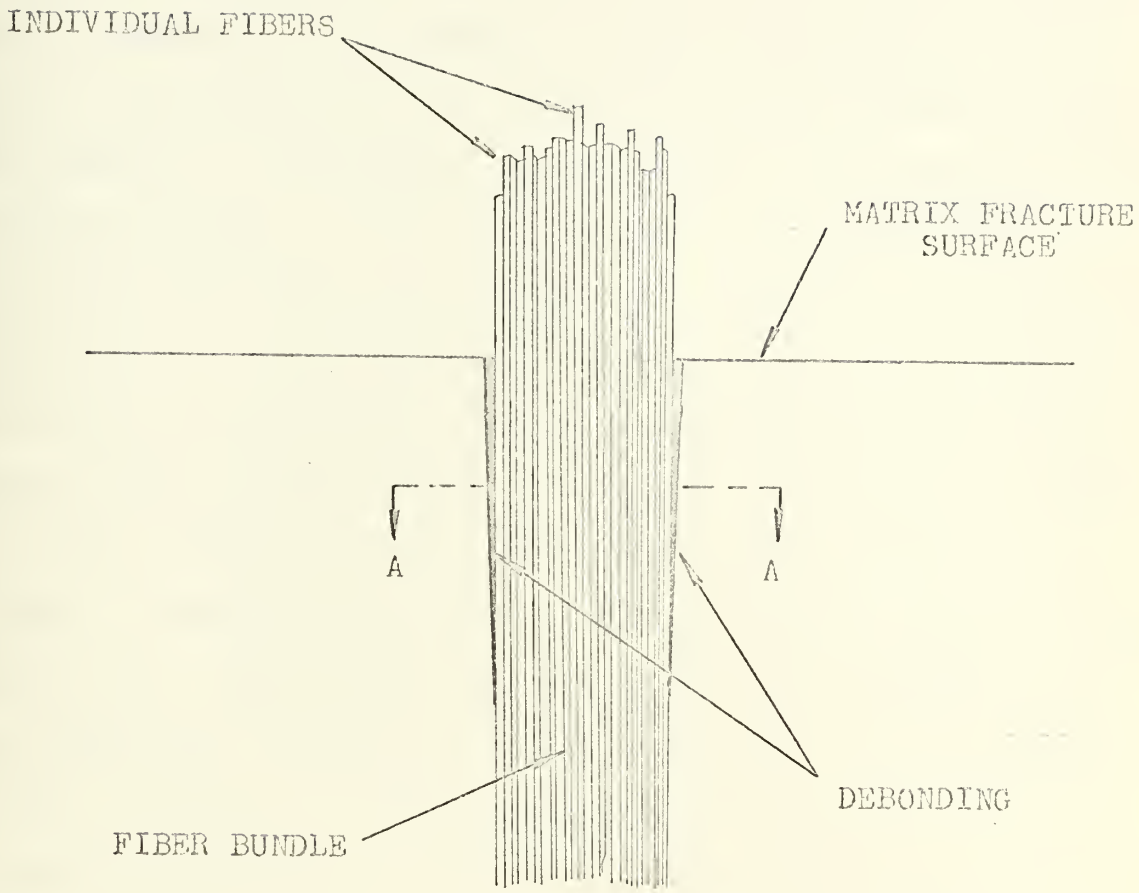

FIGURE 38 SCHEMATIC OF CROSS SECTION OF DEBONDED, FRACTURED FIBER BUNDLE

distance away from the fiber bundles in a direction perpendicular to the length of the bundles (Figure 39). This will be termed radial debonding implying debonding in a direction corresponding to the radius of the fiber bundle at a particular cross section. The extent of this debonding is a function of the characteristics of the particular fiber bundle and resin matrix materials. Qualitatively, the distance that a fiber bundle will debond along its length, as well as the distance of debonding around the cross section of the fiber bundle appears to be constant for a particular fiber-resin composite and does not vary with the density of fiber bundles (n) contained in the specimen. There may be some finite relationship between the amount of debonding along the length of the fiber and the extent of the radial debonding. As the fiber is extended by the displacement of the beams, it debonds along its length. Further extension causes the resin matrix material to want to be pulled towards the fracture surface by the fiber, subsequently increasing the extent of the radial debonding (Figure 38). For this reason, the extent of radial debonding appears to be greatest near the matrix fracture surface, and decreasing along the length of the fiber away from this surface. In general, the greater the extensibility to fracture of the fiber and the more brittle the resin matrix, the greater will be the amount of debonding. The polyester resin, which was the more brittle of the two resins used as matrix materials, always exhibited greater debonding when the same fiber was used as reinforcement in the two resins.

The load carrying capability of the fiber-resin composite is a function of the bonding between the fibers and the resin and the shear strength of the resin. The bonding between the fiber and the matrix may be either

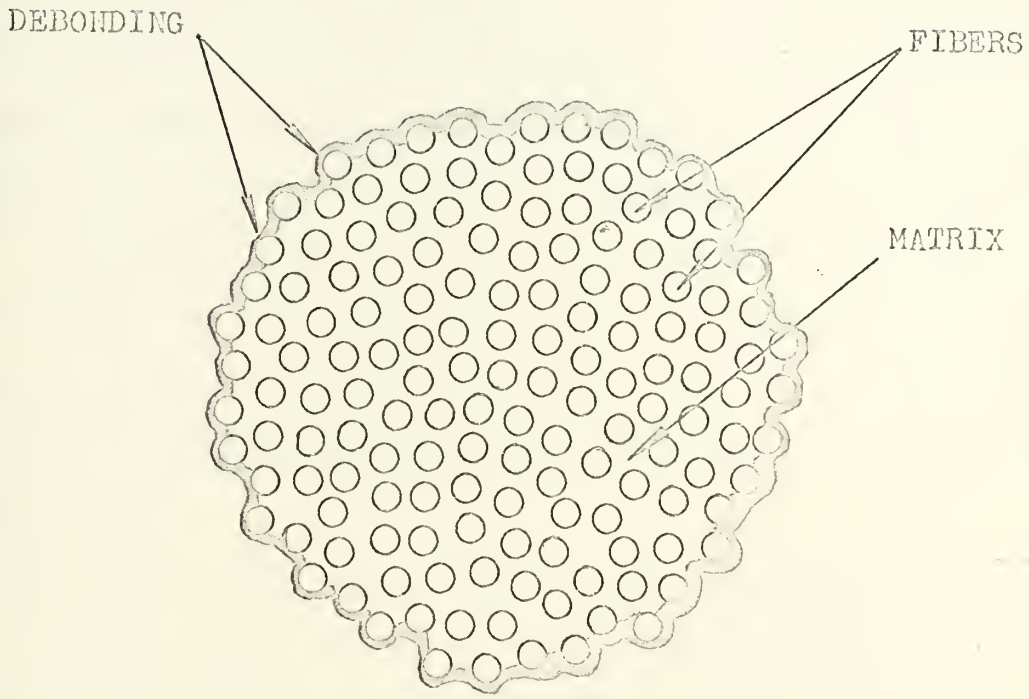

FIGURE 39 SCHEMATIC OF CROSS SECTION A-A IN FIGURE 38 .

chemical, mechanical, or a combination of these. The shear strength of the resin at the interface will greatly influence the extent of debonding along the fiber length, the lower the shear strength of the resin, the greater the extent of debonding.

As the load carrying capability of the fiber-resin interface is reduced by the debonding of the fibers, the strain in the fibers is decreased. Further deflection of the beams causes increased strain in the fibers resulting in further debonding. Although the load carrying capability of the fractured matrix material is reduced by debonding, it is not reduced to zero. The debonding process will continue along the length of the fibers until such time as there remains sufficient load transference between the matrix and the fibers to enable the fibers to reach the strain necessary for fracture. This occurs somewhere along the length of the fiber in the debonded region.

The extent of debonding of a fiber in the radial direction becomes increasingly important as the fiber density is increased (distance between fibers is decreased). The greater the extent of radial debonding associated with a particular fiber in a particular resin matrix, the lower the fiber density required for this radial debonding to begin interacting in the matrix between the fibers. As the fiber density is further increased, the overlap of the radial debonding becomes more extensive. This is manifested by a general fracturing of the matrix between fibers. As the beam deflection is increased, the matrix material that has generally fractured will begin to pull away from the intact matrix due to the elongation of the fibers giving a type of cup and cone appearance to the fracture surface between fibers. The density of fibers at which the fiber radial debonding

overlap begins to occur is a function of the brittleness of the resin matrix and the extensibility of the fibers.

The ability of a particular fiber-resin composite to exhibit a large fracture toughness is primarily linked to the ability of the composite system to have a large number of fibers carrying the load at any given time. This may be accomplished by having the crack in the matrix proceed far ahead of where the last fiber has broken leaving a large number of load bearing fibers in the resulting interval between the last broken fiber and the crack tip. This type of behavior is exhibited by both the Thornel and the Monsanto fibers in the epoxy resin matrix where even at low fiber density, there are a large number of load bearing fibers. The Thornel fibers do not exhibit the type of debonding, either radial or along the length of the bundles, normally exhibited by all of the fiber bundles used in the test specimens.

The other most significant mechanism in the fiber-resin composite system's ability to exhibit a high fracture toughness is the extent of radial debonding. With little radial debonding, the fibers tend to act individually rather than as groups resulting in a much lower percent increase in fracture toughness with increasing volume fraction of fiber percentage. Radial debonding weakens the matrix structure sufficiently to allow the fiber bundles to more evenly carry the load by having a more nearly equal strain. This type of behavior is exhibited in varying degrees by any of the glass fibers in the polyester resin, and also by the Beta-glass and flat E-glass fibers in the epoxy resin system. This ability may be evidenced by the shallow slope or the flattening of the fiber contribution to the fracture energy curves with increasing fiber density.

Any property of the fiber such as surface coatings and twist of the fiber which increases the amount of debonding of the fiber will serve to increase the toughness of the composite system at low fiber densities.

V. CONCLUSIONS

Due to the fact that the crack tip in the resin matrix material is generally at some distance ahead of the point where the last fiber has broken, the stress concentration at the tip of the crack is not sufficient to cause failure of the total composite system. Therefore, the basic Griffith Theory of brittle fracture is not applicable to fiber reinforced resin composite materials.

Fiber bundle debonding appears to be a function of the resin-fiber bond, the extensibility of the fiber and the shear strength of the resin matrix. The extent of radial debonding may be of more importance than the extent of debonding along the length of the fiber. Radial debonding will determine the ability of the individual fibers to act together in groups in carrying the load resulting in a significant increase in the fracture energy. The extent of radial debonding will determine the fiber bundle density at which significant increase in fracture energy will be exhibited.

For fiber bundles which exhibit low extensibility or strain to fracture, the principle fracture toughening mechanism appears to be the ability of the fiber-resin composite system to propagate the crack in the matrix far ahead of where the fibers are breaking. This will give rise to a large number of load bearing fibers at any time. These fibers generally exhibit very little if any radial debonding and therefore tend to act more as individual fiber bundles rather than as groups of bundles. This type of toughening mechanism gives rise to a smaller percentage increase in fracture energy with percentage increase in volume fraction of fibers than is

associated with bundles which radially debond.

Fiber-resin composite combinations which exhibit a flat fiber contribution to fracture energy vs. fiber bundle density curve will exhibit the greatest percent increase in fracture energy with percent increase in volume fraction of fibers. These combinations are generally characterized by composite systems which exhibit significant radial debonding.

VI. RECOMMENDATIONS

1) Investigate the debonding process further using a particular fiber with various surface coatings to promote or inhibit fiber debonding as an attempt to further determine the contribution of this mechanism to the fracture toughness of fiber-resin composite materials.
2) Investigate the effect of additional plies of fibers on the fracture energy of the fiber resin composite system.
3) If possible, investigate the effect of fiber extensibility using a fiber in which other properties such as geometry, modulus, and strength may be held constant while extensibility is varied.
4) Microscopy studies to further determine the interaction and effect of the radial debonding around the fibers.
5) Microscopy studies to determine the relationship between radial debonding and debonding along the length of the fibers, if any such relationship exists.

VII. REFERENCES

1) Chemical and Engineering News, (January 26, 1970); p.58.

2) Aulenbach, T. H., "Plain Strain Crack Toughness of Fiberglass Reinforced Plastic," Naval Engineer Thesis, (Department of Naval Architecture and Marine Engineering, Massachusetts Institute of Technology, May, 1969).

3) "Plain Strain Toughness Testing of High Strength Metallic Materials," ASTM Special Technical Publication No. 410, (December, 1966).

4) "Fracture Toughness Testing and Its Applications," ASTM Special Technical Publication No. 381, (June, 1964).

5) Pellini, W. S., "Evolution of Engineering Principles for Fracture Safe Design of Steel Structures," NRL Report 6957, (September 23, 1969).

6) Griffith, A. A., "The Phenomena of Rupture and Flow in Solids," Philosophical Transactions of The Royal Society, 221A, (1920); p.163.

7) Irwin, G. R., "Fracturing of Metals," ASM Symposium, (Chicago, 1947).

8) Orowan, E., Fatigue and Fracture of Metals, edited by W. M. Murray, (New York, 1952).

9) Irwin, G. R., and Kies, J. A., "Fracturing of Metals," ASM Symposium, (Chicago, 1947).

10) Outwater, J. O., and Carns, W. O., "The Fracture Energy of Composite Materials," (Final Report, University of Vermont, September 30, 1967); p. 38.

11) Mullin, J., et al., R67SD51, Space Sciences Laboratory, Missile and Space Division, General Electric Company (1967).

12) Outwater, J. O., and Murphy, M. J., "On the Fracture Energy of Unidirectional Laminates," 24th Annual Technical Conference, Reinforced Plastics/Composites Division, The Society of the Plastics Industry, Inc. (1969).

13) Berry, J. P., "Determination of Fracture Surface Energies by the Cleavage Technique," Journal of Applied Physics, Vol. 34, No. 1, (January, 1963); p. 62.

14) Berry, J. P., "General Theory of Brittle Fracture," Fracture Processes in Polymeric Solids, edited by B. Rosen, (Interscience Publishers, 1964); p. 151.

15) Broutman, L. J., and McGarry, F. J., "Fracture Surface Work Measurements on Glassy Polymers by a Cleavage Technique," Journal of Applied Physics, Vol. 9 (1965); p. 589.

16) Hoagland, R. G., "On the Use of the Double Cantilever Beam Specimen for Determining the Plane Strain Fracture Toughness of Metals," Journal of Basic Engineering, Transactions of ASME, (September, 1967); p. 525.

17) Gillis, P. J., and Gilman, J. J., "Double Cantilever Cleavage Mode of Crack Propagation," Journal of Applied Physics, Vol. 35, No. 3, (March, 1964); p. 647.

18) Sultan, Jacques N., and McGarry, F. J., "Toughening Mechanism in Polyester Resins and Composites," (Research Report R67-66, Department of Civil Engineering, Massachusetts Institute of Technology, December 1, 1967).

19) McGarry, F. J., and Willner, A. M., "Toughening of an Epoxy Resin by an Elastomeric Second Phase," (Research Report R68-8, Department of Civil Engineering, School of Engineering, Massachusetts Institute of Technology, March 1, 1968).

APPENDIX A

SPECIMEN PREPARATION

Castings are prepared in the following manner:

1) Two 12 inch x 12 inch x 1/4 inch glass plates are coated with mold release. The inner edges of the .25 inch thick neoprene edge sealing gasket are also coated with the same mold release.

2) 3mm (.118 inch) diameter pyrex glass rods approximately 8 inches long are used to space the fiber bundles away from the surface of the glass plates. For an epoxy matrix casting, two of the above glass rods are spaced approximately 1/2 inch apart in a position approximately 2 1/2 inches from one edge of the plate. Two more of the glass rods are spaced about 1/2 inch apart and positioned approximately 4 inches from the first pair. These rods are then taped to the plate using transparent tape. (Figure A-1)
For a polyester matrix specimen, single glass rods vice pairs are placed in approximately the same location as the pairs.

3) A strip of graph paper approximately 5 inches long by 1/4 inch wide with 20 divisions per inch is taped to the plate outside each pair of glass rods. (Figure A-1)
Strips of double stick transparent tape are then taped to the glass plate outside the guide strips.

4) Fiber bundles are stretched across the glass rods and taped to the double stick tape at the desired spacing. Additional transparent tape is then placed over the ends of the fibers to hold them in place. Fibers are placed in the center 4 inches of the length.

5) For an epoxy matrix casting, a quick setting polyester or epoxy resin is poured into the gap between the pairs of glass rods to hold the fibers in place during the oven cure cycle. This is necessary as the transparent tape softens during heating and allows the fiber bundles to move if they are not secured by this additional resin. This is not required for polyester matrix castings cured at room temperature.

6) When the resin used as a hold-down for the fibers has cured, the .25 inch soft rubber sealing gasket is placed on around three edges of the plate. The second plate is then placed on the gasket and spring clamps are placed around the three sealed edges. Fibers should be oriented perpendicular to the open edge of this mold.

7) Epoxy resin (EPON 828 with 5% Curing Agent D) or polyester resin (LAMINAC 4173 with 2% MEK peroxide) is prepared, the mold is placed vertically with the unsealed edge at the top, and the desired resin is poured slowly into the mold.

8) Polyester resin castings are allowed to cure overnight at room temperature. Epoxy resin castings are cured in an oven for two hours at 100° C.

9) Both resin castings are post cured for two hours at 120° C. and allowed to cool to room temperature in the oven.

10) Castings are then removed from the mold and test specimens are machined from them.

Cleavage Specimens are prepared as follows:

1) Two specimens are rough cut from the casting and trimmed to a 1.2 inch final width using a high speed router.

2) Specimens are then cut to a 7 inch length using a bandsaw. The fibers should be spaced equally about the center of the length.

3) Two 1/8 inch diameter holes are drilled approximately .2 inches in from one end and .2 inches from the top and bottom edges of the specimen. These holes are drilled to receive the loading pins.

4) Finally, the slot is cut with a .006 inch thick screw slotting saw (2 1/4 inch diameter, 60 teeth) on a milling machine. The blade rotates at approximately 175 rpm, and the specimen is fed past the blade at approximately 1 1/8 inches per minute. A lubricating fluid is sprayed on the blade and the specimen during milling to reduce blade friction thereby reducing any temperature rise in the specimen. This allows the desired depth of the slot to be machined in one pass. After the sides have been slotted, a crack is machined at one end of the specimen by increasing the depth of the slots until they intersect. The length of this crack is one inch and is called a "swallow tail" cut. The specimen is then washed clean of the lubricant and the slot cleared of water with compressed air. (Figure A-2)

Aluminum Strip Modified Cleavage Specimens are prepared as follows:

1) A metal that would remain elastic under the conditions of the test was required. A T-7075 Alclad aluminum was found to satisfy these

conditions.

2) The aluminum was machined into strips 7 inches long by .4 inches wide.

3) The face surfaces of the test specimens were thoroughly cleaned of mold release using a fine sandpaper, as were the faces of the aluminum strips. The strips were then banded to the specimen using an epoxy adhesive, EPOXIPATCH. (Figure A-3)

4) The strips were clamped to the specimen using spring clips until the adhesive had set.

5) Loading pin holes were then drilled as in the unmodified specimens.

6) The crack guide slots and "swallow tail" cut were machined in the specimen prior to the addition of the aluminum strips.

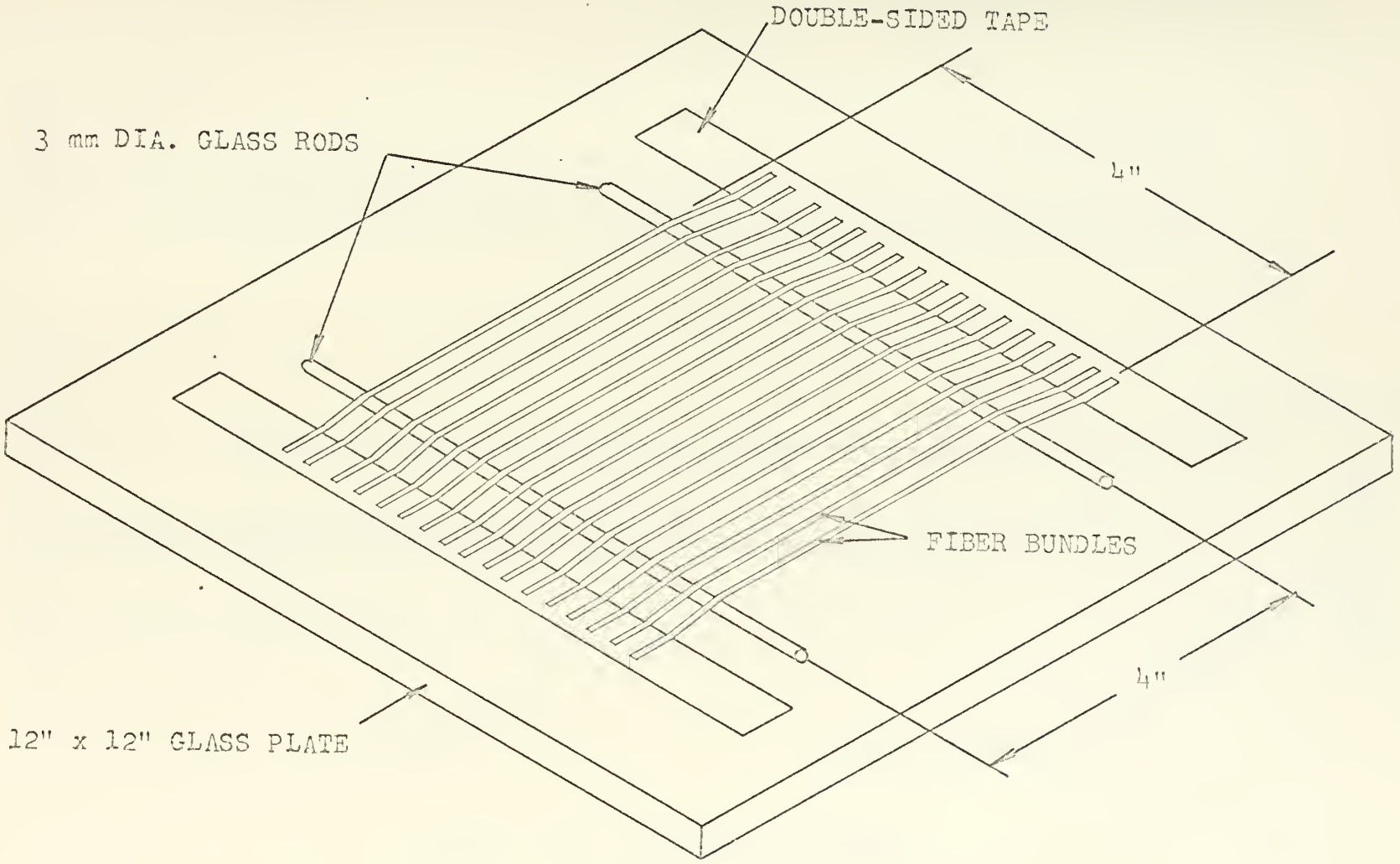

FIGURE A-1 FABRICATION OF SPECIMENS

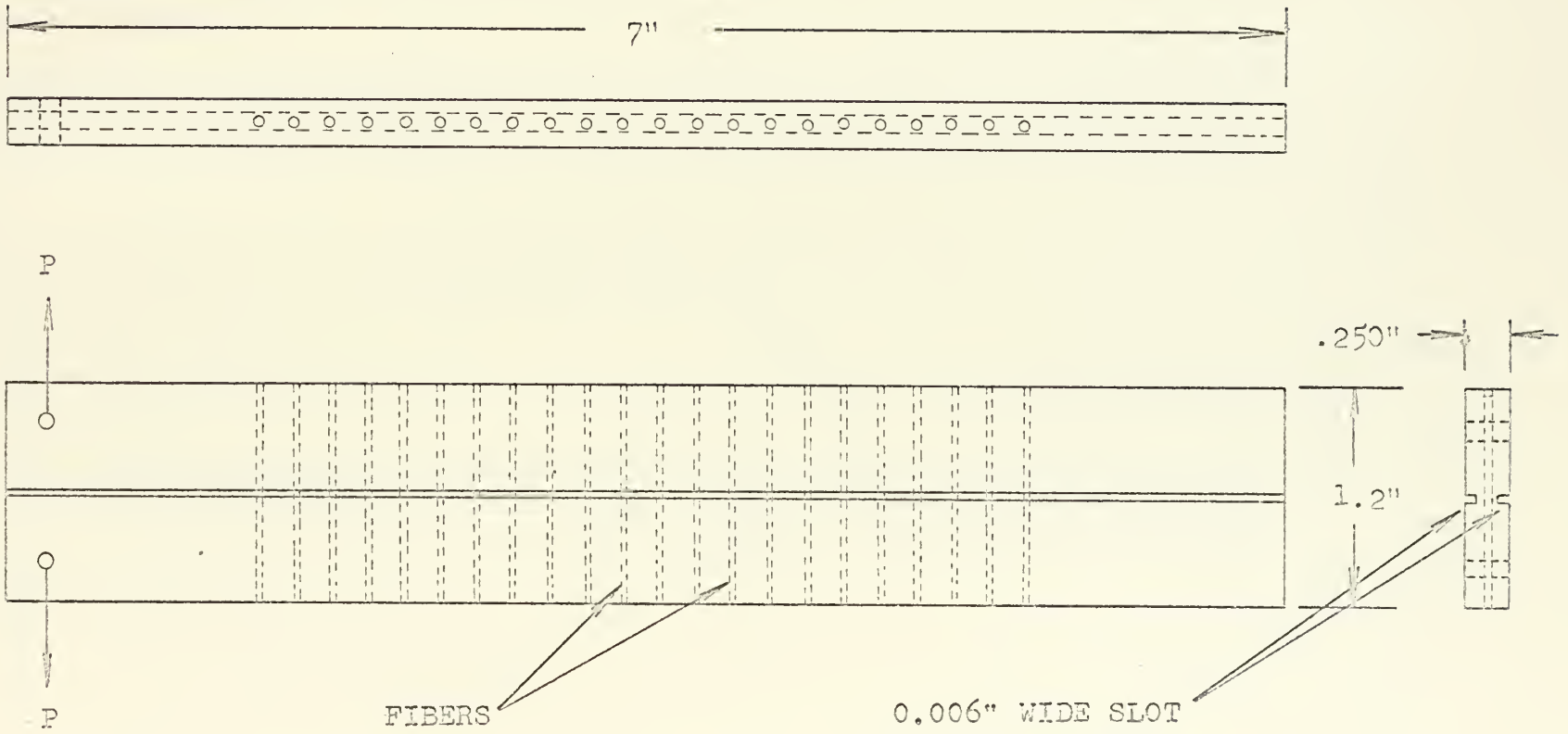

FIGURE A-2 CLEAVAGE SPECIMEN

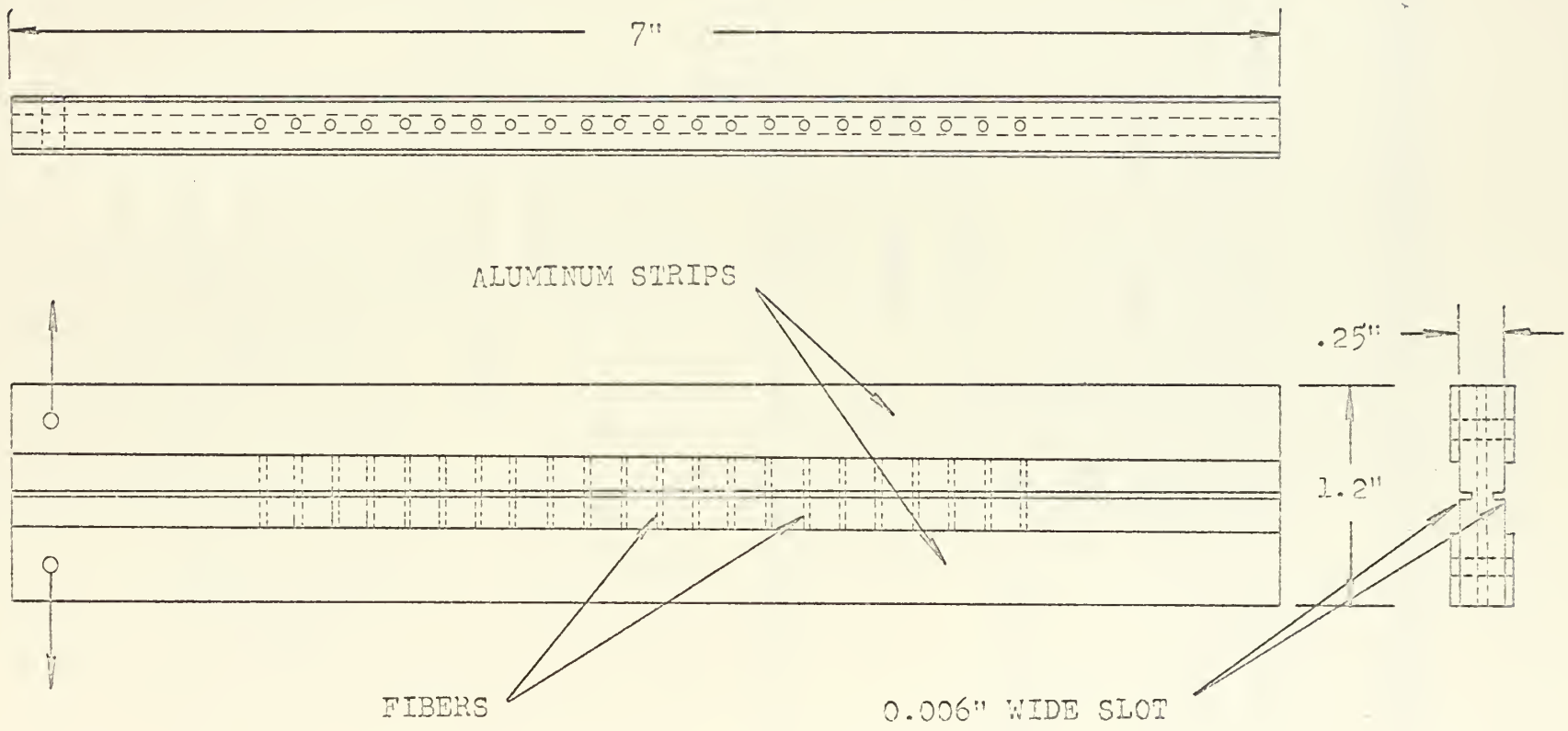

FIGURE A-3 ALUMINUM STRIP MODIFIED CLEAVAGE SPECIMEN

APPENDIX B

PROPERTIES OF MATERIALS USED IN DOUBLE CANTILEVER BEAM SPECIMENS

Resins:

1) LAMINAC 4173 Polyester Resin (American Cyanimid Company) with 2 percent Methyl Ethyl Keytone Peroxide curing agent.

LAMINAC 4173 Resin: 50% ALKYD
50% STYRENE
.015% Cobalt Metal as Napthenate

Young's Modulus: 4.63×10^5 psi

Tensile Strength: 5500 psi

Shear Strength: 1000 psi

2) EPON 828 Epoxy Resin (Shell Chemical Company) with 5 percent Curing Agent D.

Young's Modulus: 4.66×10^5 psi

Tensile Strength: 10.35×10^3 psi

Shear Strength: 2500 psi

Fiber Bundles Used as Reinforcement:

1) E-Glass Fiber Bundles.

Properties of E-Glass Fiber Bundles:

Young's Modulus: 10.5×10^6 psi

Tensile Strength: 340×10^3 psi

Elongation to Fracture: 4.8%

Density: 2.54 gms/cm^3

Fiber Bundles Used:

a) Bundles extracted from Style 181 cloth of circular cross section (Stevens Fiberglass).
Bundle diameter: 12.6×10^{-4} inches*

b) Bundles of flat rectangular cross section (ribbon).
Bundle cross section dimensions:
30.4×10^{-4} by 1.18×10^{-4} inches*

c) Single filaments of circular cross section.
Filament diameters: 1×10^{-2} inches
5×10^{-3} inches

2) Nylon 6 fiber bundles of circular cross section (Owens Corning Company).

Young's Modulus: 800×10^{3} psi

Tensile Strength: 112×10^{3} psi

Elongation to Fracture: 20%

Density: 1.14 gms/cm^3

Bundle Diameter: 16.5×10^{-4} inches*

3) Beta Glass fiber bundles of circular cross section (Owens Corning Company).

Young's Modulus: 10×10^{6} psi

Tensile Strength: 3.13×10^{5} psi

Elongation to Fracture: 3.1%

Density: 2.54 gms/cm^3

Bundle Diameter: 9.85×10^{-4} inches*

4) Thornel 50 Graphite fiber bundles of circular cross section (Union Carbide Company).

Young's Modulus: 50×10^6 psi

Tensile Strength: 285×10^3 psi

Elongation to Fracture: .5%

Density: 1.63 gms/cm^3

Bundle Diameter: 22.1×10^{-4} inches*

5) Monsanto Type I-2 synthetic fiber bundles of circular cross section (Monsanto Chemical Company).

Young's Modulus: 12.6×10^6 psi

Tensile Strength: 216×10^3 psi

Elongation to Fracture: 2.54%

Density: 1.5 gms/cm^3

Bundle Diameter: 22.4×10^{-4} inches*

* as measured

APPENDIX C

TEST SPECIMEN DATA FOR CLEAVAGE SPECIMENS

Specimen	Casting	Matrix Material	Fiber* Material	Fiber Density (n) Bundles/ Inch	Crosshead Rate Inches/ Minute	Web Thickness (t) Inches	Beam Height (h) Inches	γ ergs/cm^2 x10^{-5}	γ/n
1	1	4173	181	5	---	.04	.6	---	---
2	1	4173	181	5	---	.04	.6	---	---
3	7	4173	---	0	.05	.04	.6	---	---
4	7	4173	---	0	---	.04	.6	---	---
5	7	4173	---	0	.01	.04	.6	---	---
6	8	4173	181	5	.01	.04	.6	---	.80
7	8	4173	181	5	.01	.04	.6	---	.90
8	8	4173	181	5	.01	.04	.6	---	.98
9	9	4173	---	0	.01	.04	.6	---	---
10	9	4173	181	10	---	.04	.6	---	---
11	9	4173	181	10	.01	.04	.6	---	.78
12	9	4173	181	10	.01	.04	.6	---	.71
13	10	4173	181	20	---	.04	.6	---	---
14	10	4173	181	20	.01	.04	.6	---	.60
14A	10	4173	181	20	.005	.04	.6	---	.71
15A	10	4173	181	20	.05	.04	.6	---	.86
16	11	4173	181	40	---	.04	.6	---	---
17	11	4173	181	40	---	.04	.6	---	---
18	11	4173	181	40	---	.04	.6	---	---
19A	13	4173	181	40	.01	.04	.6	---	.69
20A	13	4173	181	40	.005	.04	.6	---	.49
21	13	4173	---	0	.01	.04	.6	---	---
22A	14	4173	181	60	.005	.04	.6	---	.93
23	15	4173	181	Varied	---	.04	.6	---	---
24	16	4173	181	1	.01	.04	.6	---	1.48

Specimen	Casting	Matrix Material	Fiber* Material	Fiber Density (n) Bundles/ Inch	Crosshead Rate Inches/ Minute	Web Thickness (t) Inches	Beam Height (h) Inches	γ ergs/cm^2 x10^{-5}	γ/n
25	16	4173	181	1	.01	.04	.6	---	1.81
26	16	4173	181	1	.01	.04	.6	---	1.27
27	18	4173	181	2	.01	.04	.6	---	1.09
28	18	4173	181	2	.01	.04	.6	---	1.17
29	18	4173	181	2	.01	.04	.6	---	1.14
30	19	4173	181	3	.01	.04	.6	---	.91
31	19	4173	181	3	.01	.04	.6	---	.96
32	19	4173	181	3	.01	.04	.6	---	1.03
33a	20	4173	181	4	.01	.04	.6	---	.76
34a	20	4173	181	4	.01	.04	.6	---	.75
35A	20	4173	181	4	.01	.04	.6	---	.82
36	21	4173	181	6	.01	.04	.6	---	.74
37	21	4173	181	6	.01	.04	.6	---	.79
38	21	4173	181	6	.02	.04	.6	---	.77
39	22	4173	181	8	.01	.04	.6	---	.77
40	22	4173	181	8	.005	.04	.6	---	.72
41	22	4173	181	8	.01	.04	.6	---	.71
42	23	4173	181	12	.01	.04	.6	---	.74
43	23	4173	181	12	.01	.04	.6	---	.80
44	23	4173	181	12	.005	.04	.6	---	.71
45	24	4173	181	14	.01	.04	.6	---	.57
46	24	4173	181	14	.01	.04	.6	---	.66
47	24	4173	181	14	.002	.04	.6	---	.56
48	25	4173	181	16	---	.04	.6	---	---
49	25	4173	181	16	.005	.04	.6	---	.67
50	25	4173	181	16	.005	.04	.6	---	.65
51	26	4173	181	18	.005	.04	.6	---	.52

APPENDIX C (Continued)

Specimen	Casting	Matrix Material	Fiber* Material	Fiber Density (n) Bundles/ Inch	Crosshead Rate Inches/ Minute	Web Thickness (t) Inches	Beam Height (h) Inches	γ ergs/cm^2 x10^{-5}	γ/n
52	26	4173	181	18	.005	.04	.6	---	.57
53	26	4173	181	18	.005	.04	.6	---	.60
54A	26	4173	181	30	.005	.04	.6	---	.60
55	28	4173	181	30	.002	.04	.6	---	.47
56A	28	4173	181	30	.005	.04	.6	---	.56
57	27	4173	181	10	.01	.04	.6	---	.67
58	27	4173	181	10	.01	.06	.6	4.85	.485
59	27	4173	181	10	.01	.08	.6	3.66	.366
60A	29	4173	181	50	.005	.06	.6	---	---
61A	29	4173	181	50	.01	.06	.6	---	---
62A	29	4173	181	50	.05	.06	.6	---	---
63A	29	4173	181	50	.002	.04	.6	---	.61
65c	45	4173	181	10	.01	.04	.6	---	.81
66c	45	4173	181	10	.01	.04	.6	---	.76
69b	34	4173	---	0	.01	.04	.6	---	---
70b	34	4173	---	0	.01	.04	.6	---	---
73c	35	4173	---	0	.01	.04	.6	---	---
79c	35	4173	---	0	.01	.04	.6	---	---
80	33	4173	---	0	.01	.04	.6	---	---
85	46	4173	181	10	.01	.04	.6	---	.824
86	46	4173	181	10	.01	.04	.6	---	.870
90	42	4173	181	40	.01	.04	.6	---	.47
91	42	4173	181	40	.01	.04	.6	---	.90
92	42	4173	181	40	.01	.04	.6	---	1.02
98c	43	4173	181	40	.01	.04	.6	---	.97
99c	43	4173	181	40	.01	.04	.6	---	.80
108c	51	4173	---	0	.01	.04	.6	---	---

APPENDIX C (Continued)

Specimen	Casting	Matrix Material	Fiber* Material	Fiber Density (n) Bundles/ Inch	Crosshead Rate Inches/ Minute	Web Thickness (t) Inches	Beam Height (h) Inches	γ ergs/cm^2 x10^{-5}	γ/n
109c	51	4173	---	0	.01	.04	.6	---	---
110c	51	4173	181	10	.01	.04	.6	---	.865
111c	51	4173	181	10	.01	.04	.6	---	.810
112	52	4173	steel	10	.01	.04	.6	fibers pulled out	
114f	53	4173	181	10	.01	.04	.6	---	.673
115f	53	4173	181	10	.01	.04	.6	---	.715
116	61	828	---	0	.01	.04	.6	---	---
118	61	828	181	10	.01	.04	.6	---	.840
119	61	828	181	10	.01	.04	.6	---	.724
120d	62	828	---	0	.01	.04	.6	---	---
121d	62	828	---	0	.01	.04	.6	---	---
122d	62	828	181	10	.01	.04	.6	---	1.62
123d	62	828	181	10	.01	.04	.6	---	1.41
124s	30	4173	181	3	.05	.05	.6	---	1.27
125s	30	4173	181	3	.05	.04	.6	---	1.09
126	---	4173	181	3@3	.005	.04	.6	---	---
127	---	4173	181	3@3	.002	.04	.6	---	---
128d	---	828	181	40	.01	.08	.6	27.8	.695
129d	---	828	181	40	.005	.08	.6	19.8	.495
130d	---	828	---	0	.01	.08	.6	---	---
131	---	4173	flat	10	.01	.08	.6	7.39	.739
132	---	4173	flat	10	.01	.08	.6	6.85	.685
133d	---	828	.01	10	.01	.08	.6	13.82	1.38
134d	---	828	.01	10	.05	.08	.6	16.5	1.65
135	---	4173	181	20	.01	.08	.6	---	---
136	---	4173	181	20	.005	.08	.6	---	---
141	---	828	.01	20	.005	.08	.6	15.55	.778

APPENDIX C (Continued)

Specimen	Casting	Matrix Material	Fiber* Material	Fiber Density (n) Bundles/ Inch	Crosshead Rate Inches/ Minute	Web Thickness (t) Inches	Beam Height (h) Inches	γ ergs/cm^2 x10^{-5}	γ/n
142	---	828	.005	20	.01	.08	.6	4.48	.224
143	---	828	.005	20	.002	.08	.6	2.53	.127
145	---	4173	flat	20	.005	.08	.6	---	---
146	100	828	flat	20	.01	.08	.6	5.00	.250
147	100	828	flat	20	.01	.08	.6	3.87	.194
148	101	828	flat	20	.01	.08	.6	6.27	.314
149	101	828	flat	20	.005	.08	.6	6.12	.306
150	102	4173	flat	20	.002	.08	.6	---	---
151	102	4173	flat	20	.005	.08	.6	---	---
150A	102	4173	flat	20	.01	.08	.6	7.50	.375
151A	102	4173	flat	20	.005	.08	.6	8.7	.435
152h	103	828	flat	20	.01	.08	.6	10.72	.541
153h	103	828	flat	20	.005	.08	.6	10.42	.521
154	104	828	181	20	.005	.08	.6	7.17	.359
155	104	828	181	20	.01	.08	.6	7.2	.360
157	105	4173	flat	10	.005	.08	.6	4.21	.421
158	105	4173	---	0	.005	.08	.6	1.09	---
159	105	4173	---	0	.005	.08	.6	1.19	---
160	106	828	flat	10	.005	.08	.6	3.31	.331
161	106	828	flat	10	.01	.08	.6	4.05	.405
162	107	4173	flat	5	.01	.08	.6	2.18	.436
163	107	4173	flat	5	.005	.08	.6	2.29	.458
164	107	4173	---	0	.01	.08	.6	1.09	---
165	108	828	flat	5	.01	.08	.6	2.60	.520
166	108	828	flat	5	.005	.08	.6	3.02	.605
167	109	828	flat	10	.005	.08	.6	4.18	.418
168	109	828	flat	10	.01	.08	.6	3.85	.385

APPENDIX C (Continued)

Specimen	Casting	Matrix Material	Fiber* Material	Fiber Density (n) Bundles/ Inch	Crosshead Rate Inches/ Minute	Web Thickness (t) Inches	Beam Height (h) Inches	γ ergs/cm^2 $\times 10^{-5}$	γ/n
169	110	4173	181	10	.005	.08	.5	4.04	.404
170	110	4173	181	10	.005	.08	.7	3.78	.378
171	111	4173	181	10	.005	.08	.5	4.37	.437
172	111	4173	181	10	.005	.08	.8	3.83	.383
173	112	828	181	10	.005	.08	.5	4.92	.492
174	112	828	181	10	.005	.08	.7	5.21	.521
175	113	828	181	10	.01	.04	.6	9.83	.983
176	113	828	181	10	.01	.06	.6	6.51	.651
177	114	828	181	10	.01	.08	.6	5.25	.525
178	114	828	181	10	.01	.10	.6	4.48	.448
179	114	828	---	0	.005	.08	.6	2.72	---
180	115	828	181	10	.01	.08	.6	---	---
181	115	828	181	10	.005	.08	.6	5.09	.509
182	116	4173	nylon	10	.005	.08	.6	---	---
182A	116	4173	nylon	10	.01	.08	.6	---	---
183	116	4173	nylon	10	.01	.08	.6	---	---
184	117	4173	nylon	20	.01	.08	.6	---	---
185A	117	4173	nylon	20	.005	.08	.6	---	---
186	118	828	181	30	.01	.08	.6	9.47	.316
187	118	828	181	30	.005	.08	.6	9.55	.318
188i	119	4173	181	10	.005	.08	.6	5.64	.564
189i	119	4173	181	10	.01	.08	.6	6.19	.619
190	120	828	181	40	.01	.08	.6	10.65	.266
191	120	828	181	40	.005	.08	.6	10.72	.269
192	121	828	flat	30	.01	.08	.6	7.42	.247
193	121	828	flat	30	.005	.08	.6	6.60	.220
194	122	828	nylon	10	.01	.08	.6	9.8	.980

APPENDIX C (Continued)

Specimen	Casting	Matrix Material	Fiber* Material	Fiber Density (n) Bundles/ Inch	Crosshead Rate Inches/ Minute	Web Thickness (t) Inches	Beam Height (h) Inches	γ ergs/cm^2 x10^{-5}	γ/n
195	122	828	mylon	10	.005	.08	.6	8.04	.804
196	123	828	thornel	10	.01	.08	.6	8.1	.810
197	123	828	thornel	10	.005	.08	.6	7.7	.770
198	124	828	thornel	20	.01	.08	.6	12.8	.640
199	124	828	thornel	20	.005	.08	.6	---	---
200	124	828	---	0	.01	.08	.6	2.33	---
201	125	828	mylon	20	.01	.08	.6	---	---
202A	125	828	mylon	20	.01	.08	.6	---	---
203	128	828	flat	20	.01	.08	.6	4.55	.228
204	128	828	flat	20	.01	.08	.6	5.4	.270
205	129	828	flat	30	.01	.08	.6	7.4	.247
206	129	828	flat	30	.01	.08	.6	7.55	.252
207	132	4173	181	30	.01	.08	.6	6.4	.213
208	132	4173	181	30	.01	.08	.6	---	---
209	132	4173	181	30	.01	.08	.6	---	---
209A	132	4173	181	30	.01	.08	.6	6.05	.202
210	133	4173	flat	10	.01	.08	.6	4.42	.442
211	133	4173	flat	10	.01	.08	.6	4.97	.497
212	133	4173	flat	10	.01	.08	.6	6.0	.600
213	127	828	181	10	.01	.08	.5	3.65	.365
214	127	828	181	10	.01	.08	1.0	3.70	.370
215	126	828	181	10	.01	.08	.8	5.50	.550
216	126	828	181	10	.01	.08	.9	4.2	.420
217	130	4173	181	10	.01	.08	.9	3.69	.369
218	130	4173	181	10	.01	.08	1.0	3.51	.351
219	131	4173	181	10	.01	.08	.7	4.16	.416
220	131	4173	181	10	.01	.08	.8	3.71	.371

APPENDIX C (Continued)

Specimen	Casting	Matrix Material	Fiber* Material	Fiber Density (n) Bundles/Inch	Crosshead Rate Inches/Minute	Web Thickness (t) Inches	Beam Height (h) Inches	γ ergs/cm^2 x10^{-5}	γ/n
221	134	4173	181	30	.01	.08	.6	---	---
222	134	4173	181	30	.005	.08	.6	---	---
223	135	4173	flat	30	.005	.08	.6	---	---
224	135	4173	flat	30	.005	.08	.6	---	---
224A	135	4173	flat	30	.01	.08	.6	11.25	.375
225	136	4173	flat	20	.01	.08	.6	---	---
225A	136	4173	flat	20	.01	.08	.6	9.1	.455
226	136	4173	flat	20	.01	.08	.6	---	---
226A	136	4173	flat	20	.01	.08	.6	9.7	.485
227	137	4173	beta	10	.01	.08	.6	2.9	.290
228	137	4173	beta	10	.01	.08	.6	4.15	.415
229	138	4173	beta	20	.01	.08	.6	---	---
229A	138	4173	beta	20	.01	.08	.6	5.4	.270
230	138	4173	beta	20	.005	.08	.6	5.47	.274
230	138	4173	beta	20	.005	.08	.6	5.47	.274
230A	138	4173	beta	20	.01	.08	.6	5.75	.288
231A	131	4173	181	10	.01	.08	.6	4.58	.458
232	139	828	---	0	.01	.04	.6	3.35	---
233	139	828	---	0	.01	.06	.6	2.65	---
234	139	828	---	0	.01	.06	.6	2.92	---
235	139	828	---	0	.01	.08	.6	2.72	---
236	139	828	---	0	.01	.08	.6	---	---
237	139	828	---	0	.01	.10	.6	2.25	---
238	139	828	---	0	.01	.10	.6	1.85	---
239	140	4173	beta	30	.005	.08	.6	---	---
239A	140	4173	beta	30	.01	.08	.6	10.05	.335
240A	140	4173	beta	30	.01	.08	.6	9.55	.318

APPENDIX C (Continued)

Specimen	Casting	Matrix Material	Fiber* Material	Fiber Density (n) Bundles/ Inch	Crosshead Rate Inches/ Minute	Web Thickness (t) Inches	Beam Height (h) Inches	γ ergs/cm^2 x10^{-5}	γ/n
241	141	828	beta	10	.01	.08	.6	3.30	.330
242	141	828	beta	10	.01	.08	.6	3.42	.342
243	142	828	beta	20	.01	.08	.6	6.25	.313
244	142	828	beta	20	.01	.08	.6	5.20	.260
245	143	4173	181	10	.01	.04	.6	---	---
246	143	4173	181	10	.01	.06	.6	5.36	.536
247	144	4173	181	10	.01	.10	.6	---	---
247A	144	4173	181	10	.01	.10	.6	3.67	.367
248	144	4173	181	10	.01	.08	.9	4.55	.455
249	145	4173	181	10	.01	.08	.6	4.65	.465
250	145	4173	181	10	.01	.08	1.0	4.47	.447
251	146	828	181	10	.01	.06	.6	6.93	.693
252	146	828	181	10	.01	.08	1.0	3.67	.367
253	147	828	181	10	.01	.08	.7	3.60	.360
254	147	828	181	10	.01	.08	.9	4.57	.457
255	148	828	181	10	.01	.04	.6	---	---
256	148	828	181	10	.01	.08	.8	4.25	.425
257	149	828	181	10	.01	.08	.6	4.98	.498
258	149	828	181	10	.01	.10	.6	3.75	.375
259	149	828	181	10	.01	.10	.6	4.44	.444
260	150	828	thornel	20	.01	.08	.6	12.8	.640
261A	150	828	thornel	20	.005	.08	.6	12.5	.625
262	151	828	thornel	30	.005	.08	.6	15.55	.518
263A	151	828	thornel	30	.005	.08	.6	16.5	.550
264A	152	4173	beta	40	.01	.08	.6	10.2	.255
265A	152	4173	beta	40	.01	.08	.6	9.15	.229
266	154	828	beta	40	.01	.08	.6	11.97	.299

APPENDIX C (Continued)

Specimen	Casting	Matrix Material	Fiber* Material	Fiber Density (n) Bundles/ Inch	Crosshead Rate Inches/ Minute	Web Thickness (t) Inches	Beam Height (h) Inches	γ ergs/cm^2 x10^{-5}	γ/n
267	154	828	beta	40	.005	.08	.6	11.82	.296
267A	154	828	beta	40	.01	.08	.6	9.85	.246
268	157	828	beta	30	.005	.08	.6	8.37	.279
269	157	828	beta	30	.01	.08	.6	7.5	.250
269A	157	828	beta	30	.01	.08	.6	10.4	.347
270	158	828	monsanto	30	.005	.08	.6	14.42	.481
271A	158	828	monsanto	30	.01	.08	.6	14.2	.473
272A	159	828	monsanto	20	.01	.08	.6	10.45	.523
273	159	828	monsanto	20	.01	.08	.6	13.4	.670
274	160	828	monsanto	10	.01	.08	.6	6.05, 6.31	.605, .631
275A	160	828	monsanto	10	.01	.08	.6	4.67	.467

* Refers to following table of fibers used as reinforcement: (See Appendix B for properties of fibers.)

181 - Style 181 cloth fiber bundles; E-glass.
Flat - E-glass fibers of flat rectangular cross section, no twist in bundles.
.01 - Single filament E-glass with .01 inch diameter.
.005 - Single filament E-glass with .005 inch diameter.
Nylon - Nylon 6 fiber bundles.
Thornel - Thornel 50 graphite fiber bundles.
Beta - Beta glass fiber bundles.
Monsanto - Monsanto Type I synthetic fiber bundles.

a. Fibers may have been cut during machining of slot.

b. Matrix modified with 4% CTBN rubber particles.

c. Matrix modified with 8% CTBN rubber particles.

d. Matrix modified with 10% CTBN rubber particles.

e. No post cure.

f. Fibers heat cleaned to remove finish.

g. Fibers coated with paraffin.

h. Fiber bundles twisted to twist of 3 twists/inch of fiber bundle.

i. Fibers coated with Plastilease mold release.

Thesis 118353
S3372 Schmidt
Fracture toughness
of reinforced plastic
composite materials.